

APPLICATION OF HIGH-IMPACT POLYSTYRENE (HIPS) AS A GRAPHENE
NANOPARTICLE REINFORCED COMPOSITE THERMOPLASTIC ADHESIVE

By

Erik Stitt

A THESIS

Submitted to
Michigan State University
in partial fulfillment of the requirements
for the degree of

Materials Science and Engineering-Master of Science

2017

ABSTRACT

APPLICATION OF HIGH-IMPACT POLYSTYRENE (HIPS) AS A GRAPHENE NANOPARTICLE REINFORCED COMPOSITE THERMOPLASTIC ADHESIVE

By

Erik Stitt

Adhesive bonding is a more efficient joining method for composites than traditional mechanical fasteners and provides advantages in weight reduction, simplicity, and cost. In addition, the utilization of mechanical fasteners introduces stress concentrations and damage to the fiber-matrix interface. Adhesive bonding with thermoset polymers distributes mechanical loads but also makes disassembly for repair and recycling difficult. The ability to utilize thermoplastic polymers as adhesives offers an approach to address these limitations and can even produce a reversible adhesive joining technology through combining conductive nanoparticles with a thermoplastic polymer. The incorporation of the conductive nanoparticles allows for selective heating of the adhesive via exposure to electromagnetic (EM) radiation and simultaneously can augment the mechanical properties of the adhesive and the adhesive joint. This approach provides a versatile mechanism for efficiently creating and reversing structural adhesive joints across a wide range of materials.

In this work, a high-impact polystyrene (HIPS) co-polymer containing butadiene as a toughness modifier is compounded with graphene nano-platelets (GnP) for investigation as a thermoplastic adhesive. The properties of the bulk composite adhesive are tailored by altering the morphology, dispersion, and concentration of GnP. The thermal response of the material to EM radiation in the microwave frequency spectrum was investigated and optimized. Surface treatments of the adhesive films were explored to enhance the viability of this nanoparticle thermoplastic polymer to function as a reversible adhesive. As a result, it has been shown that lap-shear strengths of multi-material joints produced from aforementioned thermoplastic adhesives were comparable to similar thermoset bonded joints.

ACKNOWLEDGEMENTS

Returning to Michigan State University to pursue graduate studies has been one of the most fulfilling experiences of my life. I would like to sincerely thank all those who have encouraged, supported, and educated me during the last one and a half years. I extend my appreciation to my thesis committee; Dr. Mahmoodul Haq, Dr. Lawrence Drzal, and Dr. K Jayaraman for their time and efforts spent reviewing and evaluating this work.

I owe this entire opportunity to my advisor, Dr. Mahmoodul Haq, not only for his enthusiastic encouragement to pursue graduate school, but the entirely unique opportunities he has provided for me to succeed. His financial support, mentorship, and flexibility in allowing me to choose my areas of pursuit has created an environment of constant growth and reward.

I would also like to express my gratitude to my co-advisor Dr. Lawrence Drzal. His willingness to share his expertise in polymer and nano-composite sciences has been of immense value and encouraged exploration into areas of research I would not have otherwise considered.

Dr. Markus Downey was a crucial contributor to this research in both guidance and execution. This work could not have been completed without him and I will always be grateful for his friendship and the example he instilled for operating as an exceptional graduate researcher.

The staff of the Composite Materials and Structures Center; Mike Rich, Per Askeland, Ed Drown, and Brian Rook consistently supported this work with their time and expertise. I thank them and look forward to our continued work together. My appreciation is extended to all members of my research group. Especially to Suhail Vattathurvalappil and Mario Calderon, both of whom have worked alongside me as friends, academically, and in our endeavors as researchers.

Finally, I would like to thank my family and most certainly my partner, Elizabeth, whose love and unconditional encouragement has kept me motivated through trying times and obstacles I could not have faced alone.

TABLE OF CONTENTS

LIST OF TABLES	vi
LIST OF FIGURES	vii
Chapter 1: Introduction	1
1.1 The Call for Innovation in Multi-Material Joining.....	1
1.2 Reversible Thermoplastic Adhesives.....	2
1.3 Toughening of Polymers	2
1.4 Surface Treatment of Polymers.....	3
1.5 Targeted Activation of the Composite Adhesive	4
Chapter 2: Selection of Thermoplastic Polymer for Modification.....	7
2.1 Introduction.....	7
2.2 Materials and Methods.....	10
2.3 Results and Discussion.....	12
2.4 Conclusion.....	15
Chapter 3: HIPS Adhesive Films	17
3.1 Introduction.....	17
3.2 Materials and Methods.....	24
3.2.1 Film Production.....	25
3.2.2 Surface Treatment.....	26
3.2.2.1 Abrasion.....	26
3.2.2.2 Acid Etching.....	26
3.2.2.3 Oxygen Plasma Treatment	26
3.2.3 Surface Chemical Analysis	27
3.2.4 Surface Spectroscopy and Imaging	28
3.2.5 Adhesion Shear Strength	28
3.3 Results and Discussion.....	30
3.4 Conclusion.....	45
Chapter 4: GnP and Composite Adhesive Films	48
4.1 Introduction.....	48
4.2 Materials and Methods.....	49
4.3 Results and Discussion.....	50
4.4 Conclusion.....	58
Chapter 5: Microwave Activation	60
5.1 Introduction.....	60
5.2 Materials and Methods.....	61
5.3 Results and Discussion.....	62
5.4 Conclusion.....	66
Chapter 6: Summary and Future Work	68
6.1 Summary.....	68
6.2 Future Work.....	70

6.2.1 Modification of the Bulk Adhesive.....	70
6.2.2 Further Study of Surface Treatment.....	71
6.2.3 Dispersion of GnP	72
6.2.4 Further Study on Microwave Activation	74
WORKS CITED.....	75

LIST OF TABLES

Table 1-1. Summary of surface treatment methods commonly used to prepare polymers for adhesive bonding [18].....	4
Table 2-1. Properties of Ineos Nova 6200.....	11
Table 3-1. Summary of atomic concentrations for all films analyzed via XPS	43
Table 6-1. Tabulated summary of thermal response to substrates, neat, and composite HIPS at 200W and 6.24GHz.....	70

LIST OF FIGURES

Figure 1-1. Crack toughening mechanisms in rubber-filled modified polymers: (1) shear band formation near rubber particles; (2) fracture of rubber particles after cavitation; (3) stretching; (4) debonding; and (5) tearing of rubber particles; (6) transparticle fracture; (7) debonding of hard particles; (8) crack deflection by hard particles; (9) voided/cavitated rubber particles; (10) crazing; (11) plastic zone at craze tip; (12) diffuse shear yielding; (13) shear band/craze interaction [16].....	3
Figure 2-1. Butadiene rubber particles and crazing within HIPS after undergoing deformation [31]	8
Figure 2-2. Fatty ester derivatives commonly used as internal/external lubricants in styrene polymers	9
Figure 2-3. Boundary layer of lubricant between metal surface and polymer melt [38].....	10
Figure 2-4. Composite FTIR absorbance for a 1x25mm disc of DSM processed HIPS.....	13
Figure 2-5. Stacked FTIR absorbance spectra for the control HIPS (green), stearamide (grey) and pentadecylamine (black); top, center, and lower, respectively.....	14
Figure 2-6. XPS Spectrum of HIPS after DSM processing.....	15
Figure 3-1. A comparison of secondary bonding on a poorly wetted substrate (top) and completely wetted substrate (bottom).....	18
Figure 3-2. Images captured of R.O. water droplets on HIPS film surfaces showing a high contact angle and poor wettability (top) and low contact angle indicative of superior wetting (bottom).....	19
Figure 3-3. Chemisorption of a carboxylic acid compound on the surface of aluminum oxide through the consumption of hydroxyls on the oxide surface [54].....	20
Figure 3-4. Molecular interactions with PTFE [55].....	21
Figure 3-5. Molecular schematic for oxygen plasma treatment of a polymer film [63].....	22
Figure 3-6. Pathway for oxygenation of the aromatic ring of styrene [66].....	23
Figure 3-7. XPS spectra showing the peak contribution of different oxygenated functional groups deposited during O ₂ Plasma treatment [67].....	24
Figure 3-8. HIPS as extruded from DSM (left), after pressing (center), after being trimmed for lap joint assembly (right).....	25
Figure 3-9. Digital contact angle goniometer setup	27
Figure 3-10. Lower substrates, bondline wire, and HIPS films before application of the upper substrate	29

Figure 3-11. Fixture for the manufacture of “sandwich” lap joints after thermal cycling.....	29
Figure 3-12. Profile of a bonded lap joint showing how substrate cuts create a 25x25mm bond area	30
Figure 3-13. Load vs displacement of lap-shear joints with untreated HIPS films	31
Figure 3-14. XPS full spectra for HIPS films released with PTFE coated peel-ply	31
Figure 3-15. Contact angles of R.O. water on select HIPS film surfaces.....	32
Figure 3-16. Micrograph of sharkskin on a pressed HIPS film sample at 50,000X.....	33
Figure 3-17. Contact angle of R.O. water on HIPS films versus O ₂ plasma treatment time, reference values [73] (left) and observed values (right).....	34
Figure 3-18. Load vs displacement curves for untreated and O ₂ plasma treated films in joints with Al and CFRP substrates	35
Figure 3-19. Comparison of lap joint fracture surfaces using untreated (left) and plasma treated (right) HIPS adhesive films	36
Figure 3-20. Estimations of the total surface energy for selected HIPS films	37
Figure 3-21. Relationship of polar, dispersive, and total surface energies observed for HIPS films versus plasma treatment times	38
Figure 3-22. SEM micrograph at 50X of HIPS film pressed with PTFE release film before (left) and after (right) 150sec plasma treatment.....	39
Figure 3-23. SEM micrograph at 5,000X of HIPS film pressed with PTFE release film before (left) and after (right) 150sec plasma treatment.....	39
Figure 3-24. SEM micrograph at 50,000X of HIPS film after 150sec plasma treatment (left) and 900sec (right)	40
Figure 3-25. Full XPS spectra for 150sec plasma treated film.....	41
Figure 3-26. Full XPS spectra for 900sec plasma treated film.....	42
Figure 3-27. Cs1 regional scan for 150sec plasma treated films highlighting the resulting functional groups	43
Figure 3-28. Cs1 regional scan for 900sec plasma treated films highlighting the resulting functional groups	44
Figure 3-29. Graphical summary of C1s binding energies observed in HIPS films and their coordinating functional groups.....	45
Figure 3-30. Graphical summary of atomic concentrations for all films analyzed via XPS	46

Figure 3-31. Summary of lap-shear strengths and failure displacements of untreated and plasma treated films on Al and CFRP substrates	47
Figure 4-1. Morphology of M25 (left) and C750 (right) GnP in SEM micrographs.....	49
Figure 4-2. Micrographs of HIPS fracture surface with changing C750:M25 GnP concentration top to bottom and increasing magnification left to right.....	51
Figure 4-3. Effects of GnP loading and morphology on the flexural modulus and strength of HIPS ..	52
Figure 4-4. Effects of GnP loading and morphology on the flexural strain-to-failure of HIPS.....	53
Figure 4-5. Effects of GnP loading and morphology on the tensile modulus and strength of HIPS	54
Figure 4-6. Effects of GnP loading and morphology on the flexural strain-at yield of HIPS.....	55
Figure 4-7. Effects of GnP loading and morphology on the notched impact resistance of HIPS.....	56
Figure 4-8. Effects of GnP loading and morphology on the lap-shear strength of Al-Al bonded joints	57
Figure 4-9. Effects of absolute M25 GnP content on the lap-shear strength of Al-Al bonded joints...	58
Figure 5-1. MicroCure 2100 variable frequency oven showing chamber, IR temperature probe, and glass sample stand	61
Figure 5-2. Surface temperatures of substrates, neat HIPS, and GnP composite HIPS at 200W and 6.24GHz with a 1.15GHz sweep.....	62
Figure 5-3. Maximum temperature (solid) and heating rate (striped) for 5 and 7.5% M25 composite films cycled at various constant frequencies at 250W	64
Figure 5-4. Maximum temperature (solid) and heating rate (striped) for 5 and 7.5% C750 composite films cycled at various constant frequencies at 250W	65
Figure 5-5. Thermal response of C750/M25 blended GnP composite films at 7.5%/wt when heated with 200W of power at the noted frequencies	66
Figure 6-1. Lap-shear strength of HIPS adhesive films compared to similar structural adhesives[18]	68
Figure 6-2. Graphical summary of the mechanical properties of GnP composite HIPS	69

Chapter 1: Introduction

1.1 The Call for Innovation in Multi-Material Joining

The objective of this work is to provide a solution for the joining of dissimilar materials which combines the advantages of mechanical fasteners with the benefits of adhesive bonding. In industry reviews, even with recent advancements in mechanical joining techniques, the integration of composite materials into many structural applications is still limited by efficient means of joining metallic-composite structures [1, 2]. Utilizing mechanical fasteners for the joining of composite materials adds weight and introduces stress concentrations diminishing the advantage of introducing composite components [3, 4]. The integration of mechanical fasteners in joints can result in losses in strength of up to 40-60% in tension and 15-50% in compression [5]. The use of bolted joints in laminates is especially detrimental as the post-processing delaminates the matrix surrounding these stress concentrations; further reducing load capacity, resistance to fatigue, and strain-to-failure [6-9].

Adhesive bonds are an efficient solution for the joining of metal-composite structures. When correctly integrated into design, adhesive joints provide distribution of transfer loads, improved fatigue resistance, light-weighting, and simplicity [10]. Sources agree thermoset adhesives address many of the short comings inherent in mechanical joining and their continued advancement is seen as critical for increased utilization of composite materials in industry [11-14]. However, thermoset adhesives are not without their disadvantages. Thermoset adhesive bonds, while strong, are permanent, making disassembly for repair and recycling difficult. The importance of repair and end-of-life reclamation continues to increase as more efficient, greener solutions to manufacturing are pursued. These areas are considered critical in evaluation for the feasibility of any multi-material joining solution [15]. It is this requirement especially that makes reversible adhesives a more valuable answer to composite joining than any existing method.

1.2 Reversible Thermoplastic Adhesives

The solution for the unique needs of multi-material joining is a structural adhesive that possesses the same functionality as mechanical fasteners. Nanocomposite reinforced thermoplastic adhesives are capable of creating strong, stable, structural bonds which can then be reversed and reassembled as needed for repair or end-of-life reclamation. Focusing on efficiency and viability for industrial application, this research is conducted in attempts to create a solution to fill these needs.

There are three keystone areas to the development of reversible thermoplastic adhesives to achieve a functionality which would make them suitable for industrial use. First, neat thermoplastic polymers require toughening or reinforcement to provide the strength needed for structural joints. Second; chemical, morphological, and topographical modification is needed to produce a surface suitable for adhesion. Finally, a mechanism is required for selective activation, the capacity to melt and bond the adhesive without thermal soaking of the joint. It is these three design parameters which are addressed in this work with a focus on applicable surface treatments to facilitate adhesion with engineering thermoplastics. While the focal point of this study, exceptional fulfillment of all three areas is essential to enforce reversible thermoplastic adhesives as the solution for industrial multi-material joining.

1.3 Toughening of Polymers

The augmentation of the physical or chemical structure of a polymer to allow the bulk material to absorb a greater amount of energy before ultimate failure than the neat material is known as toughening. Mechanical failure of polymers is due to the separation of polymers chains and severing of cross-linkages via cracking under strain. Reducing a polymer's ability to is a primary objective for increasing failure strain and is often done by the introduction of either lower and/or higher modulus phases. The mechanisms for toughing via crack inhibition are shown in Figure 1-1. Resistances to the formation and propagating of cracks are defined as intrinsic and

extrinsic toughening, leading and following the crack, respectively. A multi-phase approach to toughening allows one to utilize the advantages of both types of toughening. For this reason, a rubber toughened copolymer was chosen to be compounded with graphene nanoparticles. While nothing is gained for free, the combination of the low-modulus rubber and high-modulus graphene should capitalize on the improvements in toughness and strength to be gained from each particle while offsetting the inherent cost of the other to the resulting thermomechanical properties.

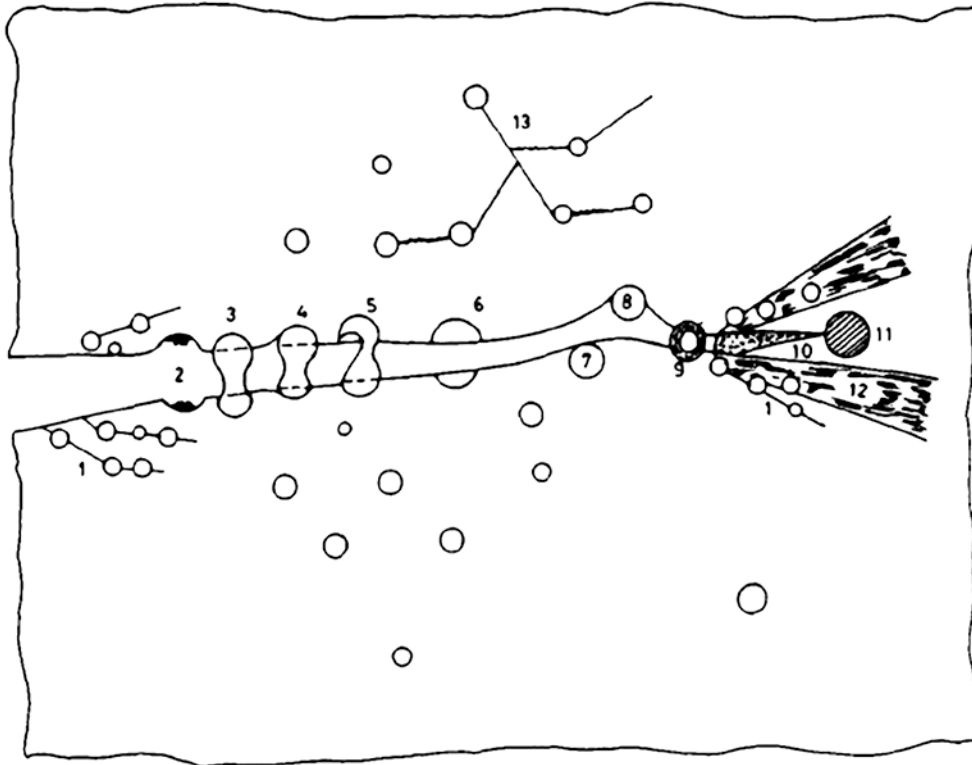


Figure 1-1. Crack toughening mechanisms in rubber-filled modified polymers: (1) shear band formation near rubber particles; (2) fracture of rubber particles after cavitation; (3) stretching; (4) debonding; and (5) tearing of rubber particles; (6) transparticle fracture; (7) debonding of hard particles; (8) crack deflection by hard particles; (9) voided/cavitated rubber particles; (10) crazing; (11) plastic zone at craze tip; (12) diffuse shear yielding; (13) shear band/craze interaction [16]

1.4 Surface Treatment of Polymers

Polymers are relatively low energy materials making their surfaces difficult to bond to without surface treatment. Thermoplastic polymers, especially, have low surface energies due to their amorphous molecular structure [17]. The low capacity for adhesion of thermoplastics is

further compounded by blends of lubricants and modifiers which are added to inhibit sticking of the liquid polymer during processing and thermoforming. In order to prepare thermoplastic polymers for bonding, modifications must be made to create an energetically favorable surface for the various mechanisms of adhesion to occur. Surface treatments employ physical and/or chemical modifications of the outer polymer structure. Table 1-1 summarizes mechanical and chemical surface treatments widely used in industry for the preparation of polymers for adhesion.

Table 1-1. Summary of surface treatment methods commonly used to prepare polymers for adhesive bonding [18]

Technology	Bond Strength	Consistency	Versatility	Capital Cost	Environment Impact
Mechanical Abrasion	Good	Poor	Very Good	Little	Dust
Solvent Wipe	Medium-Good	Fair	Good	Low	Organic vapor
Vapor Degreasing	Good	Good	Good	Medium	Organic vapor
Flame, thermal	Good	Fair	Poor	Low	Open flame
Acid etch	Very good	Good	Fair	High	Fumes, chemicals, disposal costs
Corona	Good	Good	Poor	High	Ozone
Plasma	Very good	Very good	Poor	High	Low, bottled gases

These processes function through a number of mechanisms to make changes to roughness, free-energy, chemical configuration, and stability of the surface. Each method has attributes which make it suited to specific applications. In this work solvent wipe, mechanical abrasion, acid etch, and low-pressure plasma were chosen for the preparation of the thermoplastic films for bonding. The effect of these surface treatments on the film characteristics and subsequent changes to adhesion strength are the primary focus of this work.

1.5 Targeted Activation of the Composite Adhesive

The final thrust area in the development of structural thermoplastic adhesives is developing a method to selectively heat the film within the bondline, targeted activation. Melt adhesives function by heating the material above its melting temperature to allow for flow and the formation of bonds, then freezing those bonds in place. Melt activated thermoplastic adhesives utilizing

engineering plastics are no different and require the same means to bond and de-bond from the surface, thermal energy. While the simplest solutions are to apply the adhesive in a liquid state or thermally soak the entire assembly after applying adhesive films to the bondline, neither is exceptionally efficient.

Application of liquid adhesives at the melt temperatures of structural adhesives is challenging on metal substrates. As the conductivity and the thermal mass of metals is relatively high, melt adhesives are rapidly cooled upon application causing the adhesive to skin before it can form stable bonds [19]. This requires large metal substrates to be preheated before melt adhesive application. The thermal soaking of large components is time consuming and requires much wasted energy to raise the entire temperature of a structure to heat a comparatively small area. This is true for both the preheating of substrates for liquid application or activation of adhesive films within the bonds areas. Additionally, in thermal bonding for multi-material joining, components of different composition have different rates of heating and coefficients of thermal expansion. As the three phases heat and cool, they do so at different rates and expand/contract to different specific areas. As the joint freezes, the stresses caused by these effects are locked into place, effectively pre-loading the bond.

Methods exist for the targeted heating and welding of thermoplastics augmented with conductive susceptor particles. Traditionally, ferromagnetic nanoparticles are used as the susceptors and the composite adhesive is placed within an oscillating induction field to rapidly heat the particles via hysteretic losses [20, 21]. This energy is transferred to the surrounding polymer, melting it. Ferromagnetic composite adhesives are typically used for sealing plumbing and composite pressure vessels. Induction welded thermoplastic joints in these applications have shown 25% improvements in rupture strength over alternative gluing or mechanical fastening methods [22]. While induction welding of thermoplastics is rapid, efficient, and does not require

thermal soaking to form adhesive bonds, they are extremely constrained in applications as they are not functional with conductive substrates.

The same eddy currents that induce hysteretic heating in nanoparticles, causes joule heating in conductive bulks. This rapidly heats the bonding surfaces far above the degradation temperature of conductive laminates and even the melt temperature of softer metals. The current inability to induction weld composite thermoplastics adhesives to conductive substrates severely limits their application. To overcome this limitation, a shift from induction fields to microwave energy is explored in this work. Graphene nano-structures have been shown to heat to hundreds of degrees Celsius in several seconds when exposed to microwave energy [23]. It is believed the selection of specific microwave parameters will allow penetration through substrates to facilitate heating of the adhesive within the bondline [24, 25]. To truly prove selectivity, it would be shown this can be accomplished with limited losses to the surrounding material. It is the intend of this work to examine how altering the parameters of the microwave energy and GnP loading affects the degree of energy absorption exhibited by the composite adhesive films.

Chapter 2: Selection of Thermoplastic Polymer for Modification

2.1 Introduction

Polymer selection is critical to meeting the requirements of the ultimate application of the composite adhesive. Project guidelines dictated the material must be capable of adhering to both polymer and metallic substrates, be mechanically stable over 100°C, and resistant to corrosion and moisture adsorption. Internal material requirements were designated that the material be easily processed, be susceptible to GnP integration, and readily available. Polystyrene is a glassy, chemically resistant polymer with a glass transition state around 100°C and proved an excellent candidate for use as an adhesive. While brittle in its neat form, polystyrene that has been impact modified maintains its chemical, thermal, and mechanical stability with the addition of residence to crack formation and brittle failure. An understanding of the fundamental mechanisms behind impact modification will be of value in understanding the motivations for selecting a rubber toughened polymer and how this is expected to compliment the graphene reinforcement discussed in 4.:

Impact modified styrene polymers are ones which have been augmented with a low modulus elastomer to increase toughness and resist internal crack growth [26]. In the case of the HIPS utilized in this work, that modifier is butadiene rubber which has been dispersed as distinct particles rather than within a uniform block copolymer [27]. Two-phase HIPS copolymers are produced by dissolving butadiene into the styrene monomer prior to polymerization, typically in concentrations of 3-12% [28, 29]. As bulk polymerization is initiated, agitation is applied separating the blend into a polystyrene rich phase and polybutadiene rich agglomerates which break up into discrete particles [30]. As polymerization continues, polystyrene crosslinks with modules of the butadiene creating rubber “bubbles” which are supported by the surrounding bulk as seen in Figure 2-1.

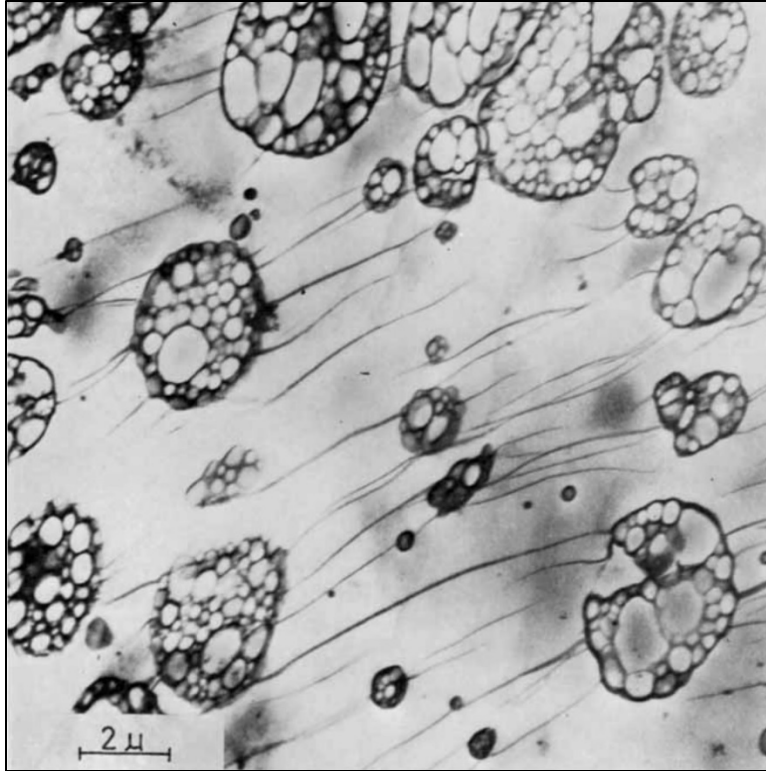


Figure 2-1. Butadiene rubber particles and crazing within HIPS after undergoing deformation [31]

These rubber bubbles enable both intrinsic and extrinsic toughening mechanisms allowing the HIPS copolymer to adsorb additional before destruction of the polymer structure. This extends load carrying capacity after damage and extending time to failure [16]. Beyond the energy absorbed by the soft butadiene during deformation, the interface between these rubber particles and the bulk polystyrene becomes the nucleation site for crazing, This is a phenomenon in which sub-micron sized voids are formed within the bulk of the polymer resisting crack formation and absorbing energy as the polymer volume increases and the rubber particles separate from the polystyrene bulk [32].

Crazing initiates at the brittle-ductile crossover point where HIPS begins to undergo plastic deformation. This is the cause of the strain-whitening seen in HIPS and other impact modified glassy polymers. In a HIPS blend with optimal butadiene particles size, crazes form at the particle boundary but are unable to pass through the rubber particles as seen in Figure 2-1. This “pinning”

prevents the propagation and agglomeration of crazes which lead to crack formation and ultimate failure. The rubber toughening in HIPS makes it an excellent candidate for composite adhesion applications. This is not only for the benefits in the mechanical properties of the material, but in addition to the role this rubber toughening can have mitigating the drawbacks of stiff nanoparticle reinforcement.

Commercially available thermoplastics are designed for specific processing methods. These application based polymers will contain a proprietary blend of additives to optimize the flow, melt, and release characteristics of the material. Typically, compounds are selected which are capable of performing several of these functions simultaneously. For example, in low molecular weight polymers, fatty acids can be used as both internal and external lubricants. To accomplish this, fatty acids with specific solubility's are selected which leads them to migrate to the surface during melting. This allows the fatty acids to enhance the internal flow properties of the adhesive while also forming a boundary layer between the polymer and processing surfaces [33]. Blends of internal/external lubricants will typically consist 1-2% of the total polymer by weight [34]. Common mold release lubricants in polystyrene blends are fatty acid esters, amides, and bis-amides [35]. It has been shown that the lengths of the fatty acid tails has a direct impact of the miscibility of the surfactant, and hence, its role in internal vs exterior lubrication [36].

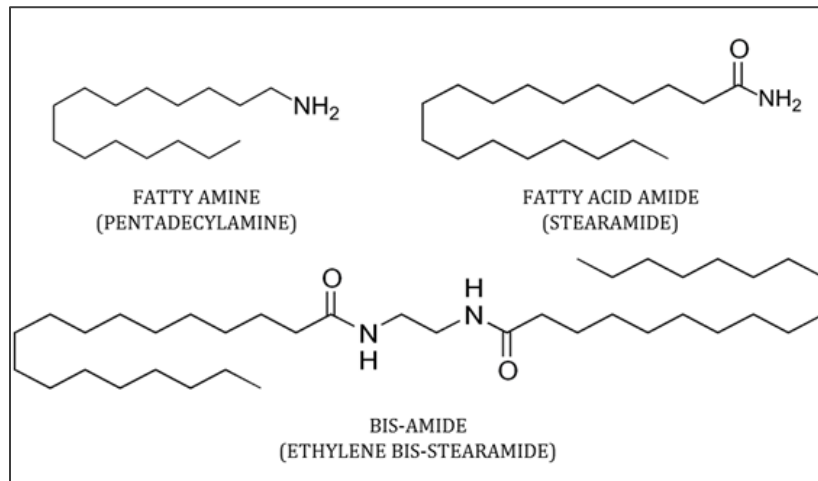


Figure 2-2. Fatty ester derivatives commonly used as internal/external lubricants in styrene polymers

Amphiphilic surfactants function by aligning their polar and nonpolar “heads and tails” into orientation with phases along a boundary according to their miscibility with each phase. As in the example of fatty acids, the insolubility of the polar constituent in the polymer bulk drives the surfactants to migrate to the surface forming a multi-molecular tail-head-tail layer [37]. This alignment creates a slip-plane as the non-polar tails form weak secondary bonds to one another. An illustrative representation of this interphase boundary is shown in Figure 2-3.

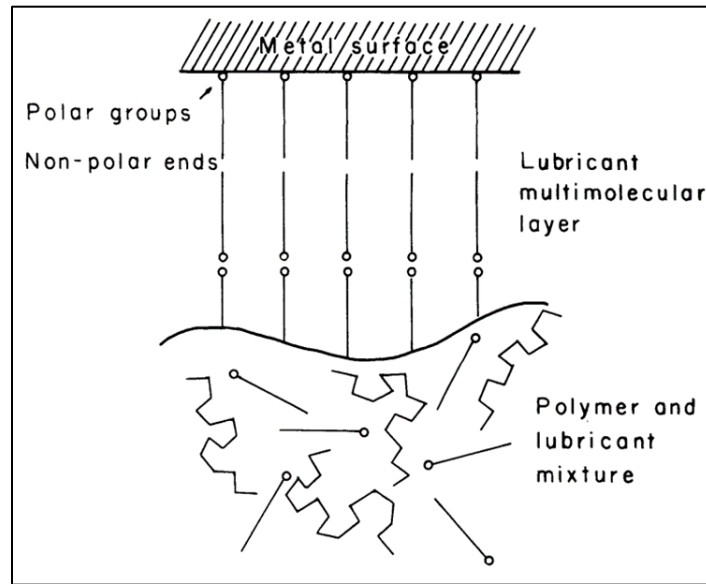


Figure 2-3. Boundary layer of lubricant between metal surface and polymer melt [38]

When these surfactants are present on the polymer surface, the thermoplastic phase is inhibited via “out competition” from chemically adhering to metallic surfaces. As it is the objective of this work is to form adhesion to thermoplastic to metallic and epoxy surfaces, these surfactants must be removed or otherwise disabled. This will be of focus in the following chapter after the presence and composition of these mold release surfactants is confirmed in this section.

2.2 Materials and Methods

In this work the thermoplastic chosen for use is Ineos Nova 6200 super high impact polystyrene. The mechanical and rheological characteristics for this polymer are listed in Table 2-1.

This material was specifically selected for its comparatively high glass transition temperature (T_g), resistance to moisture absorption, high modulus, and impact toughness. The thermoplastic was obtained as off-white pellets which were first dried for 12hr at 60°C and then stored under dry-room conditions for future use.

Table 2-1. Properties of Ineos Nova 6200

Property	Metric	Standard
Density	1.04 g/cc	ASTM D792
Mold Shrinkage	0.004-0.007 cm/cm	ASTM D955
Melt Flow	3 g/min	Condition G
Tensile Strength	25 MPa	ASTM D638
Tensile Modulus	2.135 GPa	ASTM D638
Flexural Strength	34 MPa	ASTM D790
Flexural Modulus	1.965 GPa	ASTM D790
Izod Impact (Notched)	2.24 J/cm	ASTM D256
Moisture Adsorption	<0.1 % 24hs	ASTM D570
Glass Transition	60 °C	
Deflection Temperature	85 °C	ASTM D648
Melt Temperature	190-275 °C	

All melt processing of the material was done in a 15cm³ dual screw extruder. Each batch of polymer was processed, neat or otherwise, in ~10gram batches. To compound, the material was recirculated at 250°C for 5min at a screw speed of 100RPM. The same processing conditions were used here to prepare the neat polymer as were be used to blend and mechanically disperse nanoparticles later in the work for consistency (see 4:). The thermoplastic was ejected from the extruder either to cool on a clean aluminum surface or injection molded into test geometries. For injection molding, ~2.5gram shots of polymer were ejected into a transfer cylinder held at 250°C and force injected into an 80°C mold at 0.75MPa.

Injection molded samples included tensile, flexural, and izod impact. They were produced and tested per ASTM standards; D638, D790, and D648, respectively. A minimum sample size of 6 for all material configurations and experimental variations was used for constancy. These physical testing methods were used consistently throughout this entire work unless otherwise noted.

Characterization of the chemical composition of the bulk adhesive was done using PerkinElmer Spectrum-1 Fourier transform infrared (FTIR) spectrum analyzer. The adsorption spectra was post-processed using the EssentialFTIR software suite. The adsorption peaks were initially identified using the NICODOM IR polymer demo library with additional IR spectra being obtained from the NIST Chemistry WebBook. Additional peak identification was done using *Spectrometric Identification of Organic Compounds* for reference [39].

The surface Composition of the neat material was determined using x-ray photoelectron spectroscopy (XPS). Film samples were cut into 1cm squares and attached to aluminum studs. Data collection was perform with Al X-ray (1486.6eV) and a take off angle of 45°. A pass energy of 187.85eV was used for survey and 29.35eV for regional scans. This XPS methodology is consistent for film surface analysis throughout the remainder of this work.

2.3 Results and Discussion

Results from the FTIR analysis show an absorbance spectra characteristic of organic polymers, specifically polystyrene, it is shown here in Figure 2-4. All the strong peaks identified are labeled in black. The sharp, strong peaks from 2850-3100 are indicative of alkane C-C bonds in the polymer backbone and the C-H bonds of the styrene aromatic rings. The multiple peaks between 1400 and 1600 are the result of stretching from the C=C bonds within the styrene aromatic ring. Finally, the very strong peaks from 675-1000 are from bending interactions with the C=C-H bonds of the alkene groups within the butadiene. An additional weaker peak was identified for C-O ether stretching at 1028. As HIPS is prone to oxidation of the lone C=C butadiene bond, this peak is not unexpected [26]. This interpretation matches the reference spectra for a polystyrene/butadiene blend with a high degree of certainty, 0.92/1. The additional components of the polymer blend are more challenging to identify as they exist in concentrations of only 1-5% by weight and are very similar to the bulk polymer. To determine the composition of the trace compounds within the

polymer, focus was placed on searching for strong characteristic peaks that would affect the spectra even in small concentration. For example, if nitrogen were present in nitrile functional groups, a carbon-nitrogen triple bond, there would be a strong characteristic peak from 2100-2260. As this peak is absent, nitrile based compounds can be excluded from consideration. These absent peaks labeled in grey near their expected locations on the wavenumber axis.

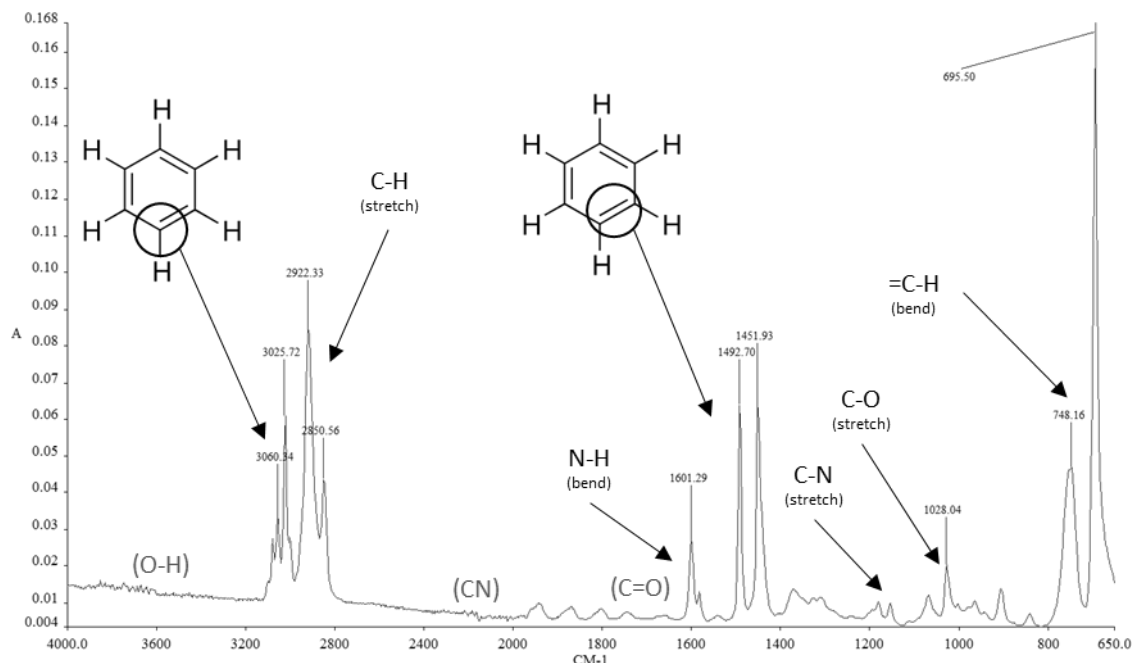


Figure 2-4. Composite FTIR absorbance for a 1x25mm disc of DSM processed HIPS

As is seen in the absorbance spectra stacked in Figure 2-5, it is highly unlikely this polymer blend contains a fatty acid amide or bisamide as the strong C=O alcohol peak from 1600-1690 and strong N-H two-band peaks from 3100-3500 are not present. These peaks are characteristic for a fatty acid amide like stearamide, see Figure 2-2 [39]. The peaks for a secondary amine however, a weak C-N band from 1080-1360 and an N-H bending peak at 1600, are plausible to be contained within the composite spectra obtained from the control HIPS sample. FTIR spectroscopy neither confirms nor denies the presence of a fatty amine surfactant within the polymer. Additional testing is required to draw confident conclusions on the additives present in the polymer blend.

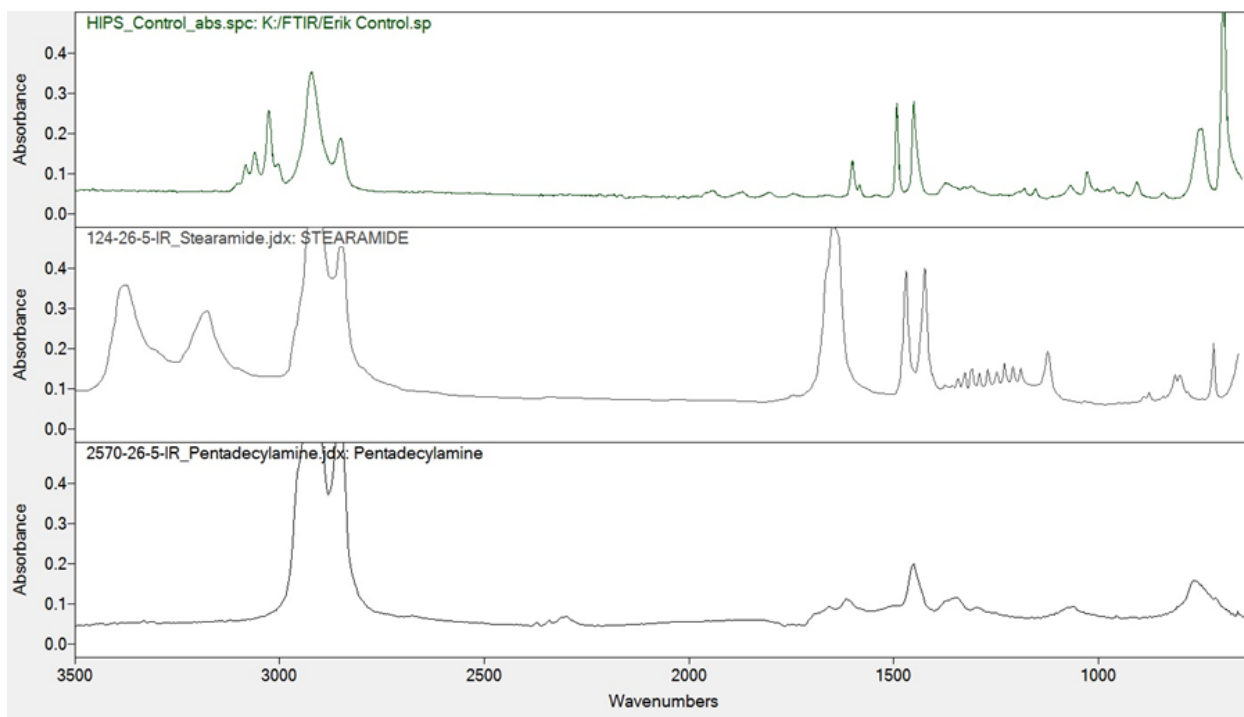


Figure 2-5. Stacked FTIR absorbance spectra for the control HIPS (green), stearamide (grey) and pentadecylamine (black); top, center, and lower, respectively

Using the nitrogen of the amine as a tag, XPS can be used to discern atomic concentrations of surface constituents and confirm the presence of these external surfactants. The penetration depth of XPS is on the order of monolayers, and the presence of nitrogen in this spectra while under vacuum would confirm the presence of a nitrogen based compound on the surface. As these lubricants are the only nitrogen containing compound suspected to be present in the polymer, assuming nitrogen present on the surface is derivative of fatty amines is appropriate while under high-vacuum.

The results of the full spectra scan of the control HIPS is shown in Figure 2-6. The full spectra of the HIPS polymer shows nitrogen, oxygen, and calcium in discernable quantities on the film surface; 0.83%, 9.59%, and 1.23%. Combining this information with the FTIR spectra, this is confirmation of a possible binary fatty amine on the polymer surface which has migrated there to function as an external mold release [40]. A moderate oxygen peak is expected in the scan of a polymer which has been exposed to atmospheric conditions. The oxygen content on the film surface

is due to mild oxidation and surface adsorption of water. The presence of calcium on the film surface is indicative of calcium carbonate, a common filler and extender added in low quantities to maintain spacing within the polymer structure and its effect on surface adhesion is not considered in this work [33].

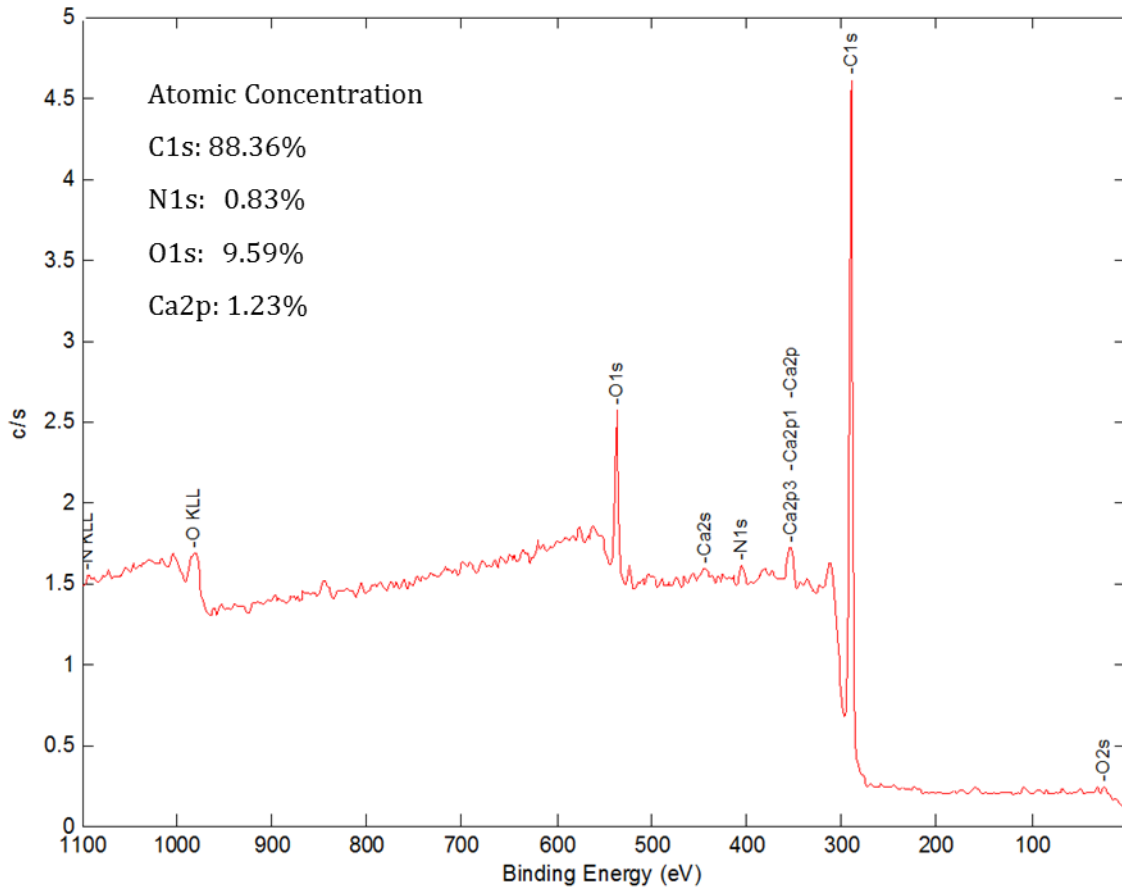


Figure 2-6. XPS Spectrum of HIPS after DSM processing

2.4 Conclusion

The findings of this chapter confirm the composition of the super high-impact polystyrene as a styrene butadiene copolymer. FTIR and XPS analysis together confirm the presence of amine based surfactants within the polymer bulk and on the polymer surface. In addition to the lubricants, a calcium based filler, most likely CaCO_3 is also identified on the film in low concentration. These finds are as expected and align with literary references as to the fillers and lubricants commonly

used in polystyrene systems. This baseline will be critical moving forward for assessment on the effects of surface treatment.

Chapter 3: HIPS Adhesive Films

3.1 Introduction

In order to present thermoplastic materials as an efficient means to replace current processes, they must be designed to function in a manner consistent with current industry processes. The adhesive films for this work are prepared by the pressing of extruded HIPS material into thin sheets. These films are “activated” via the introduction of thermal energy to raise the temperature of the adhesive above its melting point. While in contact with the substrates, the liquid thermoplastic flows forming mechanical and chemical interlocks with the surface. Upon cooling these interlocks are frozen forming bonds with the surface. These bonds create a stable joint that is resistant to shock, peel, and cracking up to the thermal yield temperature of the thermoplastic. However, when used as initially produced, these films were found to exhibit poor interfacial adhesion with slip failure occurring at the adhesive-substrate interface. This chapter explores the mechanisms at work for bonding of the adhesive films to surfaces, why there is incomplete adhesion between HIPS and the substrates, how the surface of the film can be assessed as to its bonding potential, and how this potential can be modified.

There are many theories of adhesion which have been developed to quantify the molecular interactions which hold phases together, the work of adhesion. This work will focus on the two most applicable to polymer adhesion in this way; physical adsorption, and chemical adhesion. Descriptions of these mechanisms are included for their relevance in explaining the changes observed in the adhesive behavior and are summarized from the *Handbook of Adhesives and Sealants* [18]. Adsorption theory is based on the principle that a difference in surface energy causes a low-energy liquid, the adhesive, to spread across a high-energy substrate, the adherent. This spreading, referred to as “wetting”, causes adhesive to flow into the deviations of the adherent surface. As the adhesive flows, it displaces air and allows for near intermolecular forces, Van der

Waals and hydrogen bonding, to form secondary bonds between atoms of the two phases. The formation of these secondary bonds is also referred to as physisorption. The greater the difference in surface energy, the more thermodynamically driven the wetting is, the greater the surface area between the phases will be, the more bond energy is created, and the stronger the work of adhesion is. An illustration of this mechanism is shown in Figure 3-1 highlighting the importance of contact area for physical bonding.

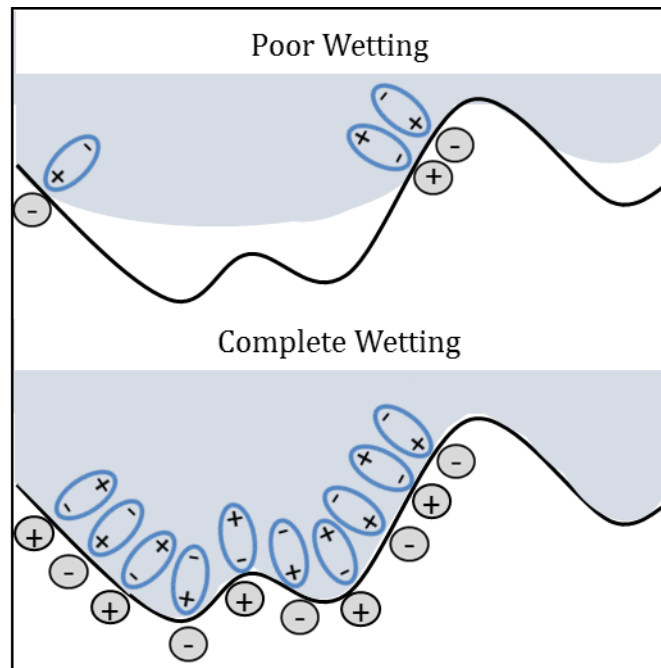


Figure 3-1. A comparison of secondary bonding on a poorly wetted substrate (top) and completely wetted substrate (bottom)

The wettability of a surface can be estimated from the contact angle of a liquid at equilibrium on its surface. The contact angles of water droplets on polymer surfaces are shown as example in Figure 3-2. The contact angle of water on a substrate is a qualitative assessment of its surface energy and has been well documented to be directly reflective of future adhesive joint strength [41-43]. Most polymers, especially polystyrene, are regarded as low-surface energy materials, they require modification of their surface to allow for wetting and strong adhesion.

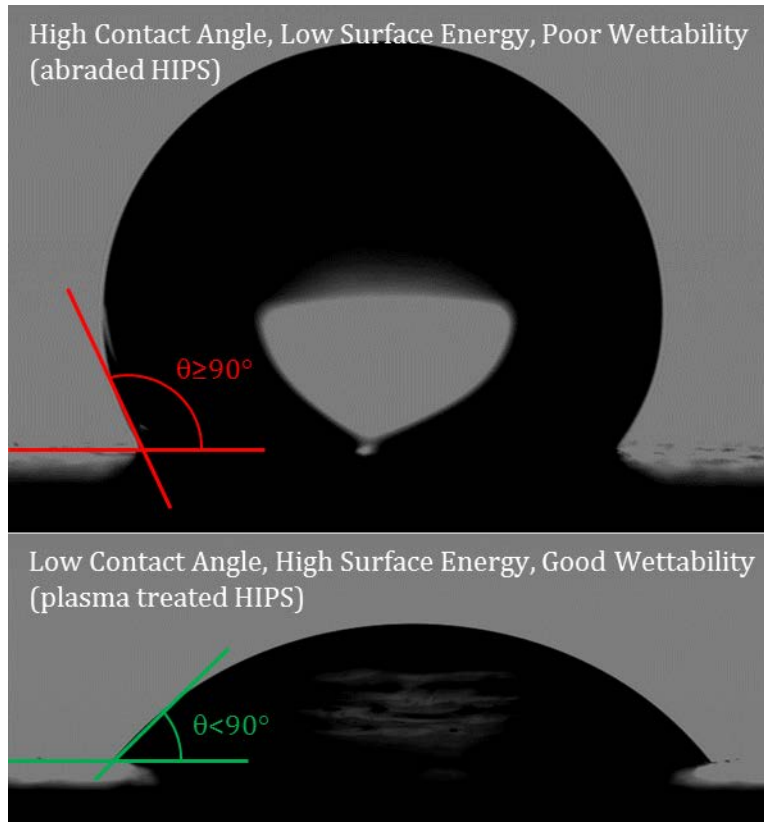


Figure 3-2. Images captured of R.O. water droplets on HIPS film surfaces showing a high contact angle and poor wettability (top) and low contact angle indicative of superior wetting (bottom)

Results in this chapter will show decreases in contact angle after specific surface treatments indicating increases in wettability and the surface energy of HIPS films. However, as increase in these properties cannot alone explain the changes observed in its adhesive response. In this work, the film acts as the adhesive rather than the substrate upon which a low-energy adhesive would spread. In addition, the surface energy of the polymer is highly dependent on its temperature, molecular weight, etc.[44, 45]. As the temperature of the thermoplastic approaches its melt temperature, the surface energy of the polymer will decrease linearly until it begins to flow [44-50]. As this reduction in surface tension takes place regardless of initial surface energy and it is the molten HIPS flowing as the adhesive, little, if any enhancement on bond strength can be explained solely by changes in physical adsorption due to an initial increase in surface energy. Other mechanisms of adhesion must be considered.

Though wettability is critical to enabling flow and thereby establishing contact area between adhesive and substrate during the adhesion process, it is a single part of a very complex mechanism. Chemical adhesion is another pathway by which phases interlock and is much stronger than physical adhesive forces. The energies of the chemical or primary bonds are on the order of 50-800KJ/mol compared to 0.1-50 KJ/mol for the secondary bonds formed during physisorption [51, 52]. Also known as chemisorption, the high bond energy in chemical adhesion is established as covalent and ionic bonds form between compatible molecular groups. In the case of polymers, these are often oxygenated functional groups; hydroxyl C-O, carbonyl C=O, and carboxyl COOH. Increased concentration of these functional groups on a polymer surface can be indicated by an increase in surface energy. An example of chemisorption is shown in Figure 3-3 as succinic acid bonds to the surface of alumina during a dehydration reaction. The carboxyl functional groups of the hydrocarbon have strong affinity for the hydroxyl groups of the aluminum oxide. As the groups near one another, they dehydrate through nucleophilic substitution, releasing an oxygen and two hydrogen atoms, in the form of water [53]. The newly formed ether bonds, O-C-O, are much stronger than the hydrogen bonding and Van der Waals forces that would have created adhesion in absence of the hydrocarbon's carboxyl functional groups.

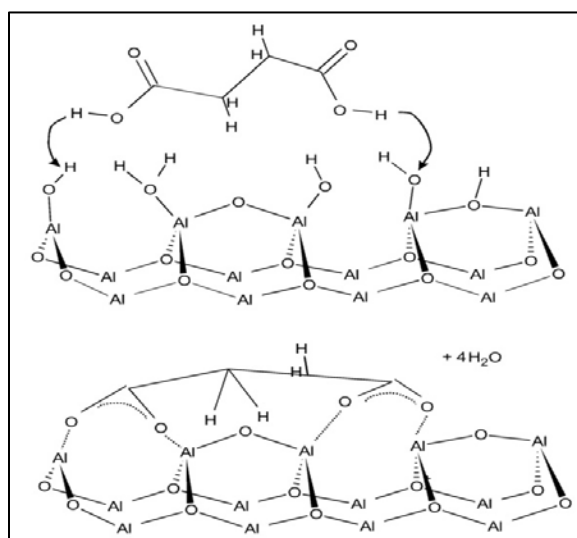


Figure 3-3. Chemisorption of a carboxylic acid compound on the surface of aluminum oxide through the consumption of hydroxyls on the oxide surface [54]

These two adhesion mechanisms, physisorption and chemisorption, will be of importance later in this section as they explain the reason for dramatic changes in the adhesion behavior of HIPS after surface treatment. While both will continue to play a role, the dominating mechanism will shift as the film morphology is altered.

Despite differences in the dominating forces of the aforementioned adhesive mechanisms, both rely on molecular proximity to initiate their bonding. One method of inhibiting bonding is to employ the use of a highly stable compound to create a barrier between compatible chemical species. Polytetrafluoroethylene (PTFE), known under the brand name Teflon, is a polymer chain composed solely of C-C and C-F bonds. As shown in Figure 3-4, the electronegativity of the C-F bond inhibits primary or secondary molecular interactions with other molecules. The low reactivity of PTFE makes it challenging to adhere it to the surfaces onto which it has been applied for its non-stick properties. Contact with PTFE coated surfaces often results in removal of some of the release agent causing contamination.

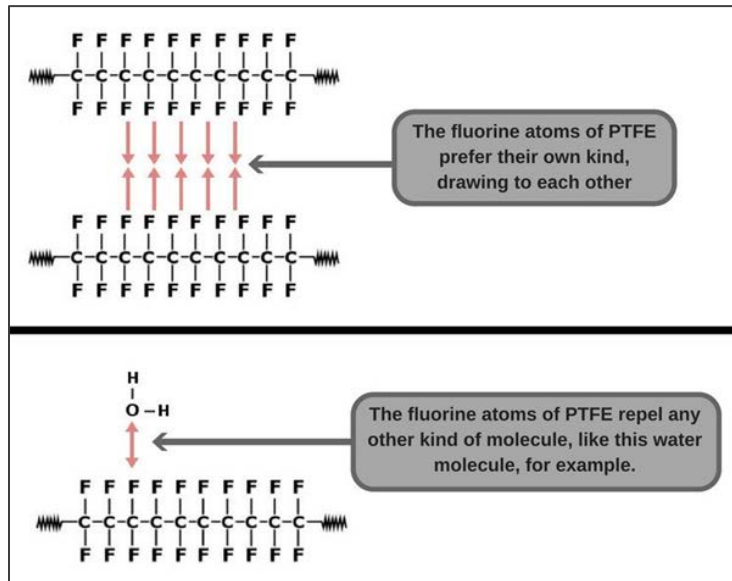


Figure 3-4. Molecular interactions with PTFE [55]

Although non-stick coatings like PTFE inhibit adhesion through interference rather than the out-competition of the surfactants in the previous chapter, and understanding of how both work is

critical for the preparation of the HIPS film surfaces for adhesion as both these materials must be removed.

Plasma surface treatment is one method of surface treatment which can be used to remove low molecular weight contaminants and will be discussed here in detail. Low-pressure plasma treatments use a variety of gasses to clean or otherwise modify surfaces for specific applications [56-60]. O_2 plasma treatment is particularly valuable for use on thermoplastics as it simultaneously removes surface contaminants, ablates, and chemically modifies the surface [61]. These three effects are all conducive to increased adhesion strength [62].

During low-pressure O_2 plasma treatment, a high-purity stream of oxygen is bled into a vacuum chamber containing the specimens to be treated. An electric field is created accelerating free electrons within the gas field forming an energized corona of plasma above the substrate's surface. Within this corona, diatomic oxygen is broken down into highly reactive oxygen radicals. As these charged plasma particles bombard the polymer surface, a chain of reactions takes place, breaking lower molecular weight bonds and forming new ones. A schematic of these surface reactions with the energized O_2 plasma is shown in Figure 3-5.

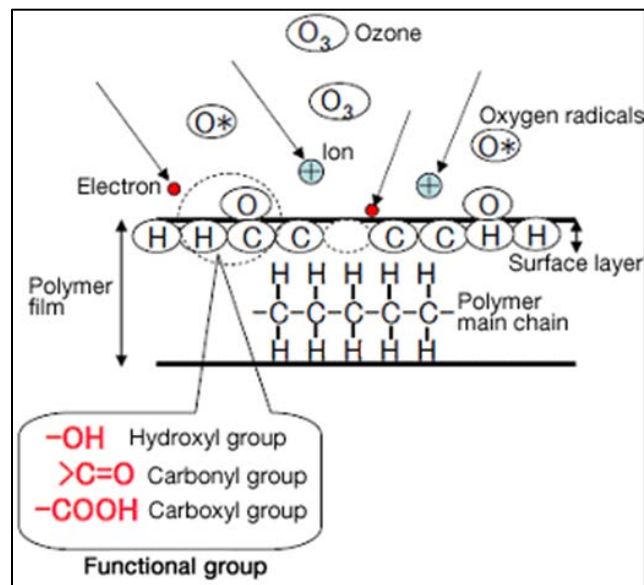


Figure 3-5. Molecular schematic for oxygen plasma treatment of a polymer film [63]

As the low molecular weight bonds are broken, they latch onto surrounding oxygen radicals forming CO₂ and H₂O which are continually evacuated through the vacuum system. This process not only removes loosely bound organic contaminants, but also ablates the surface, etching away the bulk polymer and creating additional roughness. The removal of this outer low molecular weight “skin” also adds to the stability of the surface offering layers for adhesive reaction with higher cohesive forces attaching them to the surrounding bulk. It has been observed that surface roughness of polystyrene during O₂ plasma treatment increases linearly with treatment time, with etch rates around 1nm/sec [64].

As the oxygen radicals strike the surface, many of them form covalent bonds with the hydrocarbon chains. A process known as functionalization, these covalently bonded oxygen groups open the chemically stable aromatic rings of the styrene and dramatically increase the chemical energy of the system [65]. An example chemical pathway of this reaction is shown in Figure 3-6.

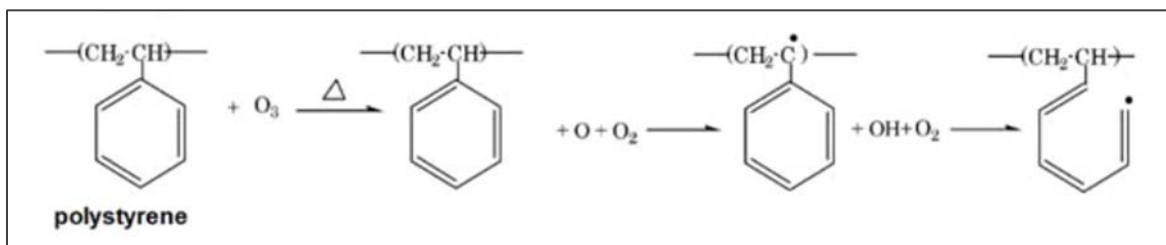


Figure 3-6. Pathway for oxygenation of the aromatic ring of styrene [66]

As oxygen radicals continue to interact with the surface, they can form bonds with carbons already containing oxygens forming secondary and tertiary functional groups. With each additional oxygen, the energy of the functional groups increases. Figure 3-7 is an XPS spectra of an oxygen functionalized polymer showing the shift in binding energy of hydroxyl, carbonyl, and carboxyl groups. All of these surface reactions are responsible for all three of the aforementioned effects of O₂ plasma treatment.

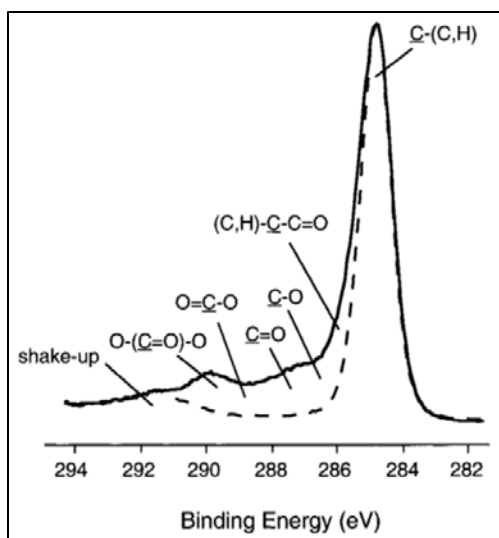


Figure 3-7. XPS spectra showing the peak contribution of different oxygenated functional groups deposited during O₂ Plasma treatment [67]

Oxygen plasma treatment is a highly effective multi-function surface treatment for polymers. Low-pressure oxygen plasma treatment simultaneously applies artifacts from multiple surface modifying mechanisms. While this is one of the inherent benefits of this treatment method, disseminating the effects of these changes to the surface, individually, on adhesion characteristics becomes difficult. It was not possible to completely access the contributions of these individual mechanisms within the scope of this work. Further experimentation is necessary to isolate the influences of cleaning, abrasion, and functionalization via plasma processes, separately.

3.2 Materials and Methods

The materials and methods for this chapter are broken into sections. The progression moves through the production of adhesive films, surface treatment of the films, analysis of film surface energies following treatment, and evaluation of the adhesive performance in lap-shear testing. All procedures outlined in this section will be continued throughout the remainder of this work unless noted otherwise.

3.2.1 Film Production

To produce adhesive films, HIPS was discharged from the dual-screw processing machine and allowed to coil and cool to ~10gram “pucks”, see Figure 3-8, left. The pucks were then loaded into a Caver press preheated to 150°C between two sheets of Airtech Release Ease 234 non-perforated peel-ply. Also added between the PTFE coated sheets are four washers of 0.75mm thickness, one at each corner. The platens were then closed at an even rate to 544kg and held for no less than 2 minutes. The films were removed from the press and placed between two 1cm thick steel sheets of 5kg mass to cool. After reaching room temperature, the films were removed from the peel ply, and bagged with a desiccant. The pressed films can be seen as removed from the press and as trimmed for use in lap-shear joints, Figure 3-8, center, left, and right, respectively.

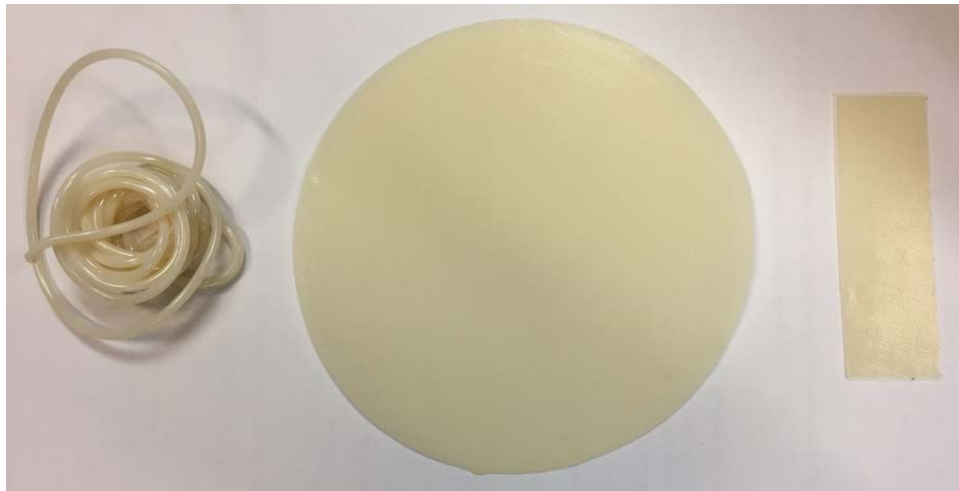


Figure 3-8. HIPS as extruded from DSM (left), after pressing (center), after being trimmed for lap joint assembly (right)

As a control, films were also produced without the use of peel-ply. These films were pressed between two mirror-polished steel platens to the same thickness. The platens and film were then removed and allowed to cool to room temperature. This was done to investigate the degree of contamination resulting from use of the PTFE coated peel-ply material.

3.2.2 Surface Treatment

Several surface treatments were attempted to alter the surface energy of the polymer films in effort to enhance their adhesive properties. All surface treatments utilized are recognized by industry as methods for the surface treatment of polystyrene based thermoplastic prior to adhesion as substrates. They are taken from ASTM and industry standard references including *Surface Preparation Techniques for Adhesive Bonding*, the *Handbook of Plastics Joining*, and *Joining of Plastics* [68-70].

3.2.2.1 Abrasion

Films to be abraded were cleaned with lab-grade isopropanol on each side to remove loose contaminants. The films were then placed in a Trino dry blasting cabinet loaded with new 120grit aluminum oxide blasting media. Operating at 0.5MPa, the films were abraded on each side until a uniform texture was obtained. The films were then sprayed with compressed air to loosen large particulates and washed three times with isopropanol in attempts to remove surface residue. The cleaned films were then bagged with desiccant.

3.2.2.2 Acid Etching

HIPS films were acid etched in a solution of 90%wt concentrated sulfuric acid and 10%/wt sodium dichromate anhydride. The solution was heated in an 890mL crystallizing dish under low stir to 100°C. The HIPS films were submerged in the acid solution for 2 minutes. After removing, the films were immediately rinsed with room temperature DI water for two minutes. Films were then dried using lint-free anti-static lab wipes and placed in a 45°C convection oven for 8 hours. The films were then bagged with desiccant.

3.2.2.3 Oxygen Plasma Treatment

Low-pressure oxygen plasma treatment was done in a Plasma Treat vacuum plasma treatment chamber. Films were placed directly on the electrode surface, four per shelf. The chamber was evacuated to 0.05Torr before starting a 0.26Torr bleed of 99.8% high-purity grade

oxygen. Samples were treated at 275W for times varying from 1sec to 15mins. The films were then turned and the reverse sides were treated for an equivalent time. After treatment, films were removed from the vacuum chamber and bagged with desiccant.

3.2.3 Surface Chemical Analysis

To document the changes in surface energy, contact angle measurements were taken using reverse osmosis (R.O.) water, ethylene glycol, and diiodomethane. 3 μ L drops of liquid were placed on the surface using a Gilmont GS-1200 micrometer syringe, one dedicated for each liquid. Exactly 15 seconds were taken to position and focus the drop before capturing a micrograph of the drop using the experimental setup shown in Figure 3-9.

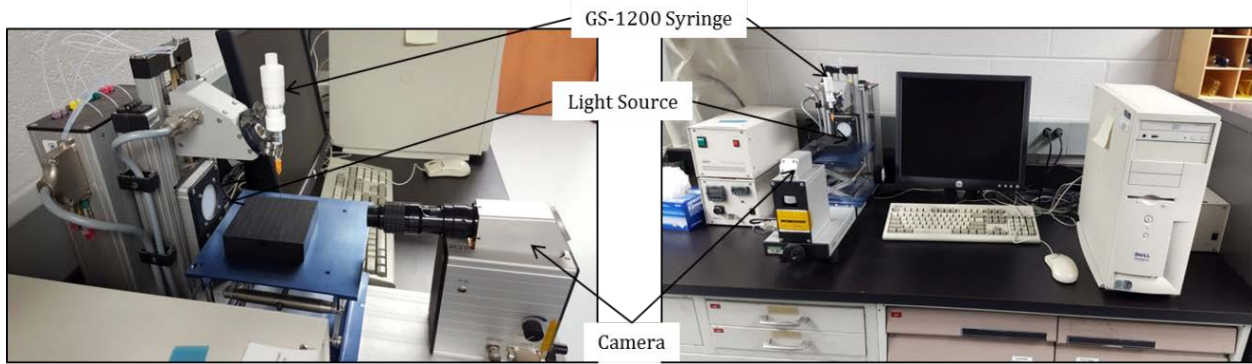


Figure 3-9. Digital contact angle goniometer setup

Once data points had been collected for all three liquids, the surface free energy was estimated using the Owens, Wendt, Rabel, and Kaelble (OWRK) method for the estimation of polar/non-polar contributions to polymer surface energies [71]. This model is outlined in Equations 1 and 2 where γ notates the contributions of the polar (P) and dispersive (D) components of the solid (S) and liquid (L) surface energies. The contact angle is denoted as θ .

$$\gamma_{SV} = \gamma_{SL} + \gamma_{LV} \cos \theta \quad (1)$$

$$\frac{\gamma_L(\cos \theta + 1)}{2\sqrt{\gamma_L^D}} = \sqrt{\gamma_S^P} \cdot \left(\frac{\sqrt{\gamma_L^P}}{\sqrt{\gamma_L^D}} \right) + \sqrt{\gamma_S^D} \quad (2)$$

The plotting of Equation 2 yields a linear line from which the slope and intercept can be derived. These values, m and b, respectively are used to solve for the polar and dispersive surface energy components using Equations 3 and 4.

$$m = \sqrt{\gamma_S^P} \rightarrow \gamma_S^P = \text{Polar Component} \quad (3)$$

$$b = \sqrt{\gamma_S^D} \rightarrow \gamma_S^D = \text{Dispersive Component} \quad (4)$$

After determining the dispersive and polar contributions, the total surface area for each film surface treatment was estimated using Equation 5, where the total free surface energy of the solid is the sum of the two components.

$$\gamma_S^P + \gamma_S^D = \text{Total Surface Energy} \quad (5)$$

3.2.4 Surface Spectroscopy and Imaging

Quantitative analysis of the surface chemistry of the films was done using x-ray photoelectron spectroscopy (XPS) using the methods from section 2.2.

Micrographs of film surfaces and features were collected using a JEOL 7500F ultra-high resolution scanning electron microscope (SEM). Film samples were cut to 1cm squares and mounted to aluminum studs before receiving a 30sec iridium coating to enhance conductivity. The microscope was operated at an accelerating voltage of 5keV and probe current of 20 μ A with a working distance of 4.5mm.

3.2.5 Adhesion Shear Strength

To measure and quantify the performance of the adhesive, lap-shear joints were assembled using thermally bonded films per ASTM D1002 in a “sandwich” configuration. To bond, substrates are loaded into a steel fixture with two 0.5mm wires across their surface 30mm off-center to maintain bondline thickness without interfering with the adhesion area of investigation. The films were trimmed to 25.4 x 85mm (Figure 3-8, right) and placed on the lower substrate (Figure 3-10)

before a second was applied above and compression was applied via toggle clamps. Strips of 3mm thick HDPE trimmed to a width of 26mm were placed between each substrate for alignment and to facilitate easy removal from the fixture after bonding.

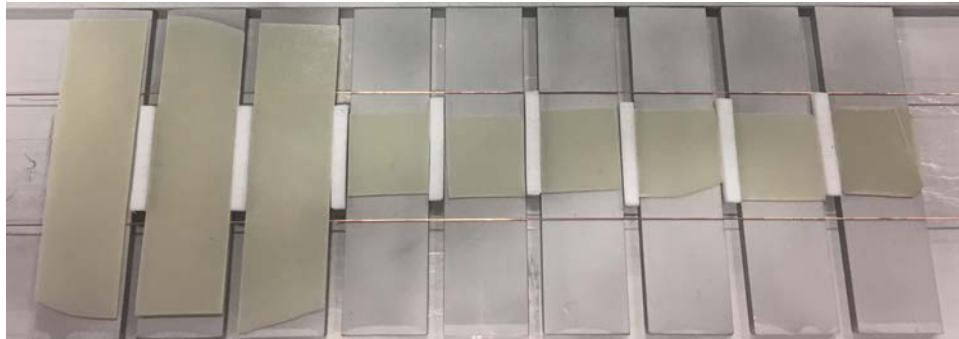


Figure 3-10. Lower substrates, bondline wire, and HIPS films before application of the upper substrate

The samples were loaded into a convection oven preheated to 225C. The bonding cycle was driven by substrate temperature and the joints were removed when the substrates were recorded to reach 175C via contact thermocouple. The fixtures with the joints were removed and allowed to cool to room temperature. Figure 3-11 shows 18 “sandwich” lap joints on the compression fixture after cooling.



Figure 3-11. Fixture for the manufacture of “sandwich” lap joints after thermal cycling

To obtain a standard 25.4 x 25.4mm bond area, a cut was made through the substrates on opposing sides 38.1 and 63.5mm measured from the same edge. The cut was made through the substrate and adhesive layer with minimal damage to the opposing substrate as seen in Figure 3-12. Production of lap joints of this geometry allowed for the simultaneous manufacture of large

sample sizes and significantly reduced scatter over alternative geometries initially investigated. The lap-shear strength of joints was determined within 24 hours of producing the joints using an MTS 810 load frame equipped with 15MPa hydraulic grips and a 50kN load cell. Reflective tape was placed on each side of the bond line to be measured via laser extensometer. Joints were pulled at a rate of 1mm/min to failure. The axial load and laser extensometer displacement were recorded. This test method was consistent for determining the lap-shear strength of all the thermoplastic films investigated throughout this work.

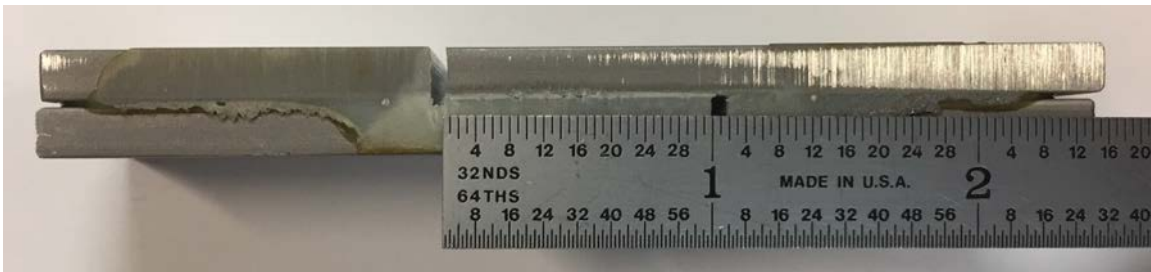


Figure 3-12. Profile of a bonded lap joint showing how substrate cuts create a 25x25mm bond area

3.3 Results and Discussion

Initial lap-shear joints assembled from pressed adhesive films showed poor adhesion characteristics. Lap-shear strengths of only 7.4MPa and 8.4MPa do not coordinate with the shear failure capacity of HIPS. This suggest there is purely interactional failure. Example load-displacement curves are presented in Figure 3-13 to illustrate the rapid slip failure of the bond. Joints assembled using both Al and CFRP showed interfacial slip failures at an average of 4.8kN and 5.4kN, respectively, when assembled with untreated films.

Analysis of the film surfaces following pressing with PTFE release films showed traces of contamination from the pressing process. A 3.59% atomic concentration of fluorine is shown on the full spectra of the PTFE pressed film in

Figure 3-14. However, lap joints assembled using films pressed both with and without release film showed equivalent failure loads and mechanisms, 4.75kN for mirror pressed and 4.77

for release pressed. It can be assumed the type of surface contaminant, either PTFE or fatty amine, is not the sole contributor to this interfacial failure because of the equivalency of these failure loads.

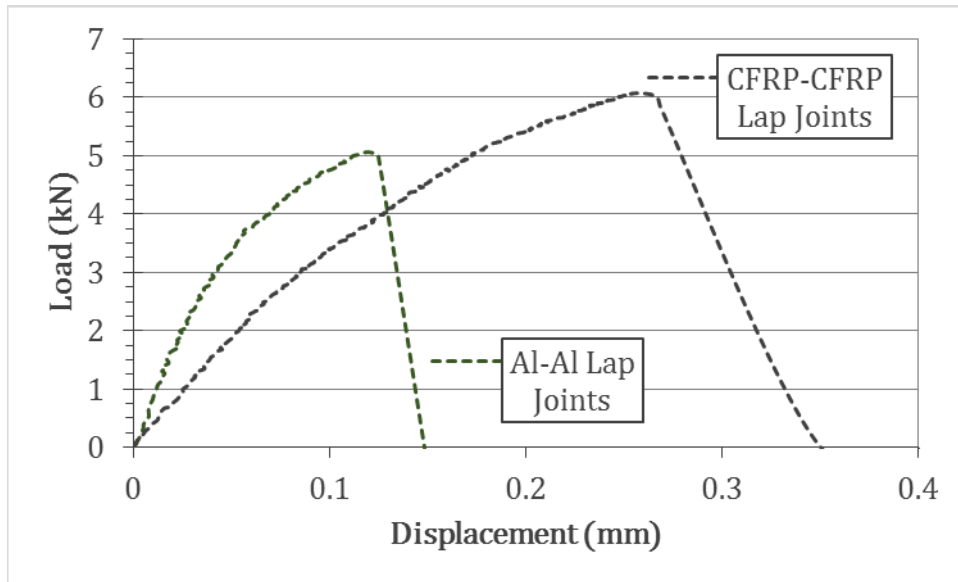


Figure 3-13. Load vs displacement of lap-shear joints with untreated HIPS films

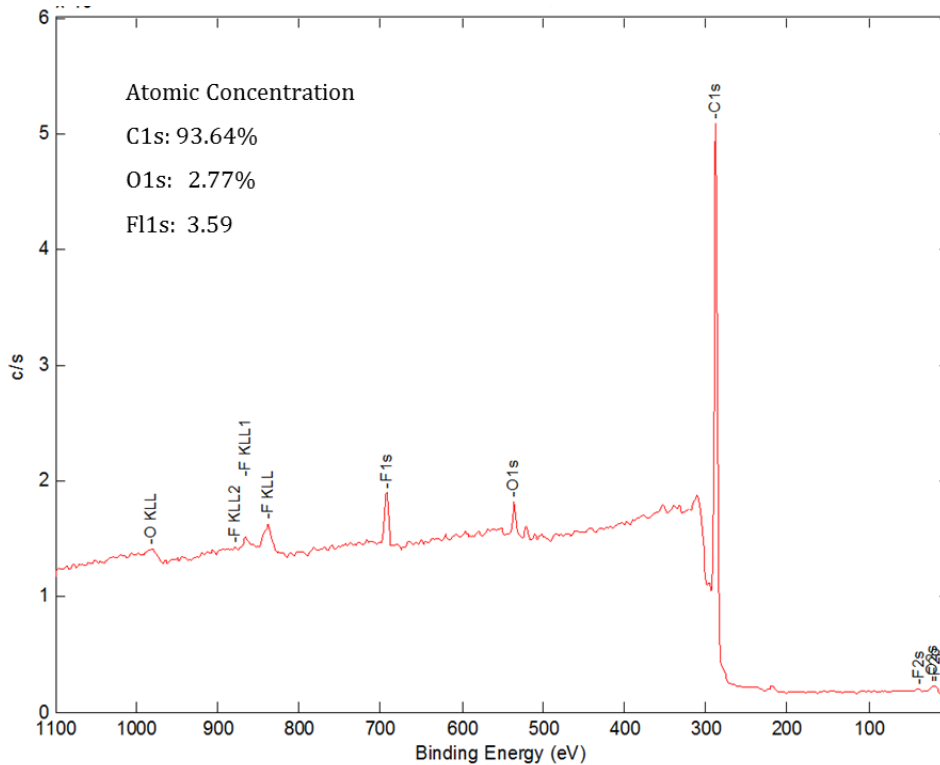


Figure 3-14. XPS full spectra for HIPS films released with PTFE coated peel-ply

Contact angles collected yielded information regarding changes to the energy of the film surfaces before and after surface treatments. An initial, qualitative assessment of the change in surface energy of HIPS films for different surface history is shown in Figure 3-15 using R.O. water only. The contact angle of the polymer surface as extruded with no additional processing was 89.4°, indicating a surface of poor wettability, $\approx 90^\circ$. It was found that pressing the extruded material between either mirrors or PTFE increased the contact angles of both to 95.2% and 97.1%, respectively. This was expected as the similarity of these surface energies is reflected in their nearly identical, $\Delta \approx 0.5\%$, lap-shear failure loads.

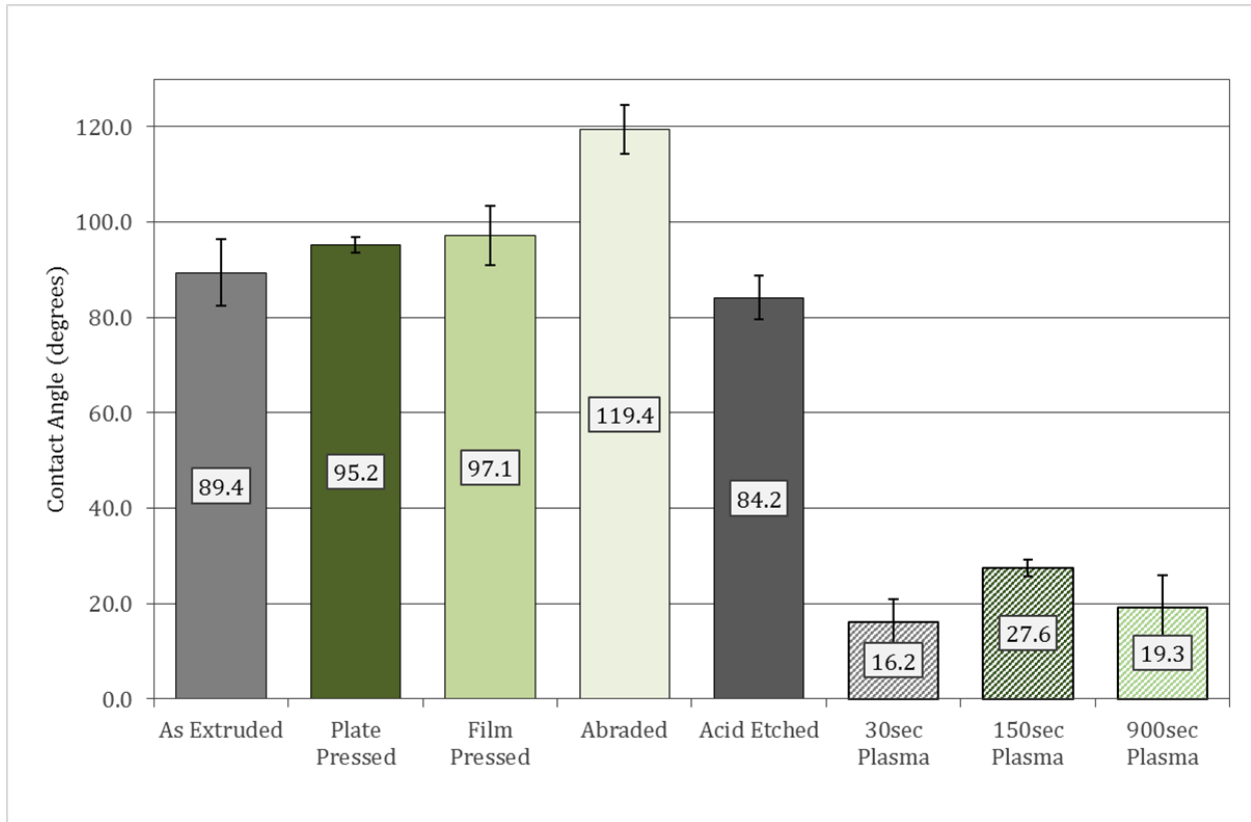


Figure 3-15. Contact angles of R.O. water on select HIPS film surfaces

This similarity in surface energy and failure loads may also be explained by topological surface effects. Both preparation methods press the HIPS pucks into films below their melt temperature. It is believed shaping the films under these conditions causes “sharkskin”, a surface

topography created by edge flow instabilities [72]. Figure 3-16 is a micrograph of sharkskin texturing on a pressed sample.

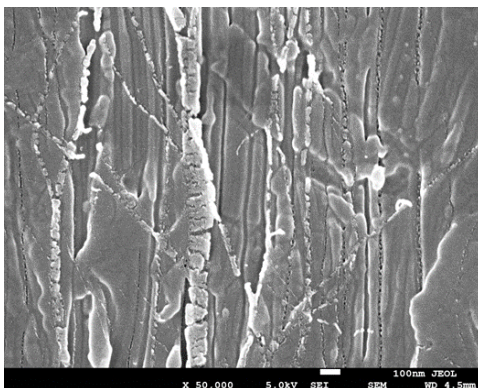


Figure 3-16. Micrograph of sharkskin on a pressed HIPS film sample at 50,000X

This low molecular weight outer layer is unstable and weakly bound to the bulk polymer. As adhesive forces act at the outer most layers, bonds made to this layer as easily pulled from the polymer, creating a weak secondary interface, lowering strength of adhesion. This boundary layer is later ablated via surface treatment, see Figure 3-24.

After characterization of the untreated polymers used for adhesion, the effects of surface treatment on contact angle was investigated to select a method most suitable for the modification of films for successful bonding. Data collected showed a significant increase in the contact angle, i.e. decrease in wettability, of the films which were abraded, 34%. This is likely due to residual alumina embedded in the surface film layer. In addition, creating a greater surface of an already non-wetting surface has been documented to further increase contact angles above 90° and decrease angles below 90° [52].

Improvements in contact angle, a decrease from that of the initial films, was observed in both acid etched and plasma treated films. Acid etching resulted in a 5.8% decrease in contact angle moving further into the wetting regime than the untreated films. The limited reduction in contact angle and additional risk from a lab safety aspect of utilizing a 100°C solution with a pH <0.1 for treatment were both taken into consideration for a go/no go decision on acid etching. It was

decided, within the scope of this work, the acid etching was unjustified and was not produced on a large enough scale for the assembled of joints. The small batch of acid etched film prepared for contact angle measurements was evaluated in the following XPS analysis and suggest investigation into polymer acid etching could be revisited in future work.

The O₂ plasma treatment showed the greatest modification of contact angle with an average decrease of 76% seen in the samples selected for Figure 3-15. Although longer treatment O₂ plasma treatment times were initially selected, it was found the treatment was effective even for short durations, less than 30 seconds. When comparison was made to literary documentation of contact angle vs treatment time, the trend observed was found to be in close agreement as seen in Figure 3-17. However, due to high data scatter at these low treatment times, durations of 150, and 900 seconds were chosen for further analysis.

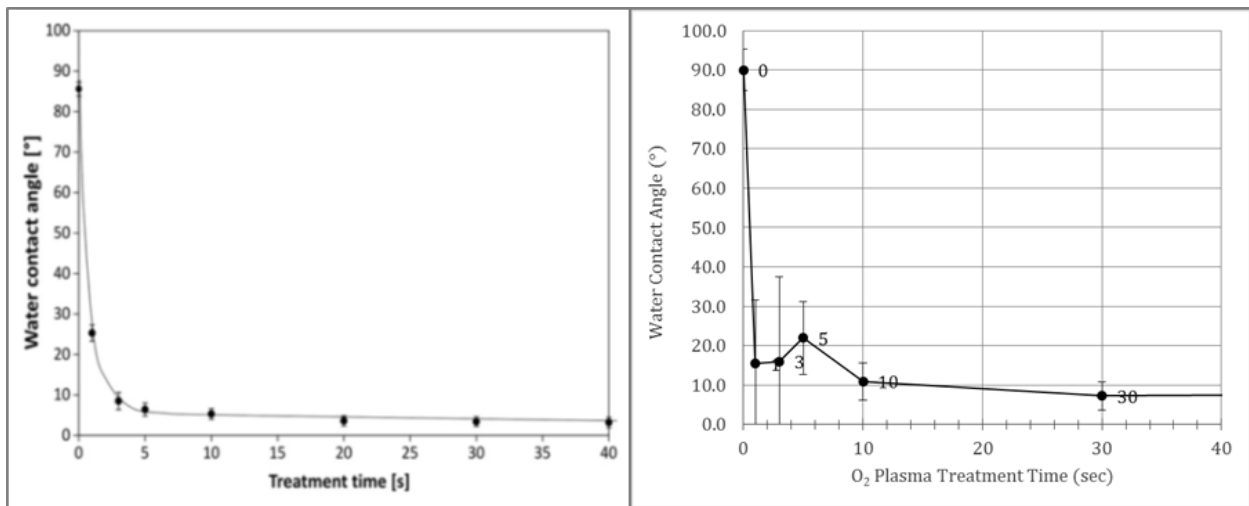


Figure 3-17. Contact angle of R.O. water on HIPS films versus O₂ plasma treatment time, reference values [73] (left) and observed values (right)

Joints were prepared with the plasma treated films and load-displacement plots of representative samples are shown in Figure 3-18. The lines in green are the response of lap-shear testing on aluminum substrates with plasma treated (solid) and untreated (dashed). The joints assembled with plasma treated films showed an average increase in peak load of 133% with a corresponding increase of 243% in displacement to ultimate failure. Also to note in Figure 3-18, is

the change in shape of the load-displacement profile. The addition of the long plastic deformation region between the peak load and ultimate failure is indicative of strain occurring within the adhesive. This plastic strain indicates load being transferred across the interfaces into the adhesive. The deformation of the polymer as it absorbs the transferred load leads to greater strength and longer strain-to-failure.

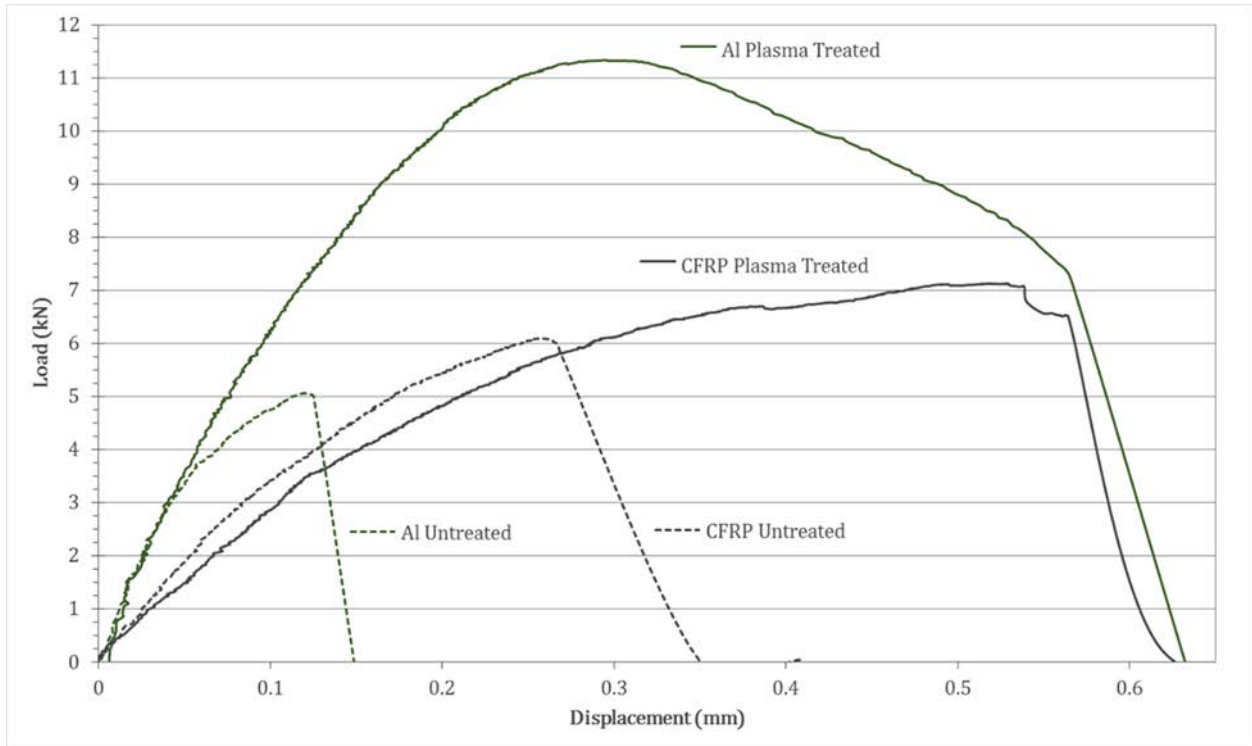


Figure 3-18. Load vs displacement curves for untreated and O₂ plasma treated films in joints with Al and CFRP substrates

The lines in black are the results of equivalent tests on samples prepared using CFRP substrates with the solid line being treated films and dashed, untreated. There again is an increase in maximum load and failure displacement of 28% and 143%, respectively. While not as substantial as the increases in the aluminum samples, it should be noted the failure in the plasma treated CFRP joints came as a result of delamination of the CFRP substrate. The adhesive bond had become stronger than the inter-laminar shear strength of the composite and thus the failure is not entirely indicative of the strength of the adhesive bond. Further testing on stronger laminate substrates is

required to draw complete conclusions of the adhesive bond strength of HIPS with epoxy based substrates.

An examination of the failure surface further confirms the change in failure mechanism from a purely interfacial failure to a more cohesive, mixed mode failure within the adhesive. As shown in Figure 3-19, there is a clear distinction in the amount of strain experienced by the plasma treated adhesive (right) and untreated (left). The strain is especially evident in the profile of the spherical inclusions within the adhesive layer. It is believed these are bubbles formed by vaporization of residual moisture in the polymer and water being released from surface reactions. It is also possible these bubbles are the result of outgassing from the substrates during curing. Future investigation is required to identify and eliminate these inclusions.

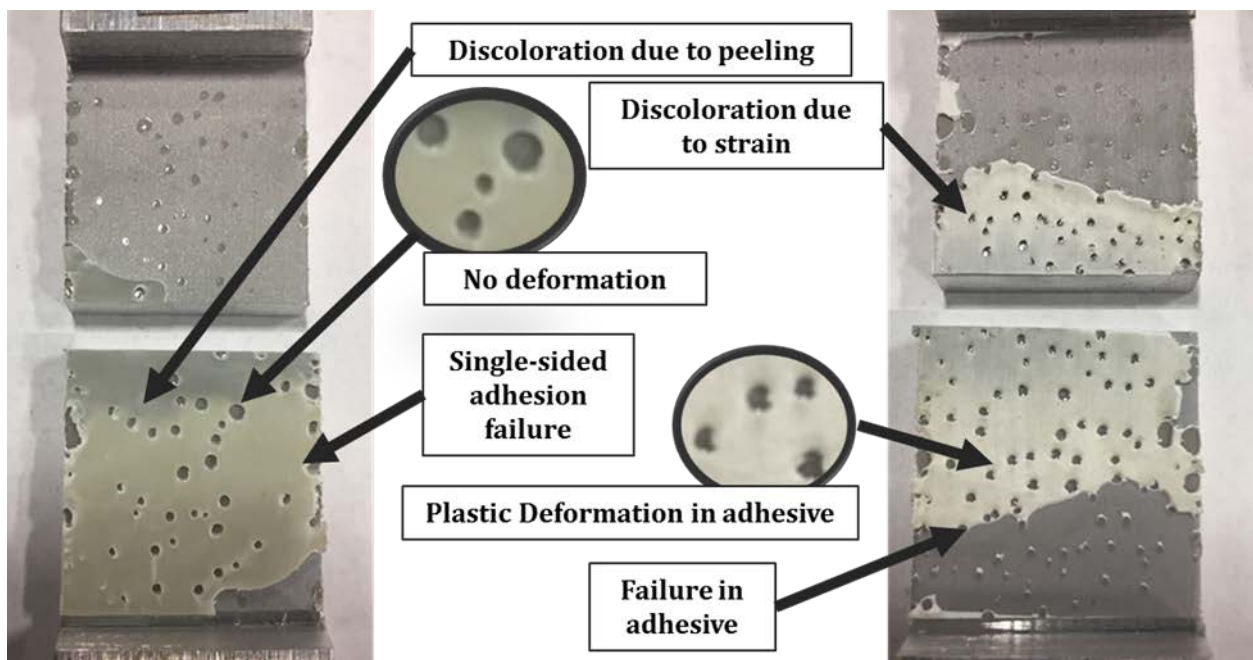


Figure 3-19. Comparison of lap joint fracture surfaces using untreated (left) and plasma treated (right) HIPS adhesive films

The successful transfer of load from the substrate to the adhesive is a critical accomplishment as it shows an increase in work of adhesion. Further strengthening of the joints can now be pursued by modifying the adhesive bulk and its cohesive properties [74].

As discussed in the introduction to this chapter, showing there is a decrease of contact angle is not enough to discern the changes to the film surface responsible for the increased work of adhesion. Total free surface energies for each treatment time were calculated and are shown in Figure 3-20. The film pressed and extruded sample surfaces match reference values of 38 dyn/cm² for neat polystyrene. All three O₂ plasma treatment times investigated showed ~50% increases in total surface energy, again in agreement with literature values of ~72 dyn/cm².

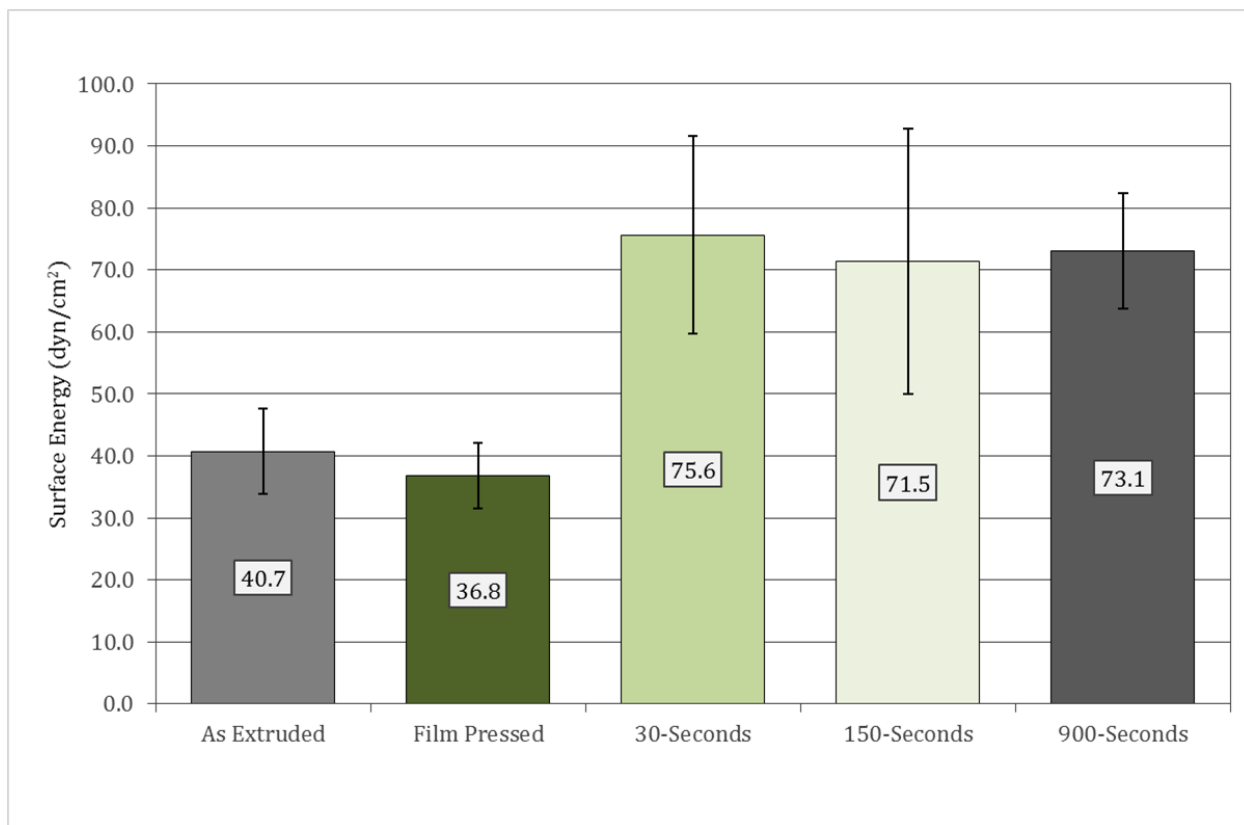


Figure 3-20. Estimations of the total surface energy for selected HIPS films

While there is a clear increase in total surface energy, analysis was made regarding the proportions of each energy component, dispersive and polar, in attempts to better understand the chemical and morphological changes taking place on the surface. It is shown that with O₂ plasma treatment, there is significant modification to the polar component of the surface energy with little change to the dispersive contribution. This trending is shown in Figure 3-21 and is consistent with oxygen functionalization taking place on the film surface during the plasma treatment. It was hoped

the data would show a “knee” in the polar surface energy change, indicating a saturation point where no additional oxygen would be deposited. This time could then be defined as an optimal treatment duration for the remainder of the study. While there is possible trending to suggest this at 30 seconds, there is too much scatter within the data to provide a conclusive answer. This was due to high variability in contact angle on some films, a result of inconsistencies in the surface texture and flatness. Further testing is required to fully confirm.

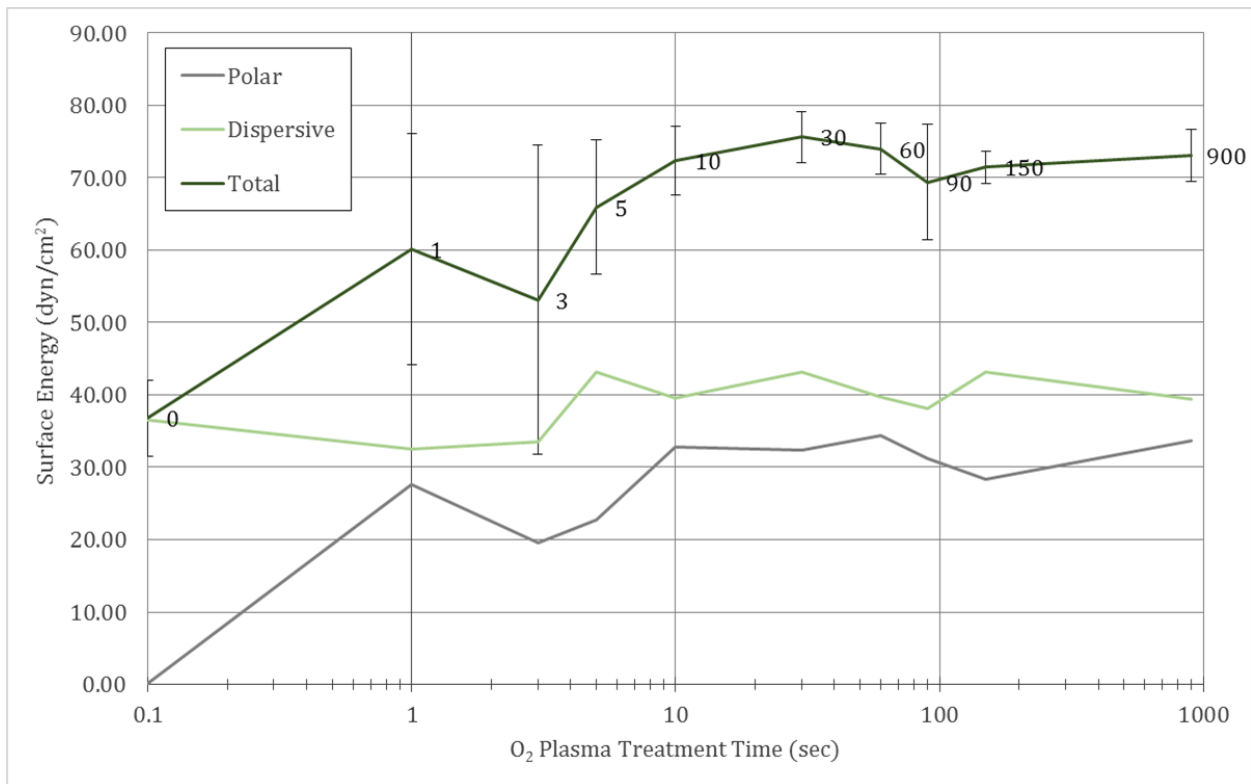


Figure 3-21. Relationship of polar, dispersive, and total surface energies observed for HIPS films versus plasma treatment times

Analysis was made into the effects of the plasma treatment on the topography of the surface using SEM analysis. A low magnification comparison of the film surfaces before and after 150sec treatment time is shown in Figure 3-22. The pattern on the polymer surface is an artifact of the texture of the release film. Note the subtle change to the finer variations on the film surface. These changes are easier to see at the higher magnification in Figure 3-23. These images were collected at 5,000x compared to the low-magnification images at 50x.

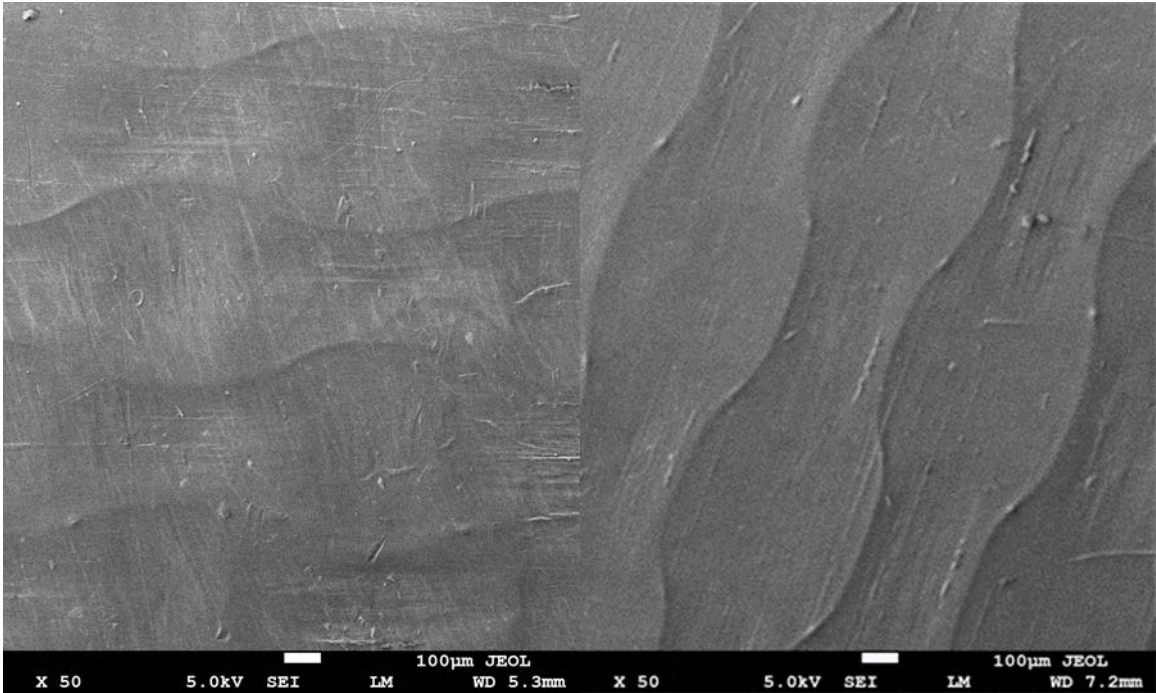


Figure 3-22. SEM micrograph at 50X of HIPS film pressed with PTFE release film before (left) and after (right) 150sec plasma treatment

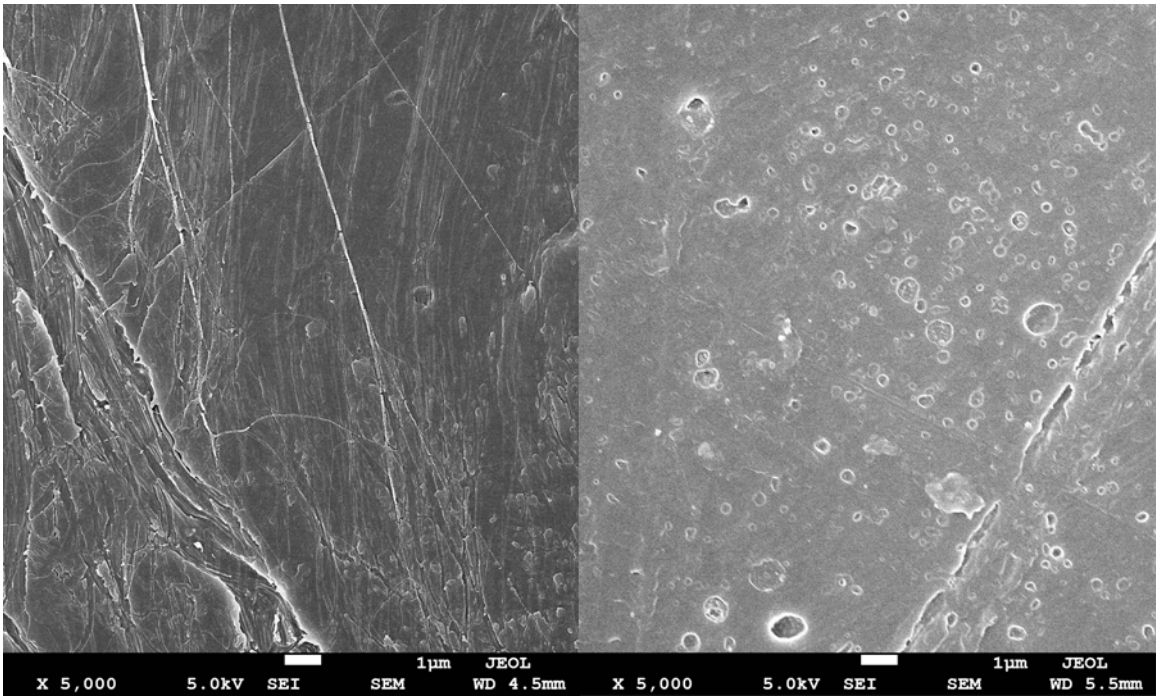


Figure 3-23. SEM micrograph at 5,000X of HIPS film pressed with PTFE release film before (left) and after (right) 150sec plasma treatment

On the left of Figure 3-23, the untreated sample is shown with the sharkskin and flow lines formed during the pressing process. After the 150sec plasma treatment, shown right, the flow lines are still visible while the cracked, laminar features of the sharkskin are gone. The low-weight monolayers have been removed exposing “fresh”, longer polystyrene chains. Note the small pitting which has occurred where acute inconsistencies in the morphology have resulted in localized removal of material. It is likely, these were surface particles of butadiene which were more rapidly ablated than the surrounding polystyrene.

Figure 3-24 shows the difference in film surface between 150sec (left) and 900sec (right). This image proves the time dependence on the amount of material removed with far more roughness seen on the 900sec sample. Future work would include micrographs or AMF analysis at more intervals to determine the time needed to remove the weak boundary layer.

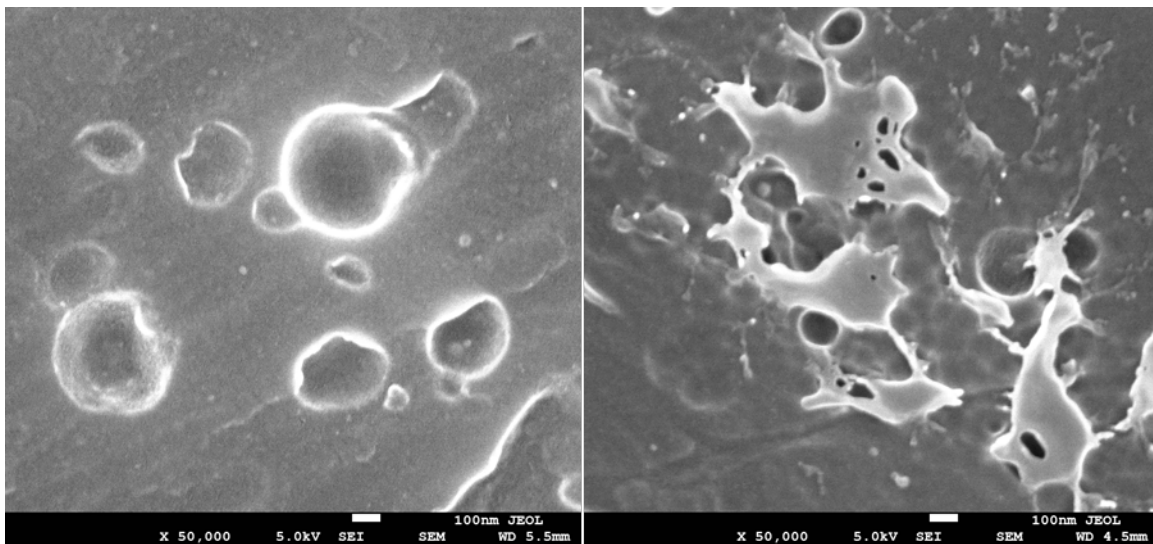


Figure 3-24. SEM micrograph at 50,000X of HIPS film after 150sec plasma treatment (left) and 900sec (right)

After plasma treatment it is shown there is considerable increase in surface oxygen content after both 150sec, Figure 3-25, and 900sec, Figure 3-26. The Os1 oxygen peak is seen at a binding energy of $\sim 532\text{eV}$ and its area is directly proportional to the amount of atomic oxygen present on the film's surface. The area of the Os1 peak is larger in the 900sec treated films at 19.7%, than for

the 150sec samples at 12.15%. This is a 9.38% increase over the untreated films and a 7.55% increase in the 750sec difference between the treatment times. This is as expected as the longer the treatment has allowed more oxygen to be functionalized onto the film surface. In addition to changes in oxygen content, neither the 150sec nor 900sec treatment spectra show any signs of fluorine or nitrogen content. This is an indication that any release agents or lubricants have been eliminated. The spectra again show indicate the presence of the calcium carbonate on the film surface with the Ca2s and Ca2p peaks found at 347eV and 440eV, respectively.

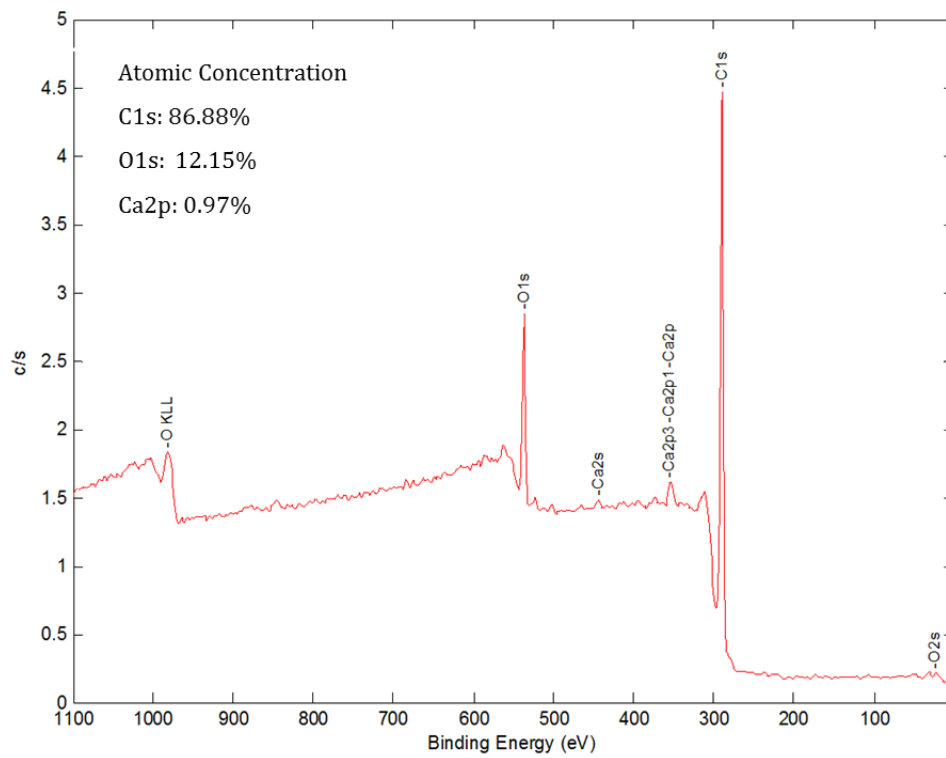


Figure 3-25. Full XPS spectra for 150sec plasma treated film

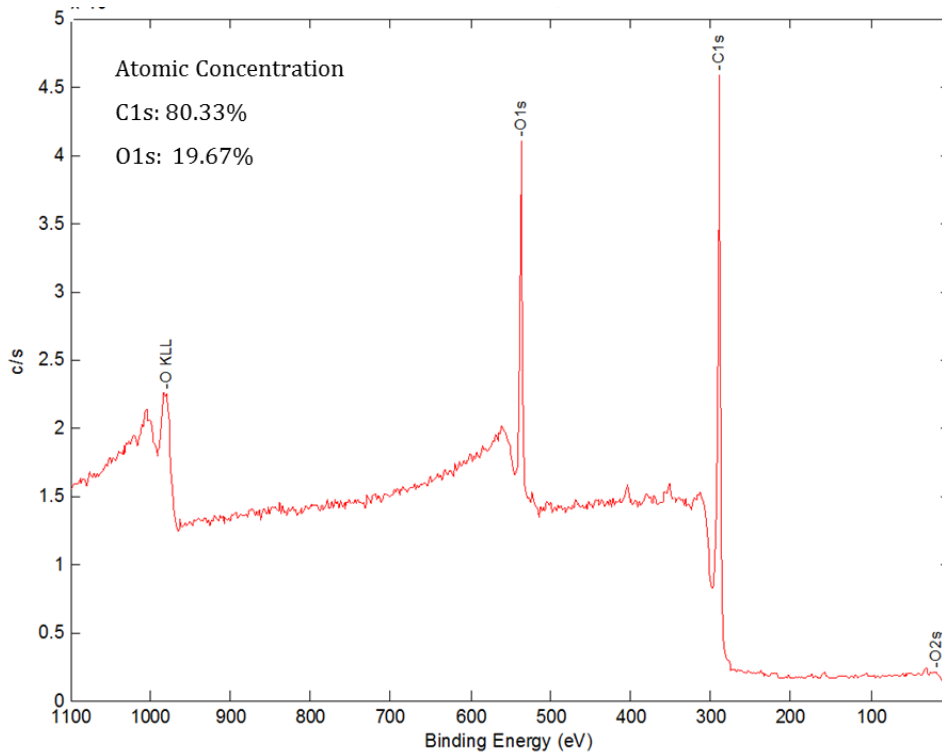


Figure 3-26. Full XPS spectra for 900sec plasma treated film

These peaks are much less pronounced on the 900sec spectra than the 150sec to the degree that they were not detected during digital post-processing through the spectra noise. While the calcium atomic concentration is expected to decrease as treatment times increase, calcium is heavier than the surrounding atomic species and will not be removed away as quickly as the polymer constituents.

The atomic concentration for all films analyzed via XPS is summarized in Table 3-1. The acid etched and 900sec plasma treated films showed the highest net oxidation at 19.2% and 19.7%. The 150sec plasma treated film showed a lower degree of oxygen functionalization at 12.15%. It should also be noted there was a large change in surface oxygen content in the extruded and film pressed HIPS, from 9.6 to 2.8%. This could be due to the driving off of surface adsorbed water during the pressing process as the film temperature is raised to 150°C. Further investigation is required to confirm.

Table 3-1. Summary of atomic concentrations for all films analyzed via XPS

Sample Name	Carbon	Nitrogen	Oxygen	Calcium	Flourine	Sulfur	Trace
Control	88.36%	0.83%	9.59%	1.23%			2.06%
Film Pressed	93.64%		2.77%		3.59%		3.59%
Acid Etched	79.71%		19.20%			1.09%	1.09%
Plasma 150sec	86.88%		12.15%	0.97%			0.97%
Plasma 900sec	80.33%		19.67%				

As the amount of oxygen functionalized onto the surface increases, it continues to bind in higher and higher order molecular configurations. As the reactivity of these molecular configurations differ, their relative concentrations on the film surface should affect the work of adhesion. Characterized by shifts in the amount of energy needed to release photoelectrons from the carbon on the sample surface, the relative concentrations of these functional groups can be determined by extrapolating the peaks of a narrow spectra around the Cs1 peak. Figure 3-27 shows the regional Cs1 scan for the 150sec treated plasma. Note the decreasing areas of the hydroxyl, carbonyl, and carboxyl functional group peaks moving as binding energy increases, right to left.

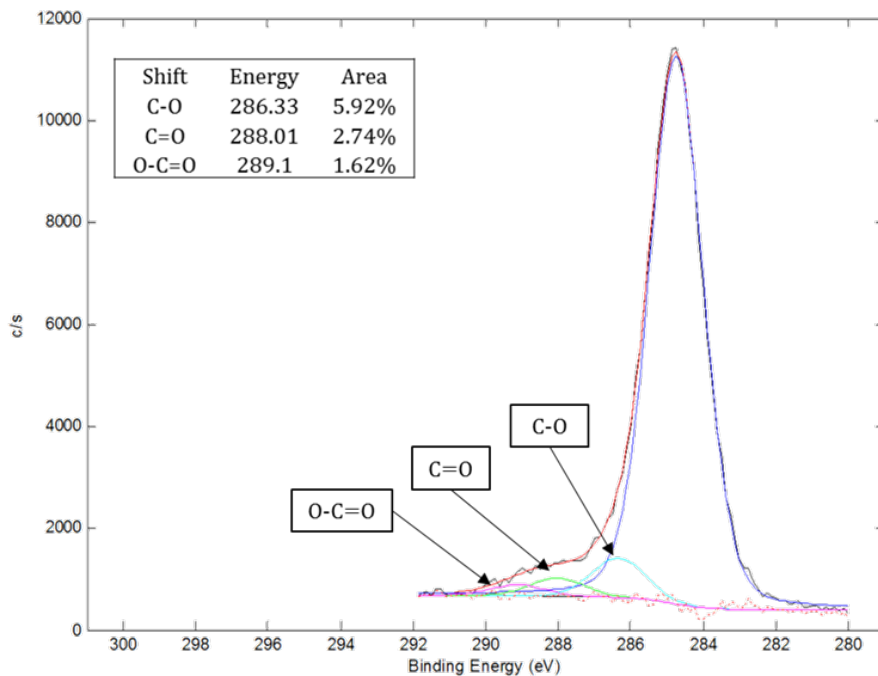


Figure 3-27. Cs1 regional scan for 150sec plasma treated films highlighting the resulting functional groups

When compared to the 150sec plasma treated sample, the increased level of oxygen functionalization on the 900sec film surface can be seen in the respective areas of the shifted CS1 peaks in Figure 3-28.

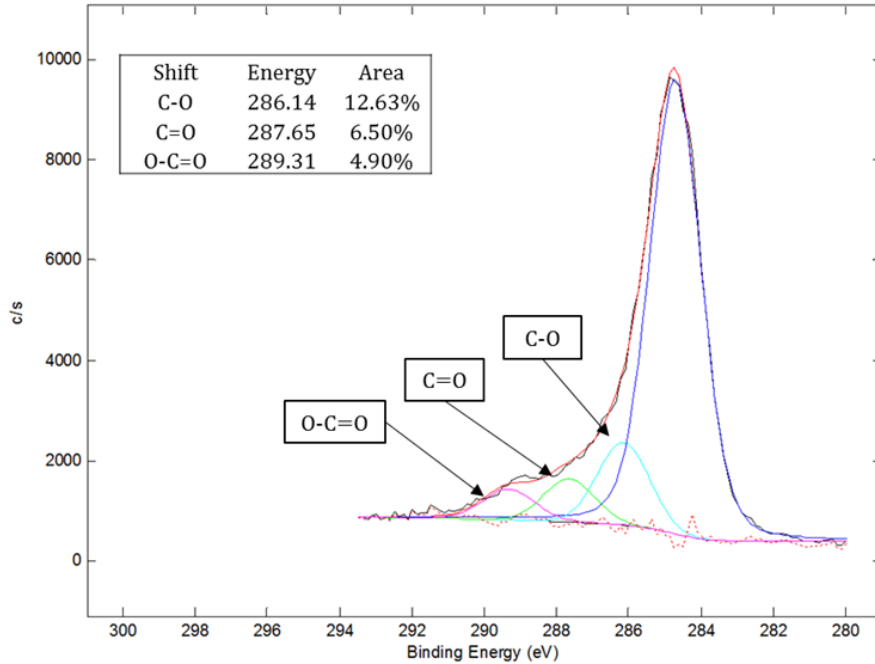


Figure 3-28. Cs1 regional scan for 900sec plasma treated films highlighting the resulting functional groups

The percent changes in the concentrations of the carbon shifts, and thereby the functional groups they support, is summarized in Figure 3-29. It is seen graphically that the acid treated and 900sec plasma treated films had the greatest degree of oxygen functionalization. When comparing how the lap-shear strength changes with the increasing total oxygen content and relative concentration of higher energy functional groups, there is no clear trend identified. While there is a slight increase in failure loads from 11.0kN for 150sec treated films and 11.2kN for 900sec films, these values lie within statistical equivalency of each other. Thus, no definite conclusion regarding “how much O₂ is enough” can be drawn from this study. By comparing relative adhesive strength with XPS spectra for a greater spread of plasma treatment times, a quantitative answer for this question will be explored in future works.

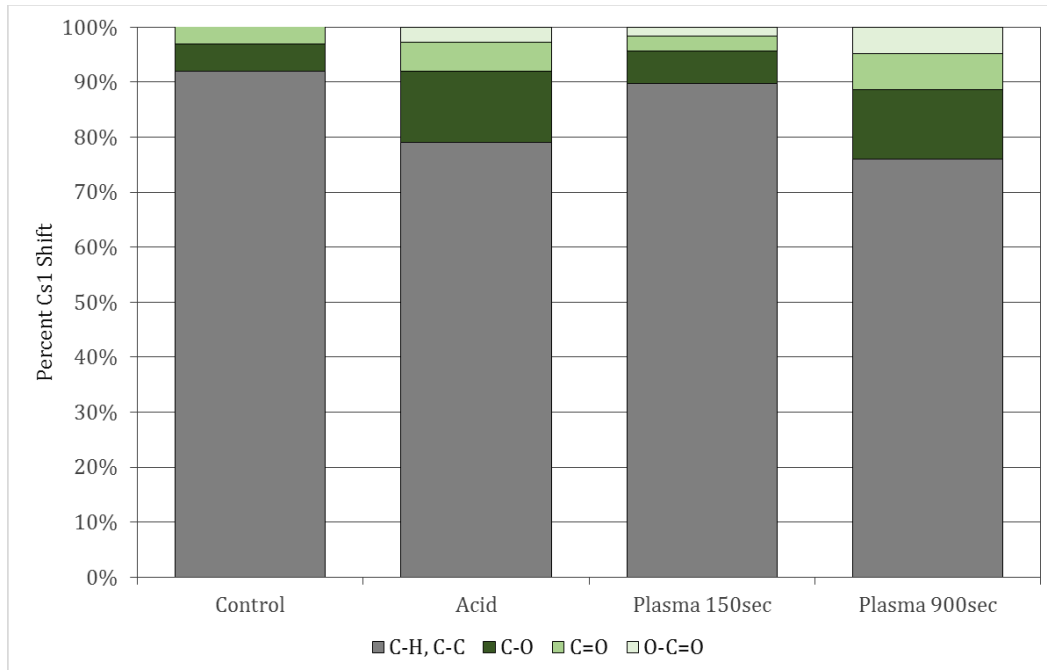


Figure 3-29. Graphical summary of C1s binding energies observed in HIPS films and their coordinating functional groups

3.4 Conclusion

It is shown that through surface treatment, adhesive films made from commercially available engineering thermoplastics can be modified to support structural failure loads with aluminum and CFRP substrates. Investigation of multiple surface treatments were made with detailed investigation of low-pressure O₂ plasma treatments being conducted after initial surface wettability comparisons. Plasma treated films showed significant changes in their adhesive strength. Changes observed in surface energy, specifically to polar surface energy contributions, before and after treatment were found to be direct indicators of adhesive strength in lap-shear testing of HIPS adhesive films. Changes in atomic composition of the film surfaces possibly responsible for these changes in energy were determined using XPS analysis. Summarized in Figure 3-30, surface treated films showed oxygen functionalization and no trace of the nitrogen and fluorine indicators of surface lubricates or release agents.

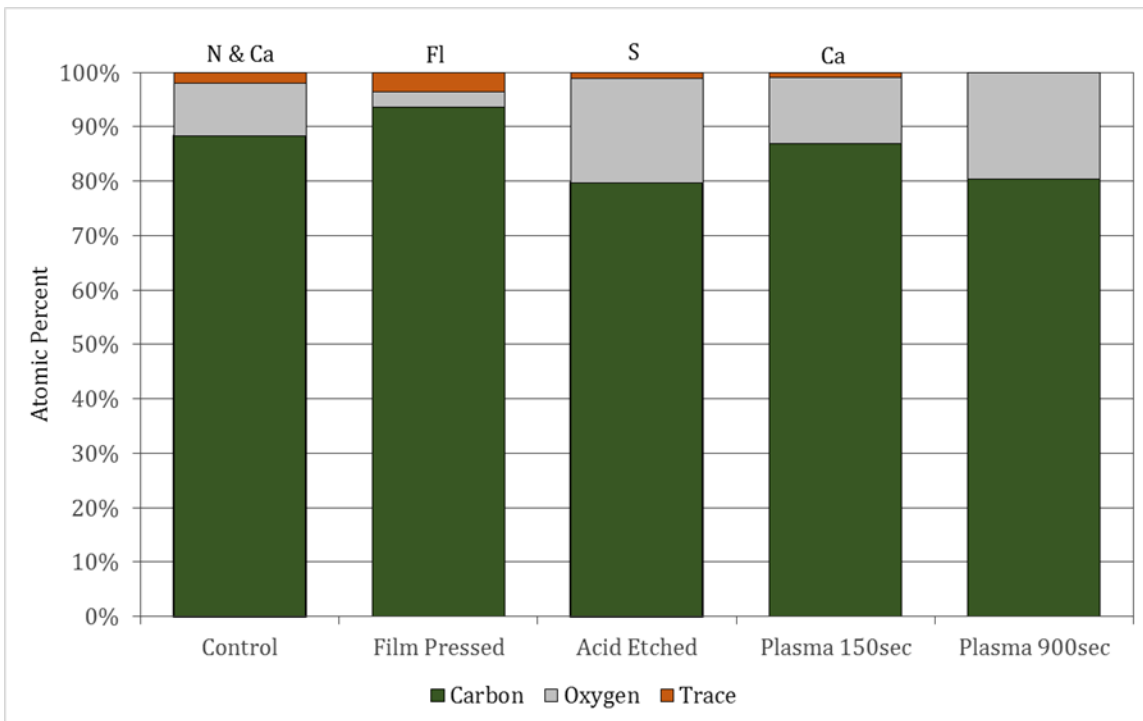


Figure 3-30. Graphical summary of atomic concentrations for all films analyzed via XPS

Low-pressure O₂ plasma treatment was shown to remove contaminants, functionalize the surface with oxygen, and add roughness, all of which contributes to the ability of surfaces to adhere. Changes to surface roughness were observed via SEM imaging including the elimination of unstable surface features on pressed films. A quantitative analysis of these changes in roughness should be made using scanning probe microscopy.

All treated film surfaces showed increased surface oxygen content of between 12.15% and 19.67%, the highest being seen in the 900sec plasma treatment. A correlation between oxygen functionalization and adhesive strength was not able to be made in this work. Acid treated films were not tested mechanically due to their low change in surface energy and high difficulty in manufacture. Results from XPS analysis suggests this method should be reconsidered in future work.

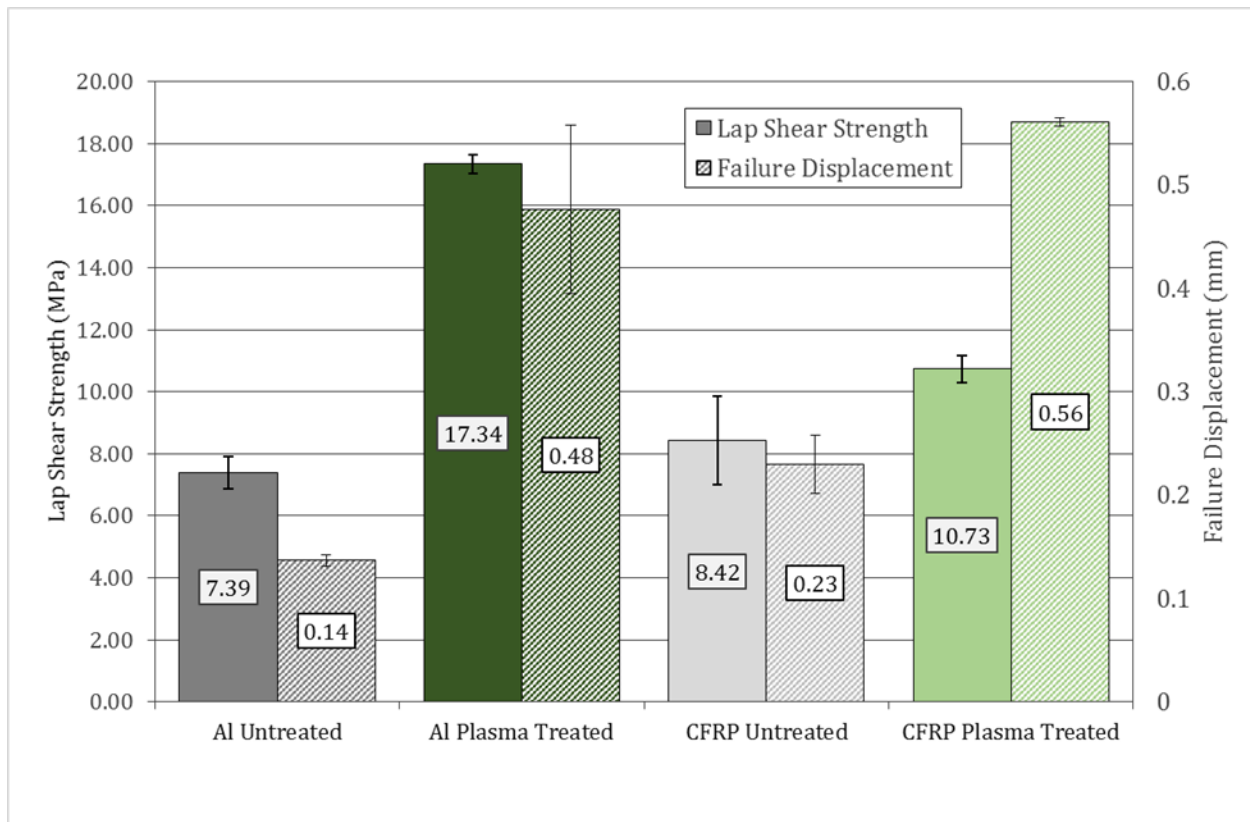


Figure 3-31. Summary of lap-shear strengths and failure displacements of untreated and plasma treated films on Al and CFRP substrates

As summarized in Figure 3-31, not only did O₂ plasma treatment result in increases to the yield loads of lap-shear joints, but also to the failure displacement. This is indicative of load transfer across the adhesive interphase and plastic deformation occurring within the adhesive. Analysis of adhesive fracture surfaces further supported this showing clear strain in the adhesive and a change from interfacial to mixed mode adhesives failures.

While all three effects of plasma treatment presented are known to increase the work of adhesion, it is not possible to identify which mechanism is predominately responsible for the 135% and 28% increase in lap-shear strength of aluminum and CFRP joints. It is believed the collected evidence suggests a clear change in dominating adhesive mechanism between the HIPS and substrates from physical to chemical bonding. Low-pressure O₂ plasma treatment is an effective method for allowing HIPS to adhere to aluminum and CFRP substrates as a melt activated adhesive.

Chapter 4: GnP and Composite Adhesive Films

4.1 Introduction

The integration of polymers with carbon-based nanoparticles is done in the pursuit of enhanced electrical, thermal, and mechanical properties [75-77]. From the standpoint of strictly mechanical strengthening, the material bulk is made stiffer by dispersing high-modulus particles in an otherwise amorphous solid. These stiff particles act as a skeleton within the polymer matrix creating a composite which combines the brittle strength of the graphene with the ease of manufacturing and compliance of the polymer. Functionalized GnP particles dispersed in thermoplastics, polyurethane in this example, at concentrations between 0.1 and 1%/wt have been shown to yield over 300% and 15% increases in tensile strength and strain-to-failure, respectively [78]. However, as the weight fraction continues to increase, the material becomes stiff yet also brittle. The increase in strength comes at the cost of strain-to-failure and impact resistance as the composite continues to behave more and more like the harder phase. A balance between the two must be made.

The objective for increasing fracture toughness is the pinning and slowing of crack growth through the material. Work incorporating GnP into thermoplastic polymers has shown increases in impact strength of 83% at 3%/wt loadings with 15 μ m diameter GnP in polypropylene indicating it can be done using high-modulus particles [79]. Enhancing fracture resistance with stiff particles is highly dependent on particle morphology and the degree adhesion between the particle and the surrounding matrix. Introducing particles which are too large and poorly bound to the matrix creates “weak links” for cracks to easily jump between, lowering impact resistance. However, by combining low and high modulus phases, it is possible to capitalize on increases in stiffness while mitigating losses in fracture toughness caused by the introduction of these interfaces.

Studies have shown that combining the GnP particles with carbonyl terminated butadiene acrylonitrile (CTBN) has mitigated the brittle behavior that can accompany integration of a stiff reinforcement with large surface area combining an over 100% increase in fracture toughness while maintaining nearly equivalent tensile and flexural moduli [80]. Attempts to achieve similar results was a motivating factor for the use of a rubber-toughened base polymer for this work with GnP. The integration of GnP into the polymer is done in this work via mechanical melt blending, a well-documented method for dispersion of carbon-based nanoparticles into similar thermoplastic polymer systems [81-83]. An addendum to the study on surface treatment featured in this work, these results are shown to supplement the validity of these materials as toughened thermoplastic adhesives. This work will be expanded on and further advanced in future research.

4.2 Materials and Methods

The GnP used in this work was obtained from XG Sciences in Lansing, MI. Two grades are utilized of differing morphologies, M25 and C750. Grade M25 nanoplatelets have an average particle diameter of 25 μ m and average surface area 135m²/g, left of Figure 4-1. The C750 is graded by surface area has an average area of 750m²/g with average particle diameters of <2 μ m, seen right in Figure 4-1.

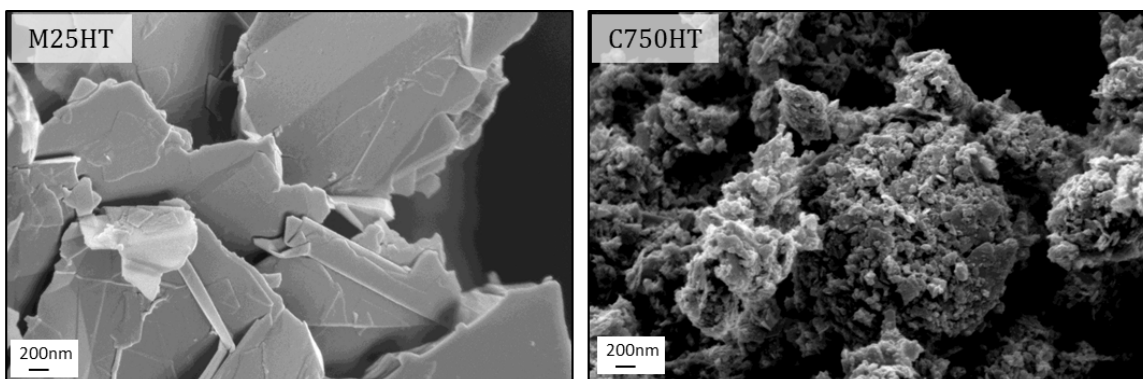


Figure 4-1. Morphology of M25 (left) and C750 (right) GnP in SEM micrographs

Before mechanically dispersing the GnP into the HIPS polymer, the GnP was heat treated to remove residual acids from the exfoliation process. Drying was done in open beaker at 100°C for 12hrs under convection before cooling and storing in an air-tight container. The dried GnP was compounded into the HIPS via DSM micro extruder consistent with the methods outlined in section 2.2. HIPS/GnP composites with absolute concentrations of 7.5% by weight were prepared with varying concentrations of M25 and C750. For the remainder of this paper, these concentrations will be identified with the notation C750:M25. For example, a 7.5%wt HIPS/GnP composite containing 25% C750 and 75% M25 would be identified as 25:75. The manufacture and testing of mechanical samples, films, and adhesive joints were completed in consistency with the methods outlined in sections 2.2 and 3.2.

4.3 Results and Discussion

The dispersion and morphology of the GnP within the HIPS polymer was evaluated in fracture surfaces via SEM. Micrographs of HIPS/GnP composites of varying weight concentrations are compiled in Figure 4-2 with increasing magnification left to right (a-c) and C750:M25 concentration moving from 0:100 to 100:00, top to bottom. The neat polymer is shown topmost for comparison. White arrows are used to indicate extrusions or pull-outs of M25 sheets and green arrows identify aggregates of C750. Row 0:100 (7.5% pure M25 GnP) of Figure 4-2 shows a high degree of surface roughness from the interlacing of GnP particles across the fracture plane. Image c of this row shows stacks of M25 that have agglomerated due to the strong desire of the M25 to oriented along compliments to its low-energy basal planes. Image 75:25-a shows a clear hole where a single M25 sheet was pulled from the surface during fracture. These features are consistent in all HIPS GnP composites containing the M25 morphology. A large pull-out feature can be seen in 75:25, the lowest M25 concentration utilized in this study.

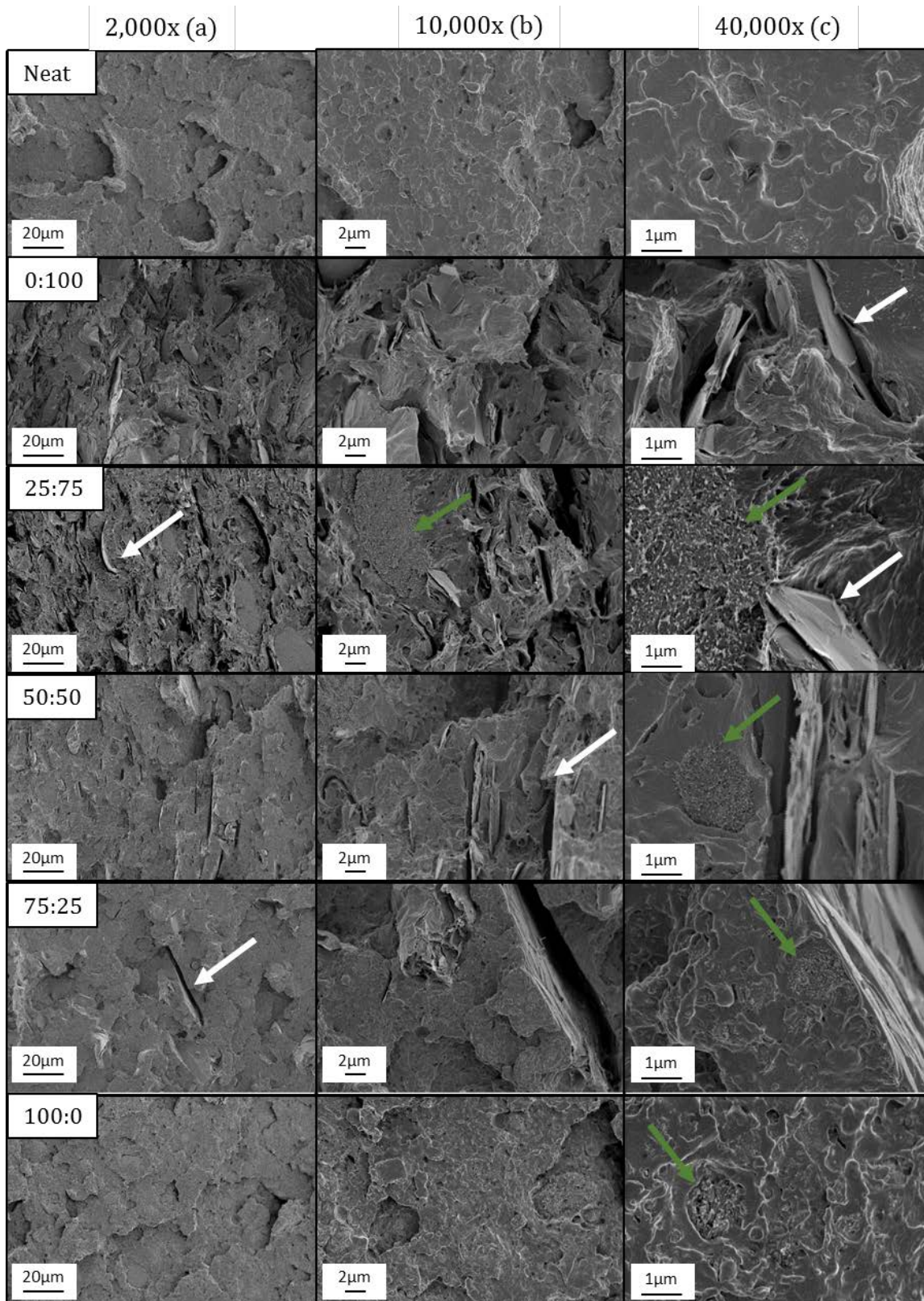


Figure 4-2. Micrographs of HIPS fracture surface with changing C750:M25 GnP concentration top to bottom and increasing magnification left to right.

The C750 particles are much smaller than the M25 sheets and more densely aggregated due to their much greater specific surface area. Image c of row 50:50 shows a C750 aggregate next to an on-plane view of an M25 sheet illustrating the difference in shape and size of the two particle types. As the morphology of the C750 is much less planar, its effect at the fracture is negligible when compared to that of the M25. The row of Neat micrographs and 100:0 (7.5% pure C750) are nearly indistinguishable compared to the considerable change in roughness caused by the introduction of M25.

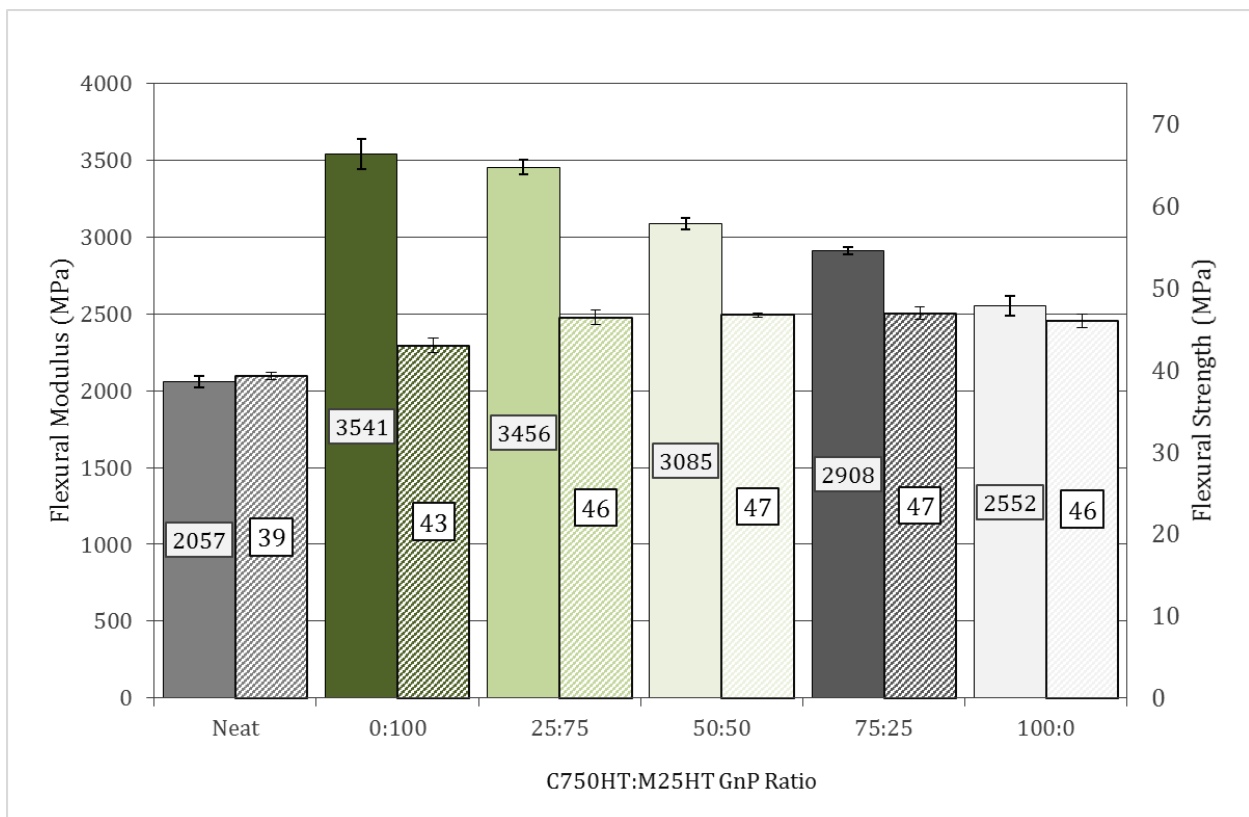


Figure 4-3. Effects of GnP loading and morphology on the flexural modulus and strength of HIPS

A graphical summary of the effects of variation in the relative concentrations of GnP morphology on the flexural properties of HIPS is shown in Figure 4-3. The composite flexural modulus was shown to be highest with 100% relative M25 content at 72% greater than the neat polymer. As the relative M25 concentration decreases, the gain in modulus decreases linearly as well to its minimum at 0% M25 concentration, 100% C750. While there is an increase in modulus in

the 7.5% pure C750 composite of 25%, the trending shows increases in modulus to be much more directly associated with M25 content. Due to the morphology of the M25 compared to the C750, this correlation is as expected. The increase in flexural strength of the composite HIPS is around 10% with at 7.5% absolute weight loading, regardless of morphology. The flexural strength of the composite HIPS is far less dependent on the relative concentrations of the GnP morphologies and varies only 7% across the entire concentration spectrum compared to 39% for the flexural modulus. This is indicative of a large change in stiffness of the material with limited change in the rupture strength of the material. This suggests weak adhesion to the polymer matrix is the ultimate failure mechanism for both particle morphologies.

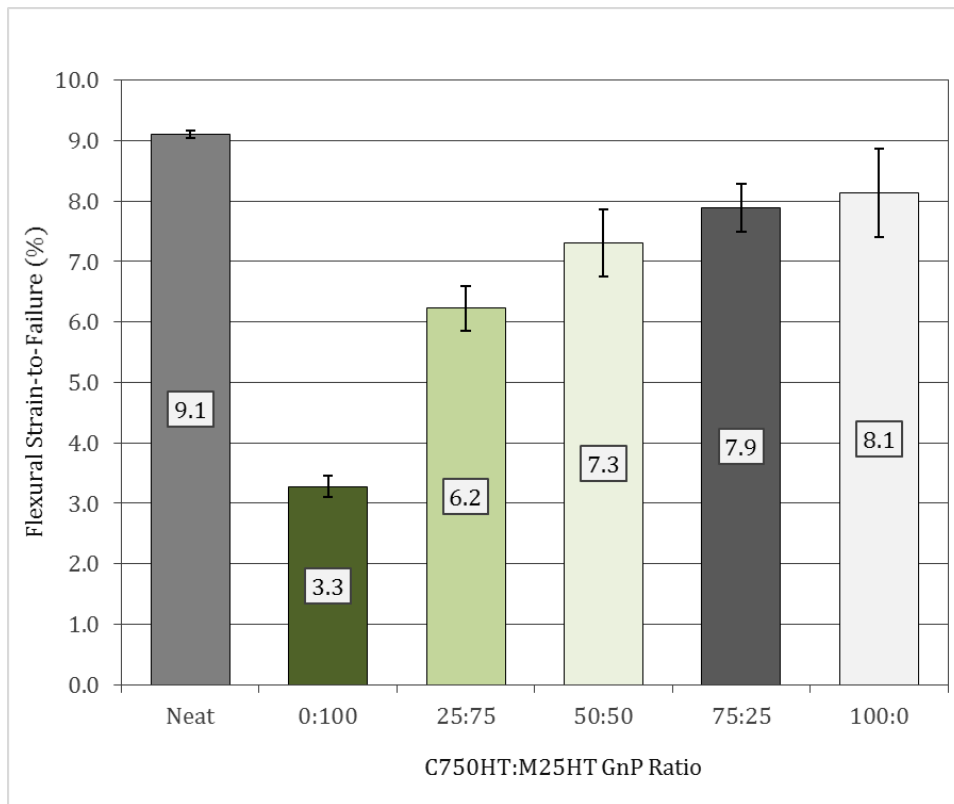


Figure 4-4. Effects of GnP loading and morphology on the flexural strain-to-failure of HIPS

The results of flexural strain-to-failure experiments are shown in Figure 4-4. The change in stiffness of the material caused by M25 content is again reflected here in a 175% loss in flexural strain-to-failure. There is a much less dramatic loss in strain-to-failure with pure C750 loading at

13%. There is a near linear correlation between the two extremes as the morphology fraction shifts. This data inversely reflects the changes in the flexural modulus as the stiffer composite blends are able to yield less before ultimate failure.

Figure 4-5 summarizes the tensile data for the HIPS composites and shows similar trends to those displayed by the material in flex. The greatest increase in tensile modulus is again with a 100% relative M25 fraction with a 76% increase over the neat polymer. However, there is a sharp decrease in this gain in the 25:75 blended composite suggesting that the addition C750 GnP negates the gains achieved in flexural modulus with the M25. This theory is further affirmed as while 22% higher than the neat polymer, there is only a 254MPa (8%) deviation across all composite blends containing C750. There is no statistically significant change in the tensile strength of any composite blends, again, suggesting the yield strength is unaffected and the failure mechanism is independent of particle morphology.

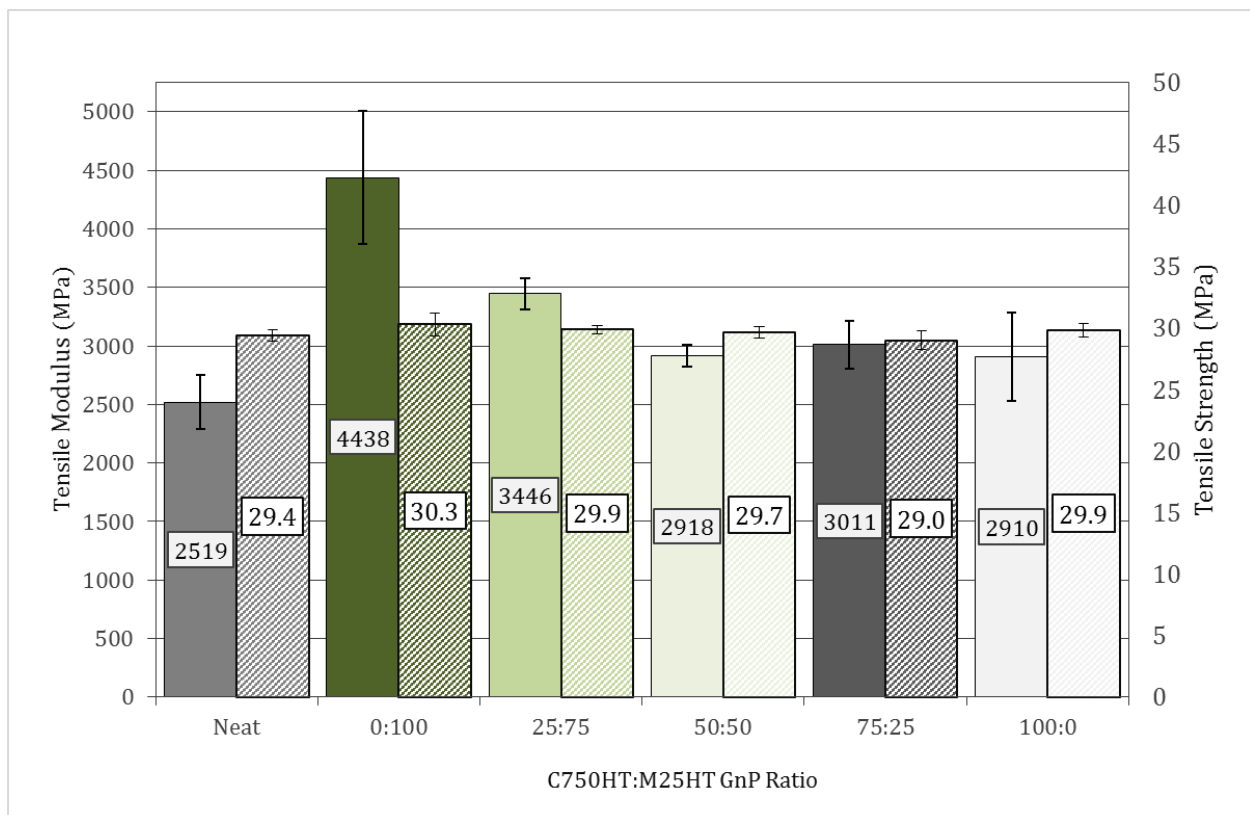


Figure 4-5. Effects of GnP loading and morphology on the tensile modulus and strength of HIPS

The strain-at-failure properties of the composite HIPS, shown in Figure 4-6, display no statistically equivalent change in the % strain at which the material enters plastic deformation across all GnP blends. This suggests that despite an increase in tensile stiffness, the yielding of the material is still completely strain driven. One could argue that this again indicates there is poor adhesion between the GnP particles and the surrounding matrix. As the strain of the polymer increases, it de-bonds from the weakly bound particles and yields around them. Thus, removing the effect of the GnP from having any influence on the net strain-at-yield. One observable trend is a significant increase in data scatter across the composite HIPS with the highest occurrence for the pure C750 fraction. Suspecting the ability of the HIPS to yield is now dependent on releasing from the surface of the GnP, the effect of dispersion and the resulting GnP surface area in contact with the polymer should play a significant role in altering the mechanical properties. However, as this adhesion appears to be weak, its net contribution, is shown to be zero within this sample base.

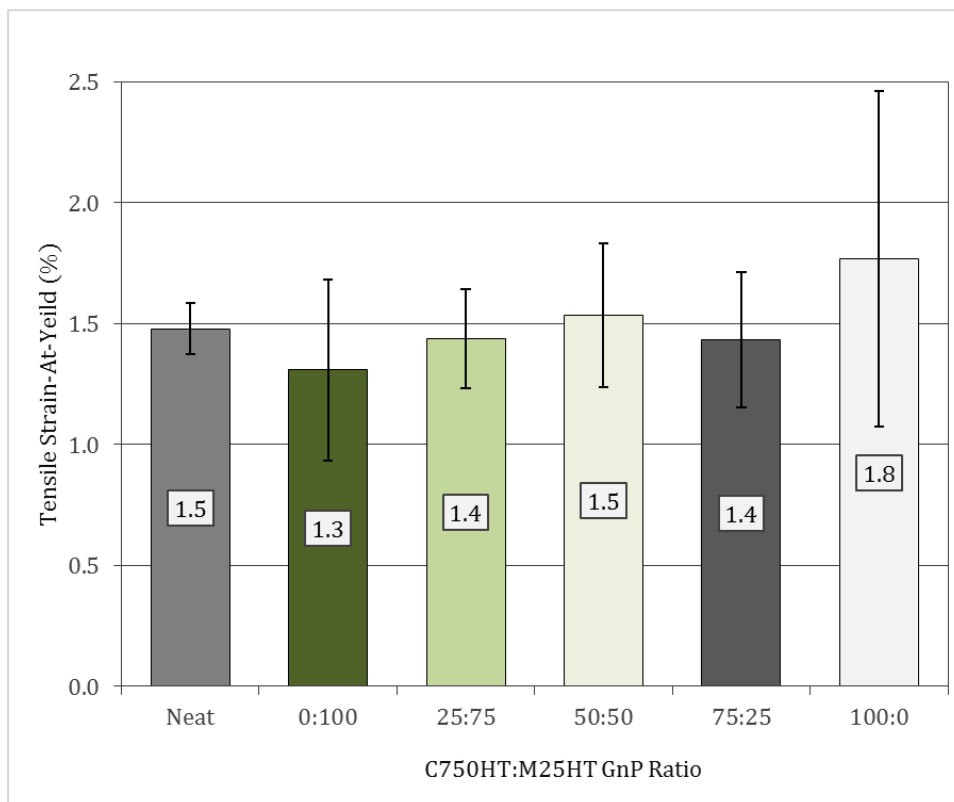


Figure 4-6. Effects of GnP loading and morphology on the flexural strain-at yield of HIPS

The notched impact results collected in this study further support the theory that the GnP is both poorly dispersed and weakly bound to the surrounding matrix. Figure 4-7 shows that 7.5% weight loading of GnP of any morphology is detrimental to the impact resistance of the material. Using un-functionalized and only mechanically dispersed GnP, there is an average loss of 72% in impact resistance with 12% deviation across all GnP morphology ratios. When reinforcing phases are weakly bound to the surrounding matrix, rather than inhibiting crack propagation, they provide slip-planes for the crack to move along with little interference. This effect is exaggerated with the M25 morphology as the agglomerations of the flat sheets are able to slide between one another in addition to at their interface with the polymer. The loss in impact resistance is shown to linearly decrease with decreasing weight fractions of M25 from 76% to 68%.

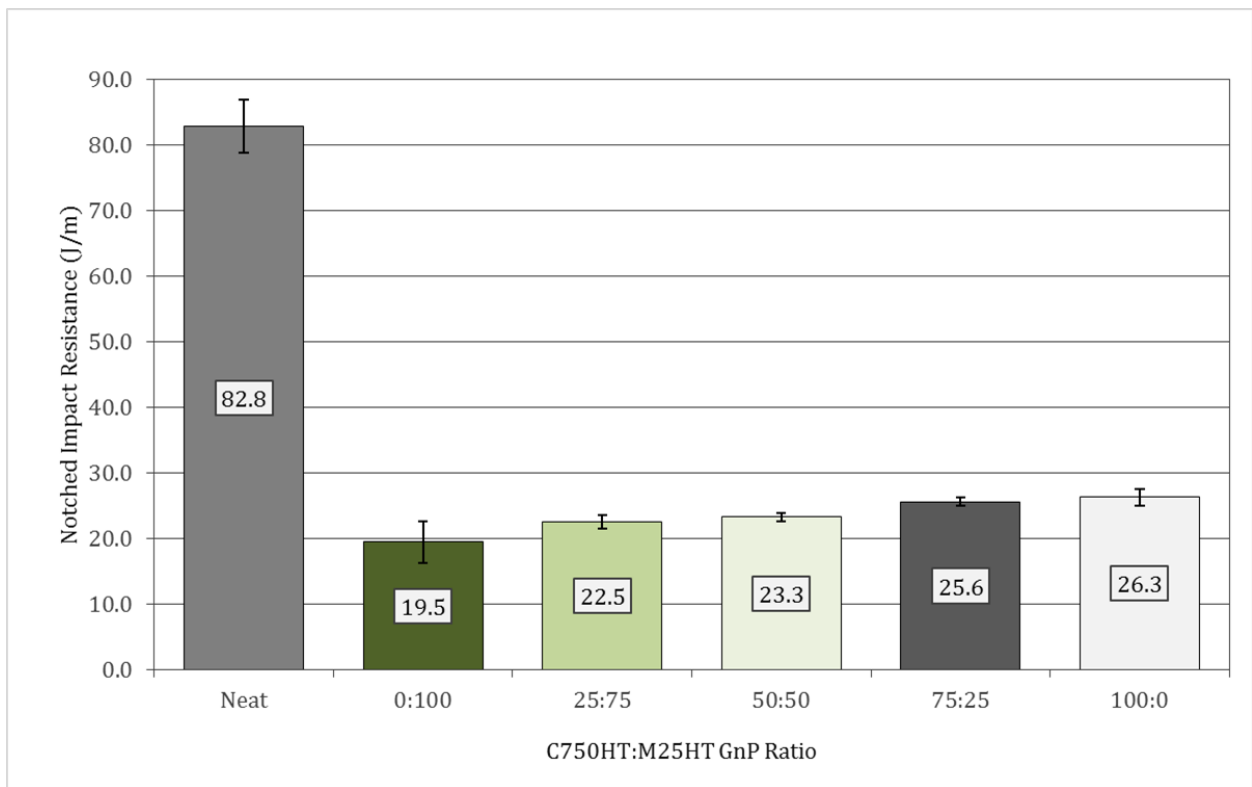


Figure 4-7. Effects of GnP loading and morphology on the notched impact resistance of HIPS

When adhesively bonded to aluminum substrates, the composite adhesive films exhibited losses in strength proportional to the M25 weight fraction. Shown in Figure 4-8, the lap-shear

strength decreases from 17.3MPa to 8.5MPa with pure 7.5% M25 composite adhesive films. This loss then decreases with decreasing M25 content to 13MPa for 75:25 composite films. The lap-shear strength is expected to continue recovering as the M25 fraction reaches zero in the pure C750 film, however, there is another drop to 11 MPa.

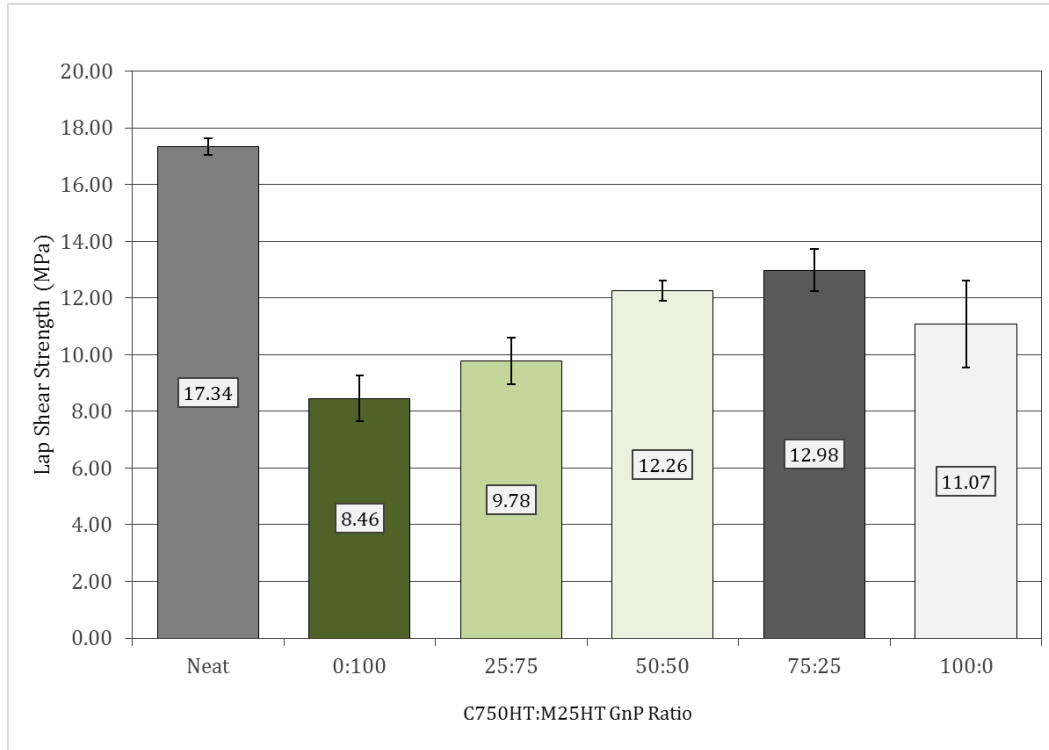


Figure 4-8. Effects of GnP loading and morphology on the lap-shear strength of Al-Al bonded joints

The inconsistent lap-shear strength of the pure C750 composite film is believed to be an experimental anomaly. This could be due to a deviation in handling of the film, the surface treatment of the substrate, or migration of the smaller particle to the film surface during processing. Additional work is required to fully understand this deviation from the expected results. When a comparison is drawn across all absolute M25 concentrations produced in this work, the strongly linear correlation shown in Figure 4-9 is obtained. The reduction in lap-shear strength of the composite films can be attributed to the increased stiffness of the higher M25 concentration composites, however, the effects of GnP on the adhesive interface must also be considered.

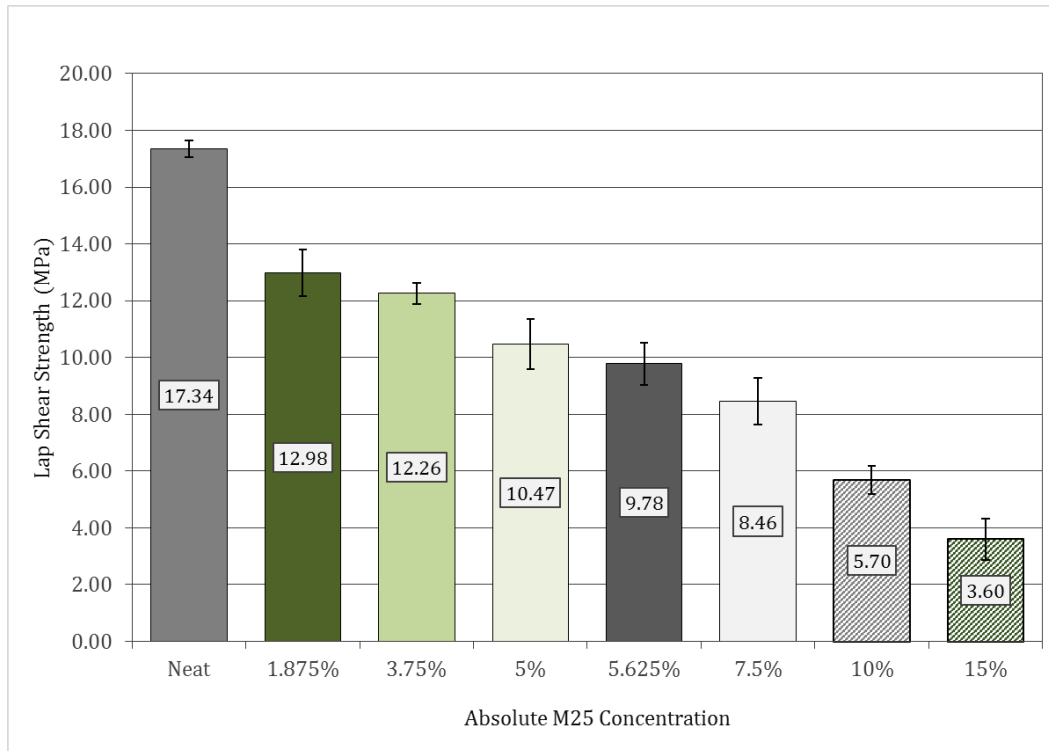


Figure 4-9. Effects of absolute M25 GnP content on the lap-shear strength of Al-Al bonded joints

Any GnP that is exposed on the surface of the adhesive film during processing or surface treatment will be a low-energy area that will not contribute to adhesion with the substrate. While it is probable that both the shear strength and adhesive force has been reduced in the composite films, in all tests conducted, the adhesive failed before the interface. The continuation of cohesive failures in the lap joints across GnP concentrations means if there is a loss in strength of adhesion, it is masked by the more brittle adhesive bulk. In future work, the same contact angle studies used for the neat films can be conducted to investigate changes to the surface energy of composite films.

4.4 Conclusion

GnP reinforcement of the HIPS thermoplastic was found to directly impact the mechanical performance of the HIPS bulk material and lap-shear joints assembled from composite adhesive films. Composite HIPS with 7.5% pure M25 loadings showed 72% and 76% gains in flexural and tensile modulus. These gains decreased with higher relative concentrations of the C750 GnP

morphology. The opposite trend was observed in flexural strain-to-failure as pure M25 loading resulted in a more significant loss, recovering with increased C750 content. The introduction of GnP in any relative concentrations resulted in an average 17% increase in flexural strength and no statistically significant change to tensile strength or tensile strain-to-yield. There was an average loss in impact resistance of 72% which recovered slightly with increased relative C750 content. The effect of GnP content on adhesive strength was shown to be inversely related to absolute M25 content with 1.875% resulting in 25% loss in strength decreasing linearly to a 51% loss at 7.5% absolute M25 content. It is believed the unexpected mechanical properties of the composite HIPS is a direct result of poor dispersion and weak particle-matrix adhesion. Solutions for these observations are considered in the Future Work section.

Chapter 5: Microwave Activation

5.1 Introduction

Similar to the previous section, this chapter briefly introduces the concept of microwave activation of GnP. Microwave energy is commonly used to rapidly and efficiently exfoliate graphite into graphene. While exfoliation is typically done at 2.4GHz to rapidly boil the acid drawn into the carbon layers for expansion, this work seeks to explore microwave frequencies which are able to heat the graphene more directly. It serves as a proof of concept showing surface temperatures of GnP composite films can be raised more rapidly than surrounding substrate materials using microwave spectrum electromagnetic radiation.

Graphene nanoparticles are shown to interact strongly with electromagnetic radiation within the microwave regime of 1-300 GHz. These frequencies are commonly used for telecommunication and radar systems. As such, much experimentation has been done investigating graphene as light-weight shielding materials for frequencies used by hand-held communication devices, 5-18GHz [84-87]. While the goal of thin-layer shielding is primarily reflection, at the correct frequencies, the adsorption of the microwave energy is very high, resulting in rapid heating. Thermal responses of varying carbon-based nanoparticles within polystyrene composites have been observed to exhibit 80°C/min heating rates for multilayer distributed graphene [88]. While ~100°C/min heating rates of GnP composites is promising, this study aims to significantly increase these heating rates to achieve polymer melt in less than 30 seconds.

As the target of this work is selective heating, the first step in providing proof of concept is to confirm a difference in the heating rate of GnP composite adhesives when compared to the proposed substrates. To demonstrate this, HIPS/GnP composite films and glass fiber reinforced polymer (GFRP), CFRP, and aluminum substrates will be exposed to c-band microwave energy while monitoring changes in the surface temperature. After proving selectivity, changes to the

thermal response of the composite films due to variation in concentration of the GnP morphologies used in this study, M25 and C750, will be observed. Finally, the effect of changes to the properties of the microwave energy, frequency and power, on heating rates will be investigated to provide a basis for future studies.

5.2 Materials and Methods

Microwave experimentation was done in a variable-frequency microwave (VFM) Microcurie 2100 (Lambda Technologies), shown in Figure 5-1, with a center frequency of 6.245GHz and a sweep of ± 1.15 GHz.



Figure 5-1. MicroCure 2100 variable frequency oven showing chamber, IR temperature probe, and glass sample stand

For study, samples are placed within the sealing chamber on a microwave translucent glass beaker below an IR temperature probe. This probe measures surface temperature in-situ during microwave operation. Samples of various compositions were tested under specific frequency and power conditions to characterize the response of the composite thermoplastics, the materials

intended to be used as adherents, and simple lap-joint structures. The parameters for the heating experiments are summarized below each figure. Samples were irradiated for 100 seconds or until their surface temperature read 200°C, whichever came first.

5.3 Results and Discussion

Initial results showed a significant difference in thermal response between neat HIPS and GnP composite HIPS as seen in Figure 5-2. The neat HIPS film experiences a ΔT of only 28.1°C over the 90sec cycle compared to a ΔT of 54°C and maximum temperature 177°C for HIPS compounded with 7.5%wt of C750 and M25 GnP, respectively. Figure 5-2 also compares the surface temperature of these adhesive films to that of GFRP, CFRP, and aluminum substrates.

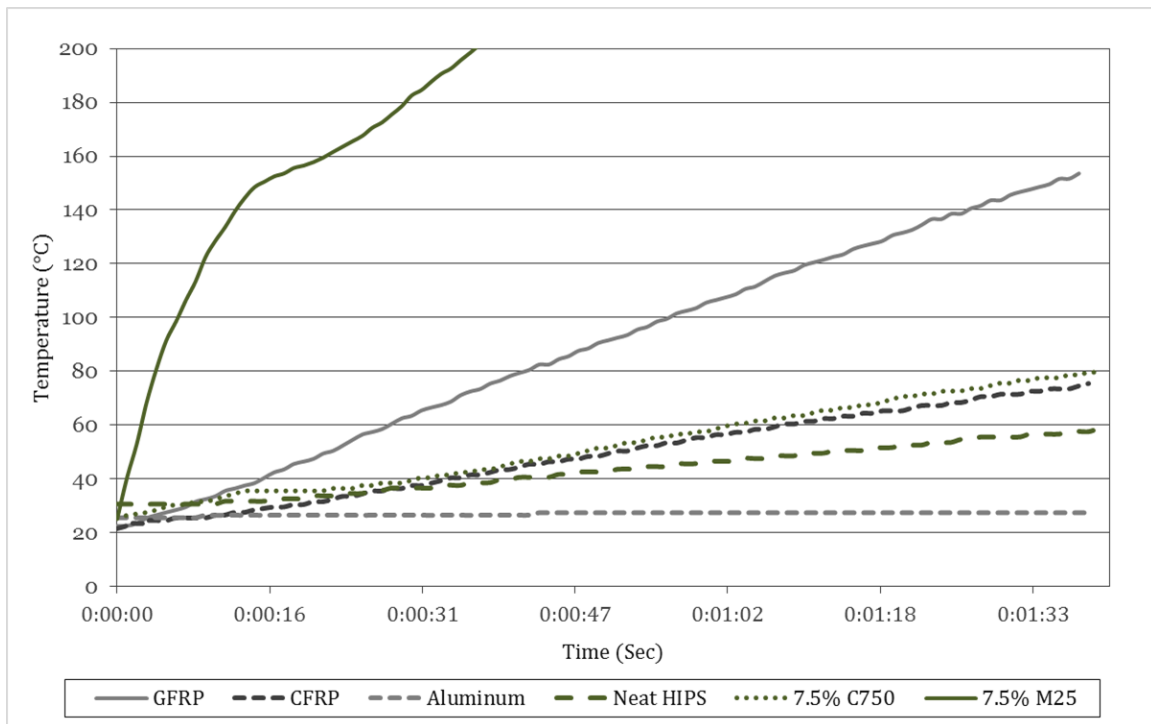


Figure 5-2. Surface temperatures of substrates, neat HIPS, and GnP composite HIPS at 200W and 6.24GHz with a 1.15GHz sweep

The ΔT of the GFRP is highest at 131°C, that of the CFRP is nearly equivalent to the C750 modified HIPS at 54°C, and the aluminum did not show any thermal response. Microwave at this at this frequency interact strongly with the “sea” of electrons unique to metallic bonds. The excited

electrons re-radiate the energy into electromagnetic fields with penetration depths of 1.2E-12m. This results in the dissipation of the electromagnetic energy on the surface and a near 100% effective refraction index [89].

The shift in the heating rate of the M25 GnP modified HIPS suggests a melt event after 15sec when the surface temperature reaches $\sim 150^{\circ}\text{C}$. While this is below the expected melt temperature of $\sim 190^{\circ}\text{C}$, this reading would be effected by distortions to the film surface as it begins to deform above its softening temperature. At an initial heating rate (0-15sec) of $502^{\circ}\text{C}/\text{min}$, the 7.5%/wt M25 GnP composite HIPS heats 12 times faster than C750 GnP modified HIPS of the same concentration and 114 times faster than neat HIPS. The M25 GnP HIPS also heats 7x faster than the most responsive substrate, GFRP. This proves the targeted heating under surface conditions and shows the potential for the same effect to be achieved within bondlines.

Experimentation was done to examine the effects of frequency and power on the thermal response of composite HIPS films. Figure 5-3 summarizes these findings for pure M25 loading of 5% and 7.5% at various frequencies. It was shown that both GnP concentration and microwave frequency have direct effects on maximum temperature and rate of heating. Key results of this experiment are high changes in thermal response with only a 1.5% difference in GnP concentration and 1.25GHz spread of frequency. At 5.85GHz, increasing the GnP content from 5% to 7.5% resulted in a 116% increase in maximum surface temperature and 328% increase heating rate observed for a 100sec cycle. For the same concentration change at 7GHz, the time to reach 200°C decreased from 29 to 21sec. Analysis of the change in thermal response from frequency showed an increase in maximum temperature of 115% (limited by the 200°C cap) and an 805% increase in heating rate for films with a consistent 5% GnP loading. While less as dramatic, the same frequency increase resulted in a 163% increase in heating rate and a decrease in time to max temperature from 53 to 21 seconds for the 7.5% composite HIPS.

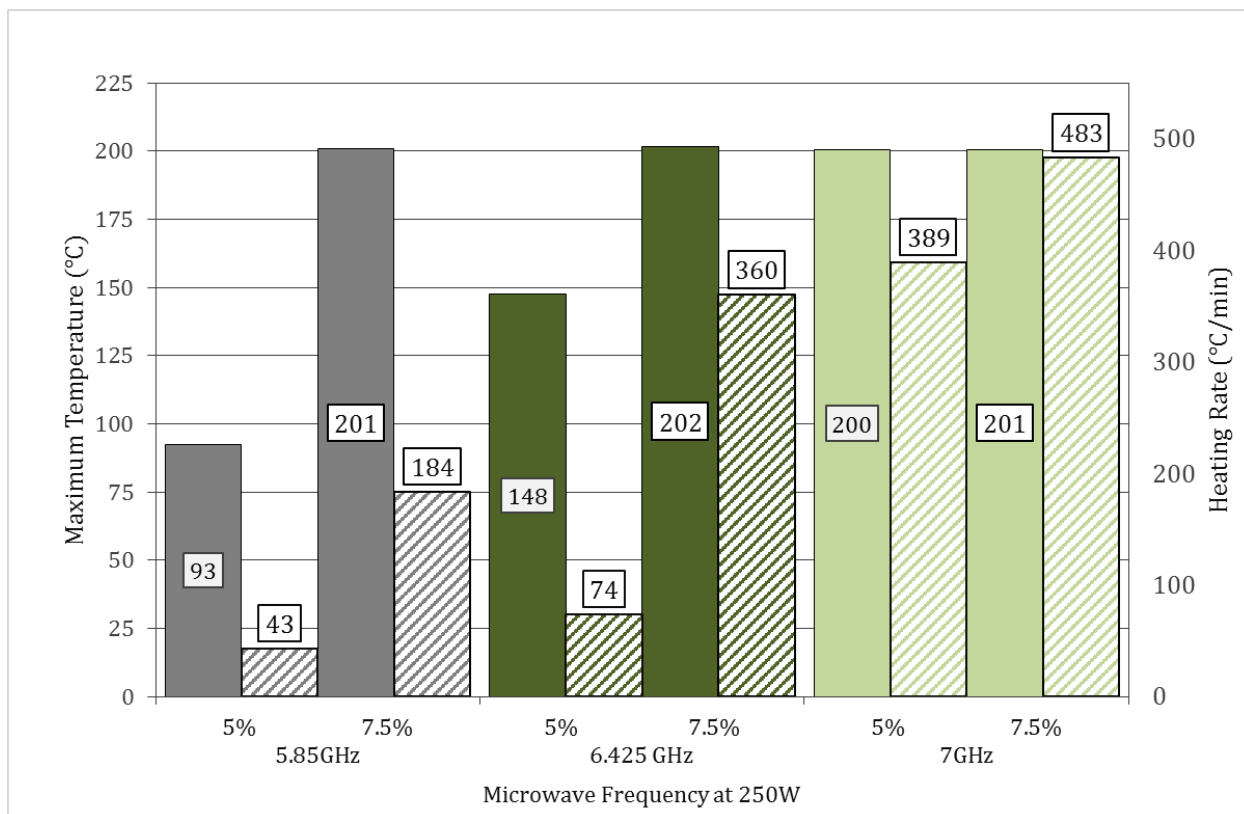


Figure 5-3. Maximum temperature (solid) and heating rate (striped) for 5 and 7.5% M25 composite films cycled at various constant frequencies at 250W

Observing such significant changes in thermal response due to relatively small changes in experimental parameters is promising as experimentation in this area continues. A high degree of control on reversible adhesive heating rates will allow efficient application to specific bonding requirements.

This experiment was repeated with composite films containing C750 GnP under equivalent conditions. Summarized in Figure 5-4, similar trends in the C750 heating response are observed to the M25. While similar correlation is observed, lower values for maximum temperatures and heating rates are observed across all concentrations and frequencies. The lower absolute heating response is in agreement with the data collected in the previous selectivity experiment. Changes to C750 concentration showed limited impact on maximum film temperature or heating with the largest change observed at 6.425GHz with 34% and 60%, respectively. While the effect of frequency

was also limited, the change from 5.85GHz to 7GHz yielded an average increase of 125% and 198% in maximum temperature and heating rate.

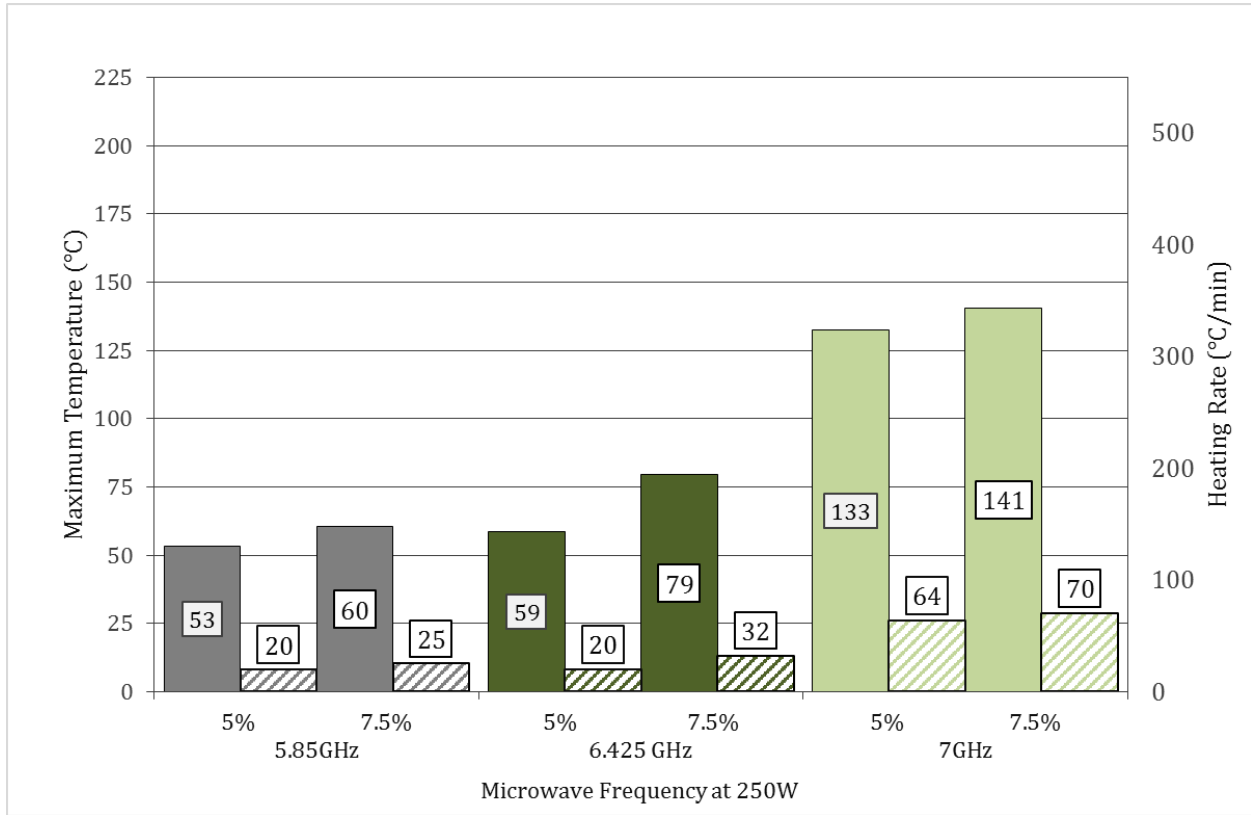


Figure 5-4. Maximum temperature (solid) and heating rate (striped) for 5 and 7.5% C750 composite films cycled at various constant frequencies at 250W

Finally, analysis was done to determine the effect on thermal response of C750/M25 blended composite films at the available frequencies. The complete range of heating profiles possible with variations in morphology concentrations and frequency is shown in Figure 5-5. In this chart, colors are representative of the relative GnP composites, 0:100-100:0 and dotted, dashed, and solid lines are indicative of 5.85, 6.425, and 7GHz frequencies, respectively. It is shown that relative M25 GnP content has the greatest effect on heating rate with rates and maximum temperature decreasing with absolute M25 content. As in the pure GnP loading frequency studies, frequency is also shown to have a direct effect on thermal response with increased frequency increasing maximum temperature and heating rate in all GnP blends tested.

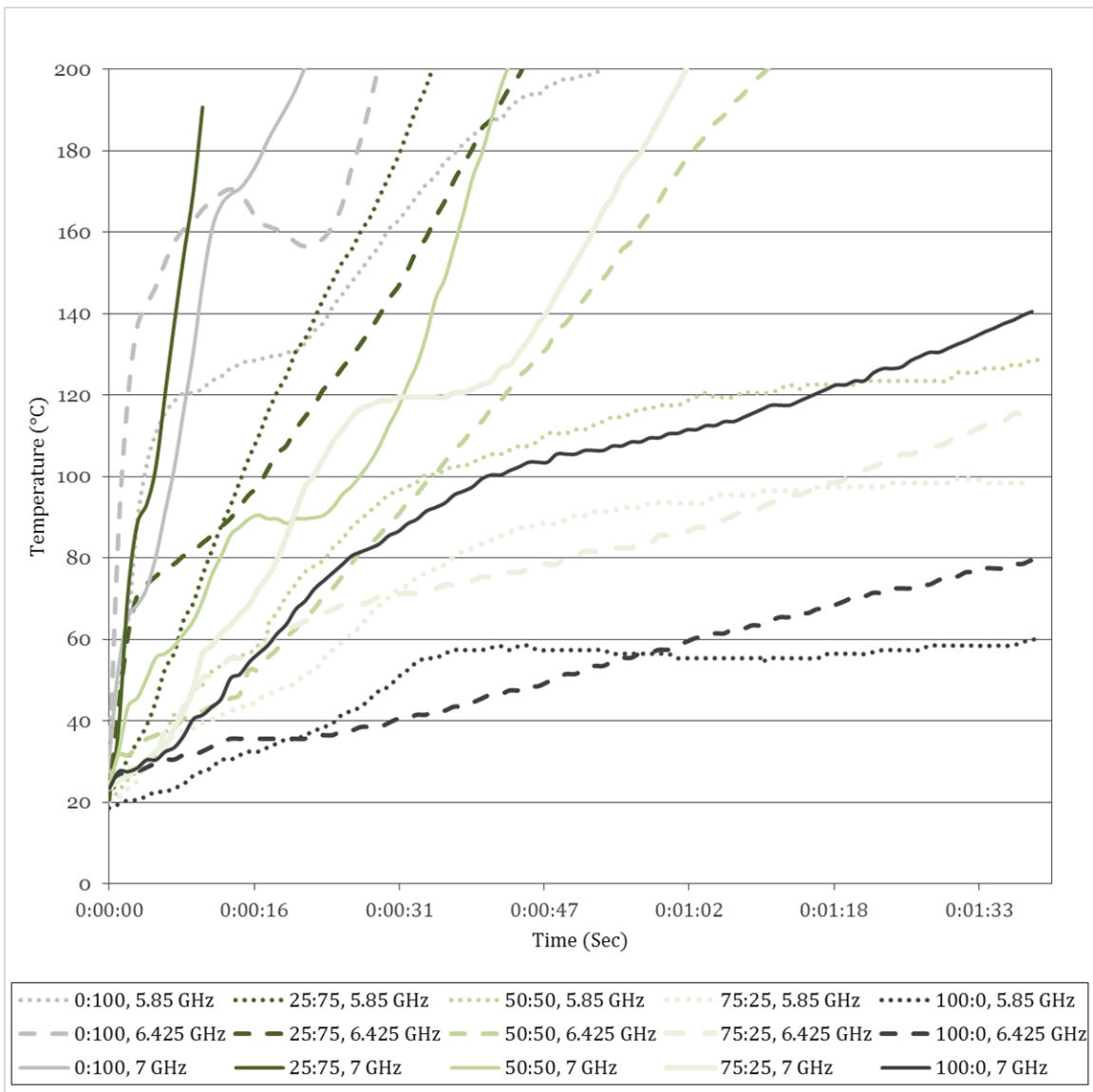


Figure 5-5. Thermal response of C750/M25 blended GnP composite films at 7.5%/wt when heated with 200W of power at the noted frequencies

5.4 Conclusion

While limited in its initial scope, this work proves that c-band microwave energy can elevate surface temperatures of HIPS/GnP composite films to higher maximum temperatures and at greater rates than those of aluminum or CFRP substrates. Films containing the M25 GnP morphology were shown to be capable of reaching the melt temperature of HIPS (200°C) in less than 30 seconds. The M25 was shown to be more efficient at heating the composite adhesive than

equivalent weight fractions of the C750 GnP. It is also proven that heating rate can be controlled via power level and frequency with higher power levels and 7GHz operating frequency giving the greatest thermal response in both particles. When used in combination, blending of the GnP morphologies and changes in frequency can be used to attain a full spectrum of thermal responses. The ability to create specific thermal responses by matching GnP blends with cycle frequencies will be of great value as application constraints require specific heating profiles. The next step of this work is to modify GnP blending and microwave parameters together to facilitate selective heating of the composite films within the bondlines of various materials.

Chapter 6: Summary and Future Work

6.1 Summary

In this work, it is shown that a commercially available engineering thermoplastic can be modified for use as an adhesive through surface treatment. Studying the effects of low-pressure O₂ plasma treatment on film surfaces showed this change in adhesive strength was due to removal of contaminants, oxygen functionalization of the surface, and an increase in roughness. Lap-shear joints assembled from oxygen plasma treated films showed a 135% increase in strength over joints assembled from untreated films. The maximum lap-shear strength of 17.6MPa observed with aluminum substrates is comparable to and even superior to the selection of structural adhesives shown in Figure 6-1. The adhesive strength of surface treated high-impact polystyrene films observed in this study justifies HIPS for continued investigation as a reversible thermoplastic adhesive.

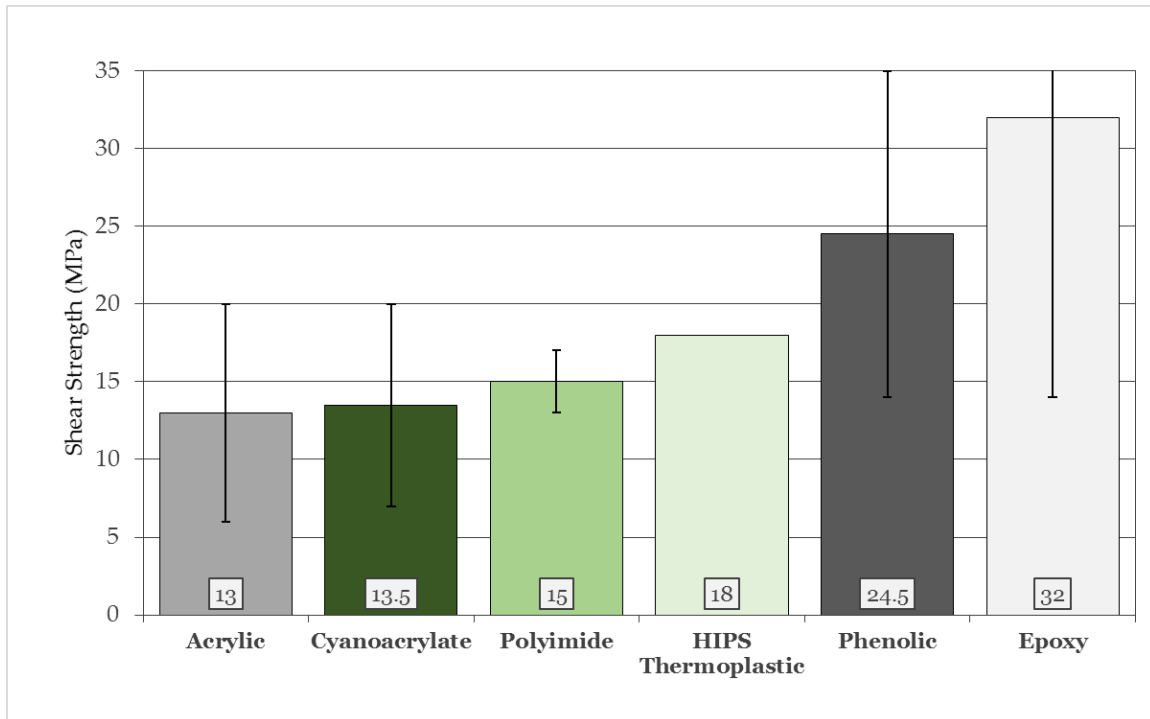


Figure 6-1. Lap-shear strength of HIPS adhesive films compared to similar structural adhesives[18]

The introduction of GnP was shown to make clear modifications to the mechanical properties of HIPS. All changes in mechanical properties are shown normalized in Figure 6-2 according to GnP content. It was shown that the use of pure M25 GnP at 7.5% concentration results in a 72% increase in flexural modulus and 76% increase in tensile modulus. The effects of GnP on other mechanical characteristics was not as expected and its suspected cause, agglomeration and inadequate interfacial adhesion, will be explored in future works.

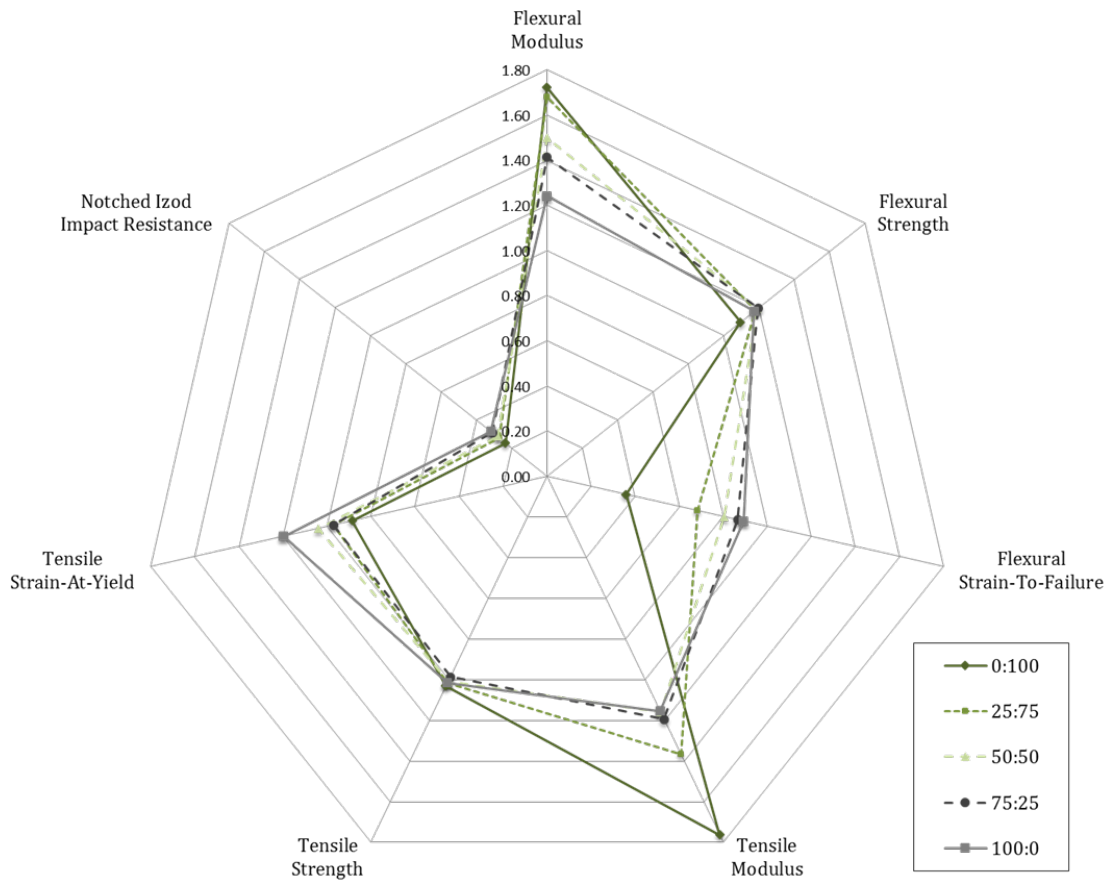


Figure 6-2. Graphical summary of the mechanical properties of GnP composite HIPS

Losses to some mechanical properties, even at these initial stages, are shown to be a trade-off for the ability to heat the adhesive via EM microwave radiation. As is summarized in Table 2-1, the change in surface temperature of open adhesives reinforced with 7.5% pure M25 GnP is significantly greater than changes observed in the studied substrates, GFRP, CFRP, and aluminum

under equivalent conditions. It is also shown the maximum surface temperature of the adhesive and rate of heating can be directly controlled via the morphology and concentration of the nanoparticle utilized in the adhesive in addition to microwave parameters. Both of these findings further enforce the feasibility of GnP/microwave heating as an efficient method for the activation of reversible thermoplastic adhesives.

Table 6-1. Tabulated summary of thermal response to substrates, neat, and composite HIPS at 200W and 6.24GHz

Material (-)	T(15sec) (°C)	T(60sec) (°C)	Tmax (°C)	ΔT (°C)	Rate (°C/min)
GRFP	40	106	154	131	72
CFRP	28	55	76	54	28
Aluminum	26	28	28	2	~0
Neat HIPS	27	41	59	28	4
0:100	151	200+	200+	177	502
100:0	36	59	79	54	40

6.2 Future Work

While this work proves commercially available thermoplastics can be modified for use as adhesives, be augmented mechanically through the introduction of GnP, and heated via microwave excitation of the GnP; further work is required to produce an adhesive ready for multi-material bonding in industrial applications. Further work should be conducted to improve ease of film preparation, enhance dispersion and interfacing of GnP, and identify specific radiation bands which allow for both substrate penetration and GnP excitation.

6.2.1 Modification of the Bulk Adhesive

Modifications to the bulk adhesive could be made to facilitate adhesive bonding without the need for such extensive post-processing. Direct production of the adhesive film geometry via continuous die extrusion would allow greater control over the uniformity of the adhesive product, orientation of the nanoparticle content, and elimination of the surface treatment required to

remove the contamination that results from secondary pressing of the films [90]. While pre-shaping the films would eliminate the PTFE contamination, the need for internal/external lubricant would still be required to utilize conventional processing techniques. Even if changes in processing methods were possible to reduce lubricant content, HIPS is still an inherently low-energy polymer. The sterically available aromatic ring of the styrene monomer is difficult to open without the use of chemical processes. As it has been shown that the chemical adhesion mechanism activated through the deposition of oxygen radicals on the film surface is far superior to that of the physical adhesion of untreated films, an oxidizing surface treatment would still be required.

6.2.2 Further Study of Surface Treatment

Further investigation into the methods of surface treatment would provide a more industrially viable solution for producing these adhesives on a larger scale. While considered overly hazardous for continued study in this work, under industrial setting, a continuous application of surface modifying chemical etchant could be utilized to eliminate the need for batch processing of adhesive films. Many additional dry, continuous treatment techniques also exist which could be utilized in film production.

Atmospheric corona discharge is a continuous surface treatment similar to low-pressure plasma treatment but done at atmospheric conditions [91]. Study would be required to assess the degree of oxygen functionalization obtained via atmospheric methods plasma treatment methods. UV surface treatments have also been shown to dramatically increase the surface energy of polystyrene films [92, 93]. However, oxygen functionalization levels obtained from UV treatments are again lower than those obtained from low-pressure O₂ plasma treatments. Finally, a review has been investigated on dielectric barrier discharge (DBD) which includes preparation of polystyrene films for adhesive bonding [94]. While similar to atmospheric corona discharge methods, DBD utilizes a knife-edge electrode to create a potential through the insulating polymer film to a ground.

The DBD atmospheric plasma treatment method has been optimized for continuous film production. This would prove particularly advantageous coupled with implementation of continuous extrusion of the composite adhesive films. Within this review, treatment of polystyrene films showed up to 75° decreases in contact angle following treatment [94]. In addition to a high degree of oxygen functionalization of the unsaturated C=C styrene bonds, the study also observed a considerably higher sensitivity to aging than low-pressure oxygen plasma treatments. While not necessarily prohibitive to the consideration of this treatment method moving forward, the effect of aging on adhesive performance would need to be considered for this and all proposed treatment methods.

Before physically exploring alternative surface treatments, it would be pertinent to modify the experiments presented here to associate the changes in adhesion to each effect of the plasma treatment. In addition, if oxygen functionalization is found to be the greatest contributor to the increase adhesive performance, the minimum level of functionalization required to achieve the bonding strengths reported in this work would should be determined. This minimal oxygen content would serve as a starting point to compare the potential of alternate oxygen functionalizing methods. Although valuable for initial comparison, this oxygen content baseline is not recommend to be the sole determinant of a treatment's potential. As all the suggested surface treatments simultaneously subject the polymer to compound modification mechanisms, additional factors may create unexpected enhancements.

6.2.3 Dispersion of GnP

The data collected in this work showed an unexpected loss in many mechanical properties after compounding with M25 and C750 GnPs. It is believed that agglomeration of the particles is creating slip interfaces as the particles are weakly bound to one another and are able to slide along their planar surfaces. More complete dispersion can be achieved through the use of surfactants,

mechanical milling, and ultrasonic dispersion before mechanical incorporation in the polymer melt [95].

However, even if greater dispersion of the particles is achieved before mixing, there is evidence to suggest that GnP particles have a tendency to reaggregate during mechanical melt mixing [96, 97]. Multiple solutions have been developed by researchers faced with the same problem. One method is to stabilize the GnP dispersion via a polymer functionalization within which the particles can then be stored and incorporated into the melt after vacuum drying [98]. Functionalization of GnP is common before incorporating into composite systems and would improve the tendency of the GnP to remain dispersed in addition to dramatically improving the strength of adhesion between the particles and surrounding matrix. Functionalization is often done using linkage molecules deposited on the particle surface [78, 95, 99, 100]. Oxidation of the graphene can also provide the same effect via the creation of oxygen groups across the low-energy platelet surfaces [101].

Another suitable solution for maintaining dispersion of the particles within the polymer is to incorporate them directly into the polymer chain. Referred to as copolymerization, the nanoparticles are dispersed within the polymer monomer in a way that they are integrated into the formation of the polymer chains. In one example, *in-situ* ultrasonication dispersed emulsion copolymerization, the dispersed graphene is directly integrated into repeating segments in a simple one pot synthesis process [102]. In fact, numerous novel methods exist for incorporating GnP directly into polystyrene systems via co-polymerization. Additional examples are reversible addition-fragmentation chain-transfer polymerization (RAFT) [103] and solvent-free dry polymerization methods [104].

All of these examples are proven solutions for the complete integration of GnP with the surrounding polymer. The investigation of chemical compounding methods is highly recommended as future scale-up will most likely find up-stream integration of the GnP more efficient than

mechanical mixing with finished materials. The mechanical performance observations made in this study should in no way be found inhibitive to the final objective of creating a GnP composite adhesive. Rather, the importance of nanoparticle dispersion and matrix compatibility has been highlighted in this work and will be of primary focus in continued experimentation.

6.2.4 Further Study on Microwave Activation

The study on microwave heating in this work is limited to the frequency range of 6.425-7GHz GHz. While it is shown that GnP is thermally responsive in this frequency regime, initial experimentation showed limited ability to heat the adhesive within the bondlines of the investigated substrates due to absorption and reflection. Studies have shown that operating within the frequency range of 2-4 GHz range can allow penetration of other polymers for bondline heating of joints [105, 106]. While GnP is still thermally responsive in this range, experiments in this study have shown a direct correlation between frequency and thermal response. A crossover point would need to be found that utilizes microwave frequencies able to penetrate materials of specific dielectric constant that are still able to be absorbed by the GnP within the adhesive. With the many combinations of substrates and GnP morphologies possible, it is of strong confidence suitable configurations will be found that maximize adhesive heating with limited losses to the surrounding substrates. The completion of this experimentation is the next step for completely verifying HIPS thermoplastic reinforced with GnP as a reversible multi-material adhesive.

WORKS CITED

WORKS CITED

1. Amancio, S.T. and J.F. dos Santos, Joining of Polymers and Polymer-Metal Hybrid Structures: Recent Developments and Trends. *POLYMER ENGINEERING AND SCIENCE*, 2009. 49(8): p. 1461-1476.
2. Ucsnik, S., et al., Experimental investigation of a novel hybrid metal-composite joining technology. *Composites Part A: Applied Science and Manufacturing*, 2010. 41(3): p. 369-374.
3. Thoppul, S.D., J. Finegan, and R.F. Gibson, Mechanics of mechanically fastened joints in polymer-matrix composite structures – A review. *Composites Science and Technology*, 2009. 69(3): p. 301-329.
4. Camanho, P.P. and F.L. Matthews, Stress analysis and strength prediction of mechanically fastened joints in FRP: a review. *Composites Part A: Applied Science and Manufacturing*, 1997. 28(6): p. 529-547.
5. Gay, D., *Composite materials: design and applications*. Third ed. 2014, Boca Raton: Taylor & Francis.
6. Dano, M.-L., G. Gendron, and A. Picard, Stress and failure analysis of mechanically fastened joints in composite laminates. *Composite Structures*, 2000. 50(3): p. 287-296.
7. Dano, M.-L., E. Kamal, and G. Gendron, Analysis of bolted joints in composite laminates: Strains and bearing stiffness predictions. *Composite Structures*, 2007. 79(4): p. 562-570.
8. Ger, G.S., K. Kawata, and M. Itabashi, Dynamic tensile strength of composite laminate joints fastened mechanically. *Theoretical and Applied Fracture Mechanics*, 1996. 24(2): p. 147-155.
9. Pramanik, A., et al., Joining of carbon fibre reinforced polymer (CFRP) composites and aluminium alloys – A review. *Composites Part A: Applied Science and Manufacturing*, 2017. 101(Supplement C): p. 1-29.
10. Patterson, E., et al., *Composite Materials and Joining Technologies for Composites, Volume 7: Proceedings of the 2012 Annual Conference on Experimental and Applied Mechanics*. 2013, Springer New York: New York, NY.
11. Joining technology of the future: high-performance structural adhesives deliver numerous advantages for constructors and processors alike. 2010, BNP Media. p. 24.
12. Brockmann, W., *Adhesive bonding: materials, applications and technology*. Rev.;1; ed. 2009, Weinheim: Wiley-VCH.
13. Silva, L.F.M., et al., *Hybrid Adhesive Joints*. 2011, Springer Berlin Heidelberg: Berlin, Heidelberg.

14. Monte, S., The adhesive advantage: Strong joints, low costs. 2009, Penton Media, Inc., Penton Business Media, Inc: Cleveland. p. 42.
15. Jahn, J., et al., Assessment Strategies for Composite-metal Joining Technologies – A Review. *Procedia CIRP*, 2016. 50(Supplement C): p. 689-694.
16. Garg, A.C. and Y.-W. Mai, Failure mechanisms in toughened epoxy resins—A review. *Composites Science and Technology*, 1988. 31(3): p. 179-223.
17. Awaja, F., et al., Adhesion of polymers. *Progress in Polymer Science*, 2009. 34(9): p. 948-968.
18. Petrie, E.M., *Handbook of adhesives and sealants*. 2nd ed. 2007, New York: McGraw-Hill.
19. Treffer, D.F. and J.G. Khinast, Why hot melts do not stick to cold surfaces. *Polymer Engineering & Science*, 2017. 57(10): p. 1083-1089.
20. Grewell, D.A., A. Benatar, and J.B. Park, *Plastics and composites welding handbook*. 2003, Munich;Hanser;Cincinnati,: Hanser Gardener.
21. Ahmed, T.J., et al., Induction welding of thermoplastic composites—an overview. *Composites Part A: Applied Science and Manufacturing*, 2006. 37(10): p. 1638-1651.
22. Kagan, V.A. and R.J. Nichols, Benefits of Induction Welding of Reinforced Thermoplastics in High Performance Applications. *Journal of Reinforced Plastics and Composites*, 2005. 24(13): p. 1345-1352.
23. Li, Z., et al., Ultrafast, dry microwave synthesis of graphene sheets. *JOURNAL OF MATERIALS CHEMISTRY*, 2010. 20(23): p. 4781-4783.
24. Sasikala, T.S. and M.T. Sebastian, Microwave Dielectric Properties of Polystyrene–Forsterite (Mg₂SiO₄) Composite. *Journal of Electronic Materials*, 2016. 45(1): p. 729-735.
25. Subodh, G., et al., Polystyrene/ composites with low dielectric loss for microwave substrate applications. *Polymer Engineering and Science*, 2009. 49(6): p. 1218.
26. Dominighaus, H., *Plastics for Engineers: Materials, Properties, Applications*. 2000: Hanser Gardner Publications.
27. Kennedy, J.F. and M. Thorley, *Concise Encyclopedia of Polymer Science and Engineering*; J.I. Kroschwitz (Ed.); John Wiley & Sons, Chichester, 1998, 1341 pages, ISBN 0-471-31856-6 £63.95. Vol. 40. 1999: Elsevier Ltd. 90-91.
28. Harper, C.A., *Handbook of plastics, elastomers, and composites*. 1996, United States.
29. Morales, G., et al., Improved Toughness in HIPS Obtained From Different Styrene/Butadiene-Graded Block Copolymers Through Modification of the Polydispersity Index of the PS Block. *Polymer Engineering & Science*, 2006. 46(10).
30. Robeson, L.M., *Polymer blends: a comprehensive review*. 2007, Munich;Cincinnati,: Hanser.

31. Seward, R.J., The observation of crazes in high-impact polystyrene by electron microscopy. *Journal of Applied Polymer Science*, 1970. 14(3): p. 852-858.
32. Trent, J.S., M.J. Miles, and E. Baer, The mechanical behaviour of high-impact polystyrene under pressure. *Journal of Materials Science*, 1979. 14(4): p. 789-799.
33. Harper, C.A., *Modern plastics handbook*. 2000, New York: McGraw-Hill.
34. Štěpek, J. and H. Daoust, *Additives for plastics*. Vol. 5. 1983, New York: Springer-Verlag.
35. Murphy, J., *Additives for plastics handbook*. 2nd;2; ed. 2001, Oxford;New York;: Elsevier Advanced Technology.
36. Williams, J.B., K.S. Geick, and J.A. Falter, Structure/performance characteristics of bisamide lubricants in ABS. *Journal of Vinyl and Additive Technology*, 1997. 3(3): p. 216-219.
37. Paul, D.R. and C.B. Bucknall, *Polymer blends*. 2000, New York: Wiley.
38. Akhmatov, A.S., *Molecular physics of boundary friction*. 1966: Israel Program for Scientific Translations.
39. Silverstein, R.M. and F.X. Webster, *Spectrometric identification of organic compounds*. 6th ed. 1998, New York: Wiley.
40. Vickerman, J.C. and I.S. Gilmore, *Surface analysis: the principal techniques*. 2009, Wiley: Chichester, U.K.
41. Kinloch, A.J., G.K.A. Kodokian, and J.F. Watts, RELATIONSHIPS BETWEEN THE SURFACE FREE-ENERGIES AND SURFACE CHEMICAL-COMPOSITIONS OF THERMOPLASTIC FIBER COMPOSITES AND ADHESIVE JOINT STRENGTHS. *JOURNAL OF MATERIALS SCIENCE LETTERS*, 1991. 10(14): p. 815-818.
42. Kodokian, G.K.A. and A.J. Kinloch, Surface pretreatment and adhesion of thermoplastic fibre-composites. *Journal of Materials Science Letters*, 1988. 7(6): p. 625-627.
43. Ebnesajjad, S. and A.H. Landrock, *Adhesives technologies handbook*. Vol. Third. 2015, London, UK: William Andrew is an imprint of Elsevier.
44. Fryer, D.S., et al., Dependence of the Glass Transition Temperature of Polymer Films on Interfacial Energy and Thickness. *Macromolecules*, 2001. 34: p. 5627-5634.
45. Park, H., et al., Effect of temperature and pressure on surface tension of polystyrene in supercritical carbon dioxide. *JOURNAL OF PHYSICAL CHEMISTRY B*, 2007. 111(15): p. 3859-3868.
46. Gaines, G.L., Surface and interfacial tension of polymer liquids -a review. *Polymer Engineering and Science*, 1972. 12(1): p. 1-11.
47. Burnett, D.J., F. Thielmann, and R.A. Ryntz, Correlating thermodynamic and mechanical adhesion phenomena for thermoplastic polyolefins. *Journal of Coatings Technology and Research*, 2007. 4(2): p. 211-215.

48. Kwok, D.Y., et al., Study on the surface tensions of polymer melts using axisymmetric drop shape analysis. *POLYMER ENGINEERING AND SCIENCE*, 1998. 38(5): p. 757-764.
49. Sauer, B.B. and G.T. Dee, Molecular Weight and Temperature Dependence of Polymer Surface Tension: Comparison of Experiment with Theory. *Macromolecules*, 1990. 24(8): p. 2124-2126.
50. Demarquette, N.R., et al., Influence of temperature, molecular weight, and molecular weight dispersity on the surface tension of polystyrene, polypropylene, and polyethylene. II. Theoretical. *Journal of Applied Polymer Science*, 2002. 83(10): p. 2201-2212.
51. Stokes, R.J. and D.F. Evans, *Fundamentals of interfacial engineering*. 1997, New York: Wiley-VCH.
52. Adamson, A.W. and A.P. Gast, *Physical chemistry of surfaces*. 6th ed. 1997, New York: Wiley.
53. Bruice, P.Y., *Organic chemistry*. 5th ed. 2007, Upper Saddle River, N.J: Pearson Prentice Hall.
54. Brand, J.v.d., et al., Interaction of Anhydride and Carboxylic Acid Compounds with Aluminum Oxide Surfaces Studied Using Infrared Reflection Absorption Spectroscopy. *Langmuir*, 2004. 20: p. 6308-6317.
55. Ashish, PTFE Molecular Interactions. 2016, ScienceABC: <http://sciabc.us/KxnDj>.
56. Kaplan, S.L. and P.W. Rose, Plasma surface treatment of plastics to enhance adhesion. *International Journal of Adhesion and Adhesives*, 1991. 11(2): p. 109-113.
57. Hegemann, D., H. Brunner, and C. Oehr, Plasma treatment of polymers for surface and adhesion improvement. *Nuclear Instruments and Methods in Physics Research Section B: Beam Interactions with Materials and Atoms*, 2003. 208: p. 281-286.
58. Hall, J.R., et al., Activated gas plasma surface treatment of polymers for adhesive bonding. *Journal of Applied Polymer Science*, 1969. 13(10): p. 2085-2096.
59. Guruvenket, S., et al., Plasma surface modification of polystyrene and polyethylene. *Applied Surface Science*, 2004. 236(1): p. 278-284.
60. J. Tyczkowski, I.K., B. Wozniak, Plasma-Surface Modification of Styrene-Butadiene Elastomers for Improved Adhesion, in *Plasma Processes and Polymers*, P.F. R. d'Agostino, C. Oehr, M. R. Wertheimer, Editor. 2005, WILEY-VCH: Weinheim;Chichester;.
61. Liston, E.M., L. Martinu, and M.R. Wertheimer, PLASMA SURFACE MODIFICATION OF POLYMERS FOR IMPROVED ADHESION - A CRITICAL-REVIEW. *JOURNAL OF ADHESION SCIENCE AND TECHNOLOGY*, 1993. 7(10): p. 1091-1127.
62. Wolf, R. and A.C. Sparavigna, Role of Plasma Surface Treatments on Wetting and Adhesion. *Engineering*, 2010. 02(06): p. 397-402.
63. Zamani Farahani, M.R., INTEGRATED MICRO PEM FUEL CELL WITH SELF-REGULATED HYDROGEN GENERATION FROM AMMONIA BORANE. 2016.

64. Ting, Y.-H., et al., Surface Roughening of Polystyrene and Poly(methyl methacrylate) in Ar/O₂ Plasma Etching. *Polymers*, 2010. 2(4): p. 649-663.
65. Landgraf, R., et al., Functionalization of Polymer Sensor Surfaces by Oxygen Plasma Treatment. *Procedia Chemistry*, 2009. 1(1): p. 1015-1018.
66. Pawlat, J., et al., RF-Powered Atmospheric-Pressure Plasma Jet in Surface Treatment of High-Impact Polystyrene. *IEEE Transactions on Plasma Science*, 2016. 44(3): p. 314-320.
67. Dupont-Gillain, C.C., et al., Plasma-oxidized polystyrene: Wetting properties and surface reconstruction. *LANGMUIR*, 2000. 16(21): p. 8194-8200.
68. Wegman, R.F. and J.v. Twisk, *Surface preparation techniques for adhesive bonding*. 2013, Elsevier/WA: Amsterdam.
69. Troughton, M.J., *Handbook of plastics joining: a practical guide*. 2nd ed. 2008, Norwich, NY; Cambridge, UK;: William Andrew.
70. Rotheiser, J., *Joining of plastics: handbook for designers and engineers*. 1999, Munich; Cincinnati, Ohio;: Hanser Publishers.
71. Owens, D.K. and R.C. Wendt, Estimation of the surface free energy of polymers. *Journal of Applied Polymer Science*, 1969. 13(8): p. 1741-1747.
72. El Kissi, N., J.M. Piau, and F. Toussaint, Sharkskin and cracking of polymer melt extrudates. *Journal of Non-Newtonian Fluid Mechanics*, 1997. 68(2): p. 271-290.
73. Vesel, A., Modification of polystyrene with a highly reactive cold oxygen plasma. *Surface and Coatings Technology*, 2010. 205(2): p. 490-497.
74. Zotti, A., et al., *Fracture Toughening Mechanisms in Epoxy Adhesives*. 2016.
75. Kaseem, M., K. Hamad, and Y.G. Ko, Fabrication and materials properties of polystyrene/carbon nanotube (PS/CNT) composites: A review. *European Polymer Journal*, 2016. 79(Supplement C): p. 36-62.
76. Saeed, M.B. and M.-S. Zhan, Adhesive strength of nano-size particles filled thermoplastic polyimides. Part-I: Multi-walled carbon nano-tubes (MWNT)-polyimide composite films. *International Journal of Adhesion and Adhesives*, 2007. 27(4): p. 306-318.
77. Shokrieh, M.M., et al., Effects of graphene nanoplatelets and graphene nanosheets on fracture toughness of epoxy nanocomposites. *Fatigue & Fracture of Engineering Materials & Structures*, 2014. 37(10): p. 1116-1123.
78. Chen, K., et al., Mechanical Reinforcement in Thermoplastic Polyurethane Nanocomposite Incorporated with Polydopamine Functionalized Graphene Nanoplatelet. *Industrial & Engineering Chemistry Research*, 2017. 56(41): p. 11827-11838.
79. Kalaitzidou, K., H. Fukushima, and L.T. Drzal, Mechanical properties and morphological characterization of exfoliated graphite-polypropylene nanocomposites. *Composites Part A*, 2007. 38(7): p. 1675-1682.

80. Wang, F., et al., Enhancement of fracture toughness, mechanical and thermal properties of rubber/epoxy composites by incorporation of graphene nanoplatelets. *Composites Part A*, 2016. 87: p. 10-22.
81. Triantou, M.I., K.I. Stathi, and P.A. Tarantili, Rheological and Thermomechanical Properties of Graphene/ABS/PP Nanocomposites. *International Journal of Chemical, Molecular, Nuclear, Materials, and Metallurgical Engineering*, 2014. 8(9).
82. Maiti, S. and B.B. Khatua, Properties of Polycarbonate (PC)/Multi-Wall Carbon Nanotube (MWCNT) Nanocomposites Prepared by Melt Blending. *JOURNAL OF NANOSCIENCE AND NANOTECHNOLOGY*, 2011. 11(10): p. 8613-8620.
83. Bhagat, N.A., et al., Development of electrical conductivity in PP/HDPE/MWCNT nanocomposite by melt mixing at very low loading of MWCNT. *Polymer Composites*, 2013. 34(5): p. 787-798.
84. Heidari, B., et al., The effect of ZnO, Fe₃O₄ and graphene oxide nanostructures on the microwave absorbing properties of polystyrene composites. *Journal of Materials Science: Materials in Electronics*, 2017. 28(1): p. 1028-1037.
85. Maiti, S., et al., Polystyrene/MWCNT/graphite nanoplate nanocomposites: efficient electromagnetic interference shielding material through graphite nanoplate-MWCNT-graphite nanoplate networking. *ACS Appl Mater Interfaces*, 2013. 5(11): p. 4712-24.
86. A. G. D'Aloia, F.M., A. Tamburrano, G. De Bellis, M.S. Sarto. Synthesis and Characterization of Graphene-Based Nanocomposites for EM Shielding Applications. in *International Symposium on Electromagnetic Compatibility*. 2013. Brugge, Belgium.
87. Saini, P., et al., Enhanced microwave absorption behavior of polyaniline-CNT/polystyrene blend in 12.4–18.0GHz range. *Synthetic Metals*, 2011. 161(15): p. 1522-1526.
88. Galindo, B., et al., Comparative study between the microwave heating efficiency of carbon nanotubes versus multilayer graphene in polypropylene nanocomposites. *Composites Part B: Engineering*, 2016. 98: p. 330-338.
89. Vollmer, M., Physics of the microwave oven. *Physics Education*, 2004. 39(1): p. 74-81.
90. McCrum, N.G., C.P. Buckley, and C.B. Bucknall, Principles of polymer engineering. 2nd ed. 1997, Oxford;New York;: Oxford University Press.
91. Onyiriuka, E.C., L.S. Hersh, and W. Hertl, SOLUBILIZATION OF CORONA DISCHARGE-TREATED AND PLASMA-TREATED POLYSTYRENE. *JOURNAL OF COLLOID AND INTERFACE SCIENCE*, 1991. 144(1): p. 98-102.
92. Zhang, D., S.M. Dougal, and M.S. Yeganeh, Effects of UV irradiation and plasma treatment on a polystyrene surface studied by IR-visible sum frequency generation spectroscopy. *LANGMUIR*, 2000. 16(10): p. 4528-4532.
93. Hozumi, A., H. Inagaki, and T. Kameyama, The hydrophilization of polystyrene substrates by 172-nm vacuum ultraviolet light. *Journal of Colloid And Interface Science*, 2004. 278(2): p. 383-392.

94. Dixon, D. and B. J. Meenan, Atmospheric Dielectric Barrier Discharge Treatments of Polyethylene, Polypropylene, Polystyrene and Poly(ethylene terephthalate) for Enhanced Adhesion. *Journal of Adhesion Science and Technology*, 2012. 26(20-21): p. 2325-2337.
95. Bhattacharya, M., Polymer Nanocomposites—A Comparison between Carbon Nanotubes, Graphene, and Clay as Nanofillers. *Materials*, 2016. 9(4): p. 262.
96. Santos, R.M., et al., Probing dispersion and re-agglomeration phenomena upon melt-mixing of polymer-functionalized graphite nanoplates. *SOFT MATTER*, 2015. 12(1): p. 77-86.
97. Vilaverde, C., et al., Dispersion and re-agglomeration of graphite nanoplates in polypropylene melts under controlled flow conditions. *COMPOSITES PART A-APPLIED SCIENCE AND MANUFACTURING*, 2015. 78: p. 143-151.
98. Wajid, A.S., et al., Polymer-stabilized graphene dispersions at high concentrations in organic solvents for composite production. *Carbon*, 2012. 50(2): p. 526-534.
99. Chandrasekaran, S., et al., Fracture toughness and failure mechanism of graphene based epoxy composites. *Composites Science and Technology*, 2014. 97(Supplement C): p. 90-99.
100. Heo, C., et al., ABS nanocomposite films based on functionalized-graphene sheets. *Journal of Applied Polymer Science*, 2011: p. n/a-n/a.
101. Bouhfid, R., F.Z. Arrakhiz, and A. Qaiss, Effect of graphene nanosheets on the mechanical, electrical, and rheological properties of polyamide 6/acrylonitrile-butadiene-styrene blends. *Polymer Composites*, 2016. 37(4): p. 998-1006.
102. Hassan, M., et al., High-yield aqueous phase exfoliation of graphene for facile nanocomposite synthesis via emulsion polymerization. *J Colloid Interface Sci*, 2013. 410: p. 43-51.
103. Lee, H., S. Perumal, and I. Cheong, Amphiphilic Fluorinated Block Copolymer Synthesized by RAFT Polymerization for Graphene Dispersions. *Polymers*, 2016. 8(3): p. 101.
104. Noh, Y.J., et al., Ultra-high dispersion of graphene in polymer composite via solvent free fabrication and functionalization. *Sci Rep*, 2015. 5: p. 9141.
105. Zhou, S. and M.C. Hawley, A study of microwave reaction rate enhancement effect in adhesive bonding of polymers and composites. *Composite Structures*, 2003. 61(4): p. 303-309.
106. So, H.W. and A. Taube, Simulation and Experimental Study of Microwave Heating of Single Lap Adhesive-Bonded Polypropylene Joint. *Polymer Engineering & Science*, 2004. 44(4): p. 728-725.